TU WIEN TECHNISCHE UNIVERSITÄT WIEN

DISSERTATION

Enhancing Frequency Stability of Islanded Microgrids via Load Step Pre-announcement and Bang-Bang Controller

ausgeführt zum Zwecke der Erlangung des akademischen Grades
eines Doktors der technischen Wissenschaften

unter der Leitung von
Univ.-Prof. Dr.-Ing. Wolfgang Gawlik
Institut für Energiesysteme und Elektrische Antriebe

eingereicht an der Technischen Universität Wien
Fakultät für Elektrotechnik und Informationstechnik

von
Yi Guo, M.Eng.
Matrikelnummer 01325308
Obere Augartenstraße 6/2
A-1020 Wien

Wien, am 24. September, 2018

_____

Yi Guo

Acknowledgement

The past five years have been an intense period of my study. Writing this doctoral thesis has a great impact on my academical and personal development. I want to thank to those people who have supported and helped me finishing this thesis.

First of all, I express my sincere gratitude to my supervisor, Univ. Prof. Dr.-Ing. Wolfgang Gawlik, for his continuous support and encouragement throughout the entire doctoral work. He made this interesting topic possible for me and offered me this opportunity to conduct my research in his group. Regular seminars and valuable advices from him helped me overcoming all obstacles in the research. His guidance gave me confidence to face and solve all the difficulties. It is a great honor for me to pursue my Ph.D. study under his supervision.

I also want to express my appreciation to all the colleagues from the Institute of Energy Systems and Electrical Drives at TU Wien for offering me a comfortable working environment and a pleasant time. I give my special thanks to a former colleague, Alexander Winter, for providing many interesting discussions, reviews and precious inputs for this thesis.

Furthermore, I give my grateful thanks to my parents, Ying Xu and Huqin Guo, for their endless love, support and trust. Their support motivates me to pursue this doctoral study abroad without any worries during these years. Their love and support made me strong and believing in myself to solve all difficult problems.

I want to thank Tobias Görlich for his love, patience and long-term support, especially during the final stages of this doctoral work. He has spent many hours to read through this thesis and offered me valuable suggestions. Many insightful discussions with him made me able to understand this work from other aspects. His feedback also helped me polishing up the content of this thesis.

Last but by no means least, I thank all my relatives and friends who were there for me and gave me kind encouragement in different ways.

Abstract

Regarding high penetration of distributed energy resources into the medium and low voltage level, power systems undergo challenges with respect to their reliability, security and stability. Aspects of microgrids, including their architecture, distributed generation, storage, and control schemes, are widely researched across the globe, as they have a promising future to integrate distributed energy resources into power systems, thereby reducing greenhouse gas emissions and increasing the reliability and security of power systems with a large amount of distributed generation. Microgrids can be described as decentralized electrical power systems comprising distributed generation, local loads and storage. They can be operated both in grid-parallel and islanded mode. Frequency stability is a common issue to be addressed, especially in islanded microgrids. The focus of this thesis is the development and investigation of a control method for islanded microgrids to regulate their frequency.

In islanded mode, microgrids tend to have a low inertia in comparison to large traditional power systems, especially when there is a high penetration of power electronic interfaced power sources in the microgrid. Thus, frequency changes more quickly when there is a power mismatch between generation and demand. In large power systems, frequency control is an important task. For this thesis, its implementation in islanded microgrids to regulate and maintain the frequency is investigated. However, frequency control is much more difficult to be achieved without the support from the utility grid. An additional control method, including load step pre-announcement and a bang-bang controller, is developed in this thesis to assist frequency control to keep frequency stable within islanded microgrids. The concept of the proposed control method is to anticipate active power changes, which result in imbalances between load and generation, by proactively delaying them for a specific time interval, so that any dynamic effect on frequency deviations caused by them is smoothed. Active power infeed of conventional generation based on directly coupled rotating machines can be controlled, and thus, frequency control in islanded microgrids is supported.

In this thesis, a simulation model of an islanded microgrid, including a conventional

generator, a photovoltaic generator and a lumped load, is used as a study case. Dynamic simulation results of the islanded microgrid are presented and analyzed. The results between the islanded microgrids with and without the proposed control method are compared. The feasibility and effectiveness of the implementation of load step pre-announcement and bang-bang controller are validated using simulation results. Set values of the two time parameters, preset and total time, of the control method regarding different cases are optimized. A discussion regarding still existing problems is given. This includes the influence of frequency measurement time delay on the proposed control method as well as frequency oscillation that may be caused by repeated reconnection of distributed generation.

Kurzfassung

Die zunehmende Integration von erneuerbaren Energien in das Mittel- und Niederspannungsnetz in den letzten Jahren führt zu Herausforderungen an die Energiesysteme in Bezug auf die Zuverlässigkeit, Sicherheit und Stabilität. Verschiedene Aspekte von Microgrids, insbesondere ihre Architektur, dezentrale Stromerzeugung, Speicher und Regelungstechniken, werden global erforscht, da sie ein großes Potential bezüglich der Integration dezentraler Stromerzeugung in elektrische Netze bergen und damit eine Verringerung des Treibhausgasausstoßes bei zugleich zuverlässiger und sicherer Energieversorgung ermöglichen. Microgrids können als dezentrale elektrische Energiesysteme beschrieben werden, die dezentrale Stromerzeugung, lokale Lasten und Speicher umfassen. Sie können sowohl parallel zum Netz als auch als Insel betrieben werden. Frequenzstabilität ist dabei ein häufiges Problem, vor allem in Inselnetzen. Der Schwerpunkt dieser Arbeit liegt auf der Entwicklung einer Frequenzregelungsverfahren für Inselnetze.

Aufgrund der geringen Trägheit von Inselnetzen im Vergleich zu großen konventionellen Stromnetzen sind Frequenzänderungen schneller, wenn es ein Leistungsungleichgewicht zwischen Erzeugung und Last in Inselnetzen gibt. Frequenzregelung ist eine wichtige Aufgabe in großen Stromnetzen. In dieser Arbeit wird ihre Umsetzung in einem Inselnetz untersucht. Allerdings ist die Frequenzregelung ohne die Unterstützung des Versorgungsnetzes schwierig umzusetzen. Es wird ein zusätzliches Regelungsverfahren, einschließlich Load Step Pre-announcement und eines Bang-Bang-Controllers, entwickelt, um die Frequenzregelung zu unterstützen und die Frequenz in Inselnetzen stabil zu halten. Das Konzept besteht darin, Wirkleistungsänderungen zuvorzukommen, die zu einem Ungleichgewicht zwischen Last und Erzeugung führen, indem sie künstlich verzögert werden, so dass dynamische Frequenzabweichungen, die dadurch verursacht werden, geglättet werden. Die Wirkleistung des Generators wird reguliert und somit kann die Frequenzregelung in Inselnetzen unterstützt werden.

In dieser Arbeit wird ein Modell eines Inselnetzes, bestehend aus einem Generator, einer Photovoltaik-Anlage und einer kumulierten Last als Fallstudie simuliert. Die Ergebnisse der dynamischen Simulationen des Inselnetzes werden vorgestellt und analysiert. Die Un-

terschiede zwischen den Inselnetzen mit und ohne das vorgeschlagene Regelungsverfahren werden aufgezeigt. Die Machbarkeit und Effektivität von Load Step Pre-announcement und Bang-Bang-Controller werden durch Simulationsergebnisse validiert. Die Werte der beiden Zeitparameter des Regelungsverfahrens werden für verschiedene Fälle optimiert. Eine Diskussion über noch bestehende Probleme wird geführt. Dazu zählen der Einfluss einer Frequenzmessungsverzögerung auf das vorgeschlagene Regelungsverfahren und Frequenzoszillation, die durch Wiederverbindung von verteilten Erzeugungsanlagen verursacht werden kann.

Contents

Chapter 1

Introduction

1.1 Background

Electrical power supply (or energy supply) is an indispensable requirement for households, industry, business, services, research, information technology and communication, technical advance and many more, and therefore, basis to maintain and further develop modern society. Electricity provides people lighting and heat and is essential for many appliances in households, such as ovens, refrigerators, washing machines, televisions and computers. It makes transportation and worldwide communication possible. Electricity is also fundamental in modern health care. Furthermore, power supply plays a key role to keep commercial and industrial facilities running, and thus, ensures smooth production and services in business and industry. A 30% rise of global energy demand in the year 2040 in comparison to the year 2016 is expected [1]. This growing demand of energy will result in increasing the size and complexity of electrical power systems. Since modern technology and its further development are strongly dependent on electrical power, social and industrial development will benefit from more efficient, secure and reliable power systems.

The continuous increase of global temperature in the last 136 years has been recorded by the National Aeronautics and Space Administration (NASA) [2]. This increase is above the level of natural variability, due to greenhouse gas (GHG) emissions [3]. Since an unstopped increase of average global temperature is expected to have dramatic effects on the world's ecosystem [4], climate change has become an increasingly important issue, especially in energy generation. Therefore, countries across the world set up their own energy policies to decrease GHG emissions. Also, renewable energy resources are essential for decreasing the dependence on fossil fuels. For example, in Europe approx-

imately 53.5% of gross energy consumption was dependent on the imported sources in 2014 [5]. Meanwhile, European citizens focus greatly on issues of climate change and pollution [6]. Thus, the European Commission proposed headline targets in 2010 which should be achieved for smart, sustainable and inclusive growth by the year 2020 - European "20/20/20" targets [7]. The goals that are set in the field of energy production and consumption, are stated as following:

- GHG emissions should be reduced by at least 20% in comparison to 1990 levels (or by 30% if the conditions are right);

- the share of renewable energy should be increased to 20%;

- energy efficiency should be improved by 20%.

More recently, the Paris Agreement, which makes a global action plan to avoid dangerous climate change by limiting global average temperature increase well below 2°C, was reached in December 2015 [8]. In order to achieve these goals, one important measure is to develop and implement renewable energy generation, which is often based on distributed generation (DG) technologies. DG, which also refers to distributed energy resources (DER), covers a wide range of renewable energy and storage technologies, such as photovoltaic (PV) generation, wind power systems, fuel cells and combined heat power. It is typically small scale power generation and is located close to the end users [9, 10]. Electrical energy then can be generated and stored at the consumption points, which is a way to meet customer demands with an emphasis on reliability and power quality, providing economic, environmental and technical benefits [11, p. 3]. However, with the high penetration of DG, electrical power systems go through challenges regarding their operation, stability and control. In contrast to conventional power systems with centralized large generation, deployment of DG into the distribution networks changes the traditional pattern that power flows from a high voltage (HV) level to a low voltage (LV) level. Due to integration of DG, the power flow may be reversed in the distribution network and additional power flow may appear in the transmission level [12]. These challenges of integrating DG require changes in control schemes and operation methods of power systems, which stimulates the interest in microgrid (MG) research.

1.2   Development of Installed Renewable Energy Resources

Since renewable energy resources are able to provide an environmentally friendly and increasingly economical way to produce electrical energy, they have become mainstream
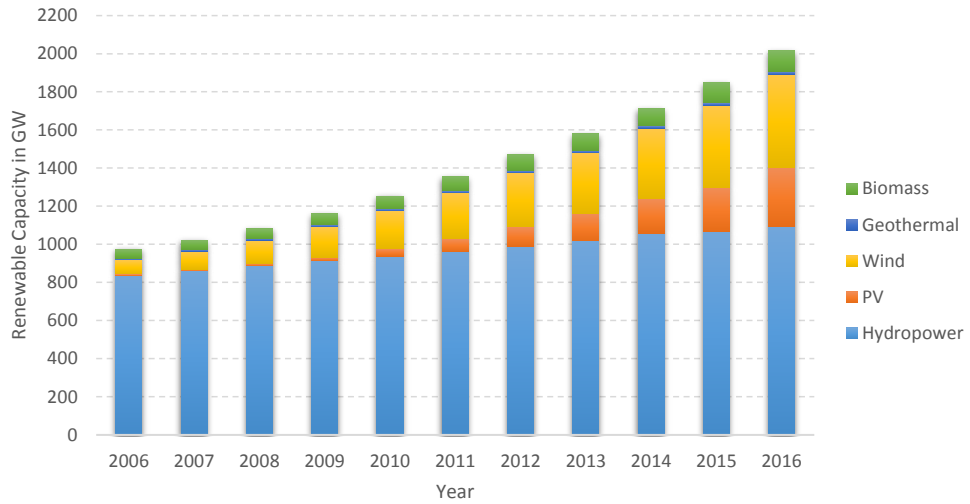
Figure 1.1: Global installed renewable electricity capacity until 2016 [13]

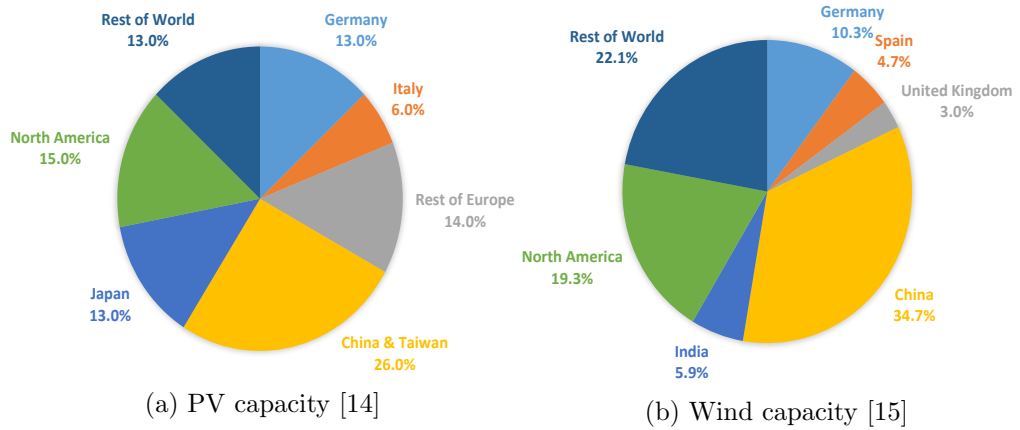(a) PV capacity [14]

(b) Wind capacity [15]

Figure 1.2: Global cumulative PV and wind generation installation by region in 2016

energy sources. The latest renewable energy data book [13] published in December 2017 gives an overview of development in global installed renewable energy resources. The cumulative global installed renewable electricity capacity was 2,016 gigawatts (GW) in 2016, which grew by 9.1% in comparison to 1,848 GW in 2015. This continued the steady growth of 7.5% per year of the compound annual growth rate from 2006 to 2016. Figure 1.1 presents the global installed renewable electricity capacity in recent years. Until 2016, China had the most cumulative total renewable installed capacity, cumulative wind and hydropower capacity and grid-connected solar PV capacity, while the United States led in installed geothermal and biomass capacity. In 2016, renewable energy resources accounted for nearly 26% of all electricity generation worldwide, which was 6,211 terawatt-hours (TWh) [13].

Integration of renewable energy resources in power systems is a way to react on challenges like climate change and finite fossil resources along with a growing demand of power generation. Hence the amount of renewable energy resources installed in total electricity generation is expected to rise further. As shown in Figure 1.1, installed hydropower capacity is the largest among all globally installed renewable energy resources, while installed PV and wind capacity grew fastest in the past years. Global cumulative installed PV capacity and wind capacity increased by 33% and 12% in 2016, respectively [13]. This shows the growing interest in PV and wind generation, especially in regions like China, North America and Germany. The global cumulative PV and wind installation of different regions in 2016 are shown in Figure 1.2 [14, 15].

1.3   Challenges of Microgrid Control

PV generation, which is one of the most important renewable energy sources apart from wind and hydro power generation, had the most dynamic growth in the global market in the recent years as presented in section 1.2. Germany had the world's biggest installation of PV generation until 2014. Germany accounted for about 13% of the global cumulative installed PV capacity and approximately 7% of German electricity demand is covered by PV generation in 2016 [14]. Thus, as an example, installation data of PV in the electrical network in Germany is presented.

Figure 1.3 shows the distribution of PV generation over the typical voltage levels of the German power system. The installed PV capacity in the distribution network (medium voltage (MV) and low voltage (LV) levels) accounts for approximately 92.8% of the total installed capacity. Only around 7.2% of the total installed PV generation is integrated into high voltage (HV) and extra high voltage (EHV) levels. PV generation behaves differently than conventional generation, e.g. it normally has no rotating mass and does
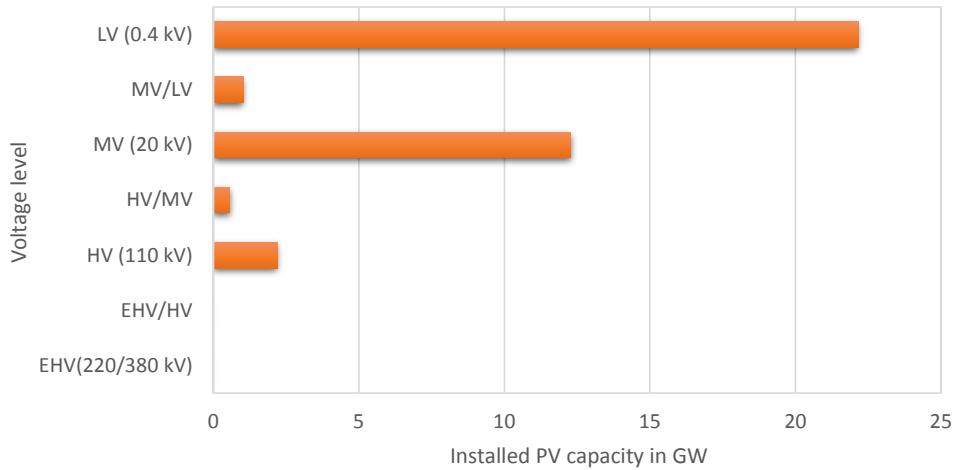
Figure 1.3: Distribution of PV generation in the German power system in
2014 [Source: energymap, bundesnetzagentur]

not contribute to the total system inertia as will be described in chapter 4. High pen-
etration of PV generation and other kinds of DG into electrical distribution networks
causes technical challenges, for instance, reversing power flow in power systems, addi-
tional power flow in transmission networks and grid instability problems [12].
The MG concept has been introduced as an effective solution for the control of grids
under high penetration of DG. Although a more detailed definition of MGs is still under
discussion, MGs can be described as decentralized electrical power systems comprising
DG, local loads and storage, plus necessary control [16]. An example of a MG is pre-
sented in Figure 1.4.
The most important characteristic of MGs is that they can be operated both in grid-
parallel and islanded mode [17]. Under normal operation conditions, MGs are connected
to the utility grid as a single controlled and coordinated unit. Once disturbances occur
either in the utility grid or in local networks, MGs have the possibility to automatically
disconnect from the utility network. When the faults are cleared or the disturbances
are overcome and operation can be resumed, MGs can connect to the utility grid again.
Operation of MGs will be further described in chapter 2.
On one hand, MGs can make effective DG integration possible and ensure energy sup-
ply during an emergency case. During both grid-parallel and islanded mode, DG can
provide power supply continuously. Therefore, loads that can be supplied by DG in-
side MGs would not necessarily suffer from power supply interruptions. In addition,
DG includes various renewable energy resources and can provide energy to end users

locally within MGs. Therefore, DG does not suffer from large power lines' operating
costs and losses [18]. On the other hand, the control of MGs is a major challenge.
Unlike large conventional power plants, DG commonly has low or no inertia [19]. The
inertia of power systems decreases with increasing the amount of inverter based DG. In
grid-parallel mode, system frequency is controlled by the main grid. When MGs operate
in islanded mode, there is no additional support from the utility grid, hence frequency
has to be controlled via coordination of DG within MGs. The low inertia of MGs can
cause fast frequency change if there is a mismatch between power generation and load
demand. Thus, balancing load and generation and frequency stability within islanded
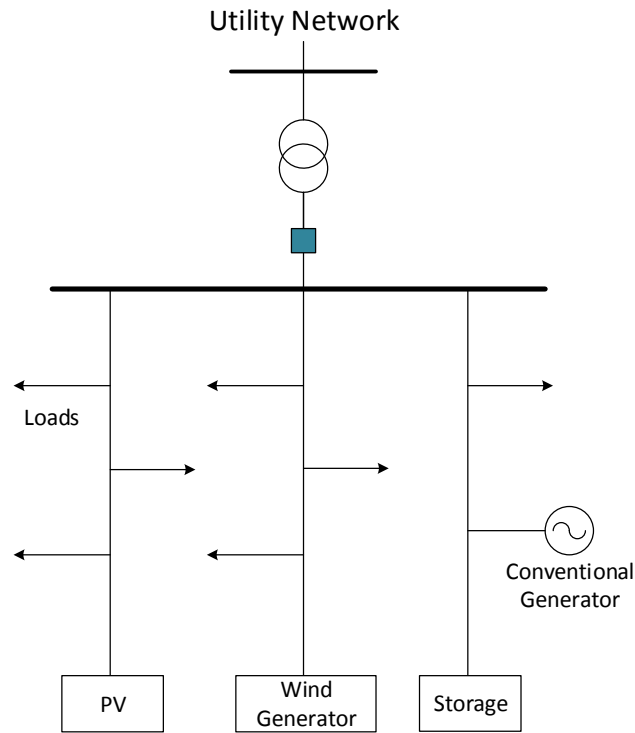MGs are major concerns.

Figure 1.4: An example of a microgrid, self-created based on [18]

1.4   Outline of Thesis

This thesis focuses on frequency control and stability of islanded MGs. A novel control
method, including load step pre-announcement (LSP) and a bang-bang (BB) controller,

is introduced to improve dynamic behavior of islanded MGs when there is a power mismatch between generation and consumption. This leads to the following essential research questions:

- Can the proposed control method benefit frequency stability of islanded MGs?

- Which parameters influence the control effect of LSP and BB controller?

- How can those parameters be adapted to obtain the optimal performance of the proposed scheme?

- Would the control effect of LSP and BB controller be worsened if MGs are not operated under ideal conditions, e.g. in case the system has measurement and communication delay?

This thesis is structured as following:

Chapter 2 gives a review of the existing control strategies used in worldwide microgrid projects. The part of the control strategies review has been published in an earlier paper [20]. Besides, the basics of the swing equation as well as frequency control, including primary, secondary and tertiary control, are presented.

Chapter 3 introduces the concept of the proposed control method - LSP and BB controller. LSP and BB controller have been firstly introduced and published in [17]. A further development of this method, including its control algorithm, control architecture and communication infrastructure, is illustrated.

Chapter 4 presents the simulated islanded MG model that is based on the swing equation. The whole set-up of the simulated model is given. Different parts of the islanded MG, consisting of a conventional generator, a PV generator and lumped load, are introduced separately.

Chapter 5 gives an analytical contemplation. Important parameters that are defined in the simulation are described. The steady state limit of the simulated MG is given based on the system settings. The dynamic behavior of the islanded MG is presented in order to analyze its dynamic limit. In addition, the approximation of the frequency nadir caused by load change in the MG is given. The relation between the preset time of the BB controller and system frequency is described. Three optimization criteria for the two time parameters are given.

Chapter 6 presents and analyzes the simulation results. A comparison between the islanded MG with and without the proposed control method is made. The effect of LSP and the BB control is illustrated. An approximation of optimal set values of the two time parameters for the control method regarding different incidents is presented. A discussion regarding still existing problems, like the reliability of the control method in

an islanded MG with time delay on frequency measurements and frequency oscillation can be caused by repeated PV reconnection, is given. Parts of simulation results and the discussion of PV reconnection issues have already been published in [21, 22].

Chapter 7 gives a conclusion that summarizes the simulation results and an outlook of possible further development.

1.5   List of Publications

The following publications are made during the elaboration of this thesis:

- Y. Guo and W. Gawlik. "A survey of control strategies applied in worldwide microgrid projects." Tagungsband ComForEn 2014 (2014): 47 - 54.

- Y. Guo and W. Gawlik. "A Novel Control Approach for Microgrids Islanded Operation - Load Step Pre-announcement and Bang-Bang Control."; Vortrag: 14. Symposium Energieinnovation EnInnov2016, Graz; 10.02.2016 - 12.02.2016; in: "EnInnov 2016 - Energie für unser Europa", Verlag der Technischen Universität Graz, (2016), ISBN: 978-3-85125-447-1; P. 1 - 14.

- Y. Guo and W. Gawlik. "Defining control strategies for photovoltaic reconnection in islanded microgrids." e & i Elektrotechnik und Informationstechnik 133.8 (2016): 402 - 406.

- Y. Guo, T. Görlich and W. Gawlik. "Load Step Pre-announcement and Bang-Bang controller Implemented in Islanded Microgrids to Improve Frequency Stability."; Vortrag: CIRED, Ljubljana, Slowenien; 07.06.2018 - 08.06.2018; in: "CIRED Workshop 2018 "Microgrids and local energy communities"", (2018), Paper-Nr. 0086, 4 pages.

Chapter 2

State of the Art

2.1 Review of Control Strategies of Microgrids

Different countries around the world have their own interests to develop the MG concept. As mentioned in chapter 1, the European Commission has proposed European "20/20/20" targets. The United States of America was the largest greenhouse gas (GHG) producer in the world before 2004 [23]. In 2009, the goal to reduce GHG emissions in the USA by around 17% in 2020 in comparison to 2005 was committed. Moreover, a big part of energy demand was supplied by imported petroleum [24], therefore, change of energy supply patterns was required. Likewise, China became the leading emitter of greenhouse gases due to its rapid economic growth after 2004. Lots of countries have made energy policies to push green energy supply technologies forward. Since Microgrids (MGs) have a promising future to a more secure, reliable and environmentally-friendly power system, they gained great research interest and plenty of projects regarding the concept and operation of MGs have been carried out worldwide.

The earlier work [20] published during the elaboration of this thesis reviews control strategies that are applied in worldwide MG projects. More than 50 existing MG projects in regions like Europe, America and Asia have been surveyed. A general topology of MGs is shown in Figure 2.1. MGs are normally connected to the utility grid via a point of common coupling (PCC), from where MGs are also able to disconnect from the utility grid. Islanded MGs, which are MGs without PCC, constantly operate independently from the utility grid because of either technical or economic constraints [16].

Information, including MG configuration, amount of PCCs, voltage level, total installed capacity of distributed generation (DG), storage capacity and maximum load demand, have been collected in the survey. The current state of control strategies used in the
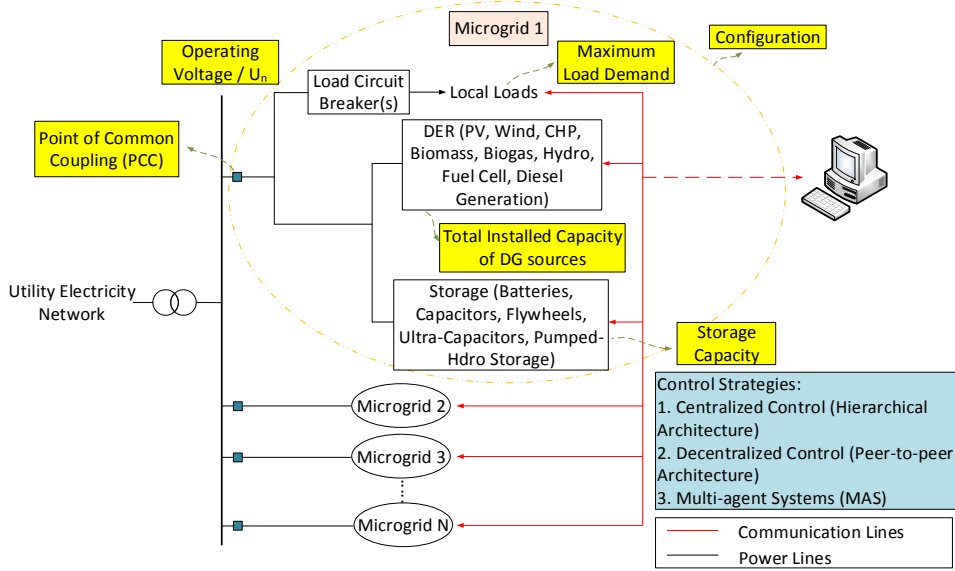
Figure 2.1: A general topology of MG

MGs is presented in [20]. It also gives the correlation between volatile DG and storage systems, and between loads and storage systems. Three control architectures, including centralized, decentralized and multi agents system (MAS), are illustrated in the work.

2.1.1   Centralized Control

Centralized control, which can also be called hierarchical control, normally includes a microgrid central controller (MGCC), which controls all the components of the MG, and local controllers (LCs). The MGCC gathers locally measured data from LCs and performs calculations. It determines control actions for the LCs and provides the LC instructions, such as set points of active and reactive power. The centralized control has been used to control frequency in large electrical power systems for years and was implemented in MGs for voltage and frequency restoration in recent years [25].
Information between the MGCC and LCs is exchanged regularly in a centralized control architecture, thus special attention should be paid to the communication systems. A failure in communication paths could lead to huge problems in the grid operation and control, which would lower the system reliability. Hence, fast and reliable communication systems are strongly required [16, 26]. Additionally, the MGCC is the essential element. If the MGCC fails, the whole control system cannot work. The upper-left side of Figure 2.2 presents an example of a centralized control structure.
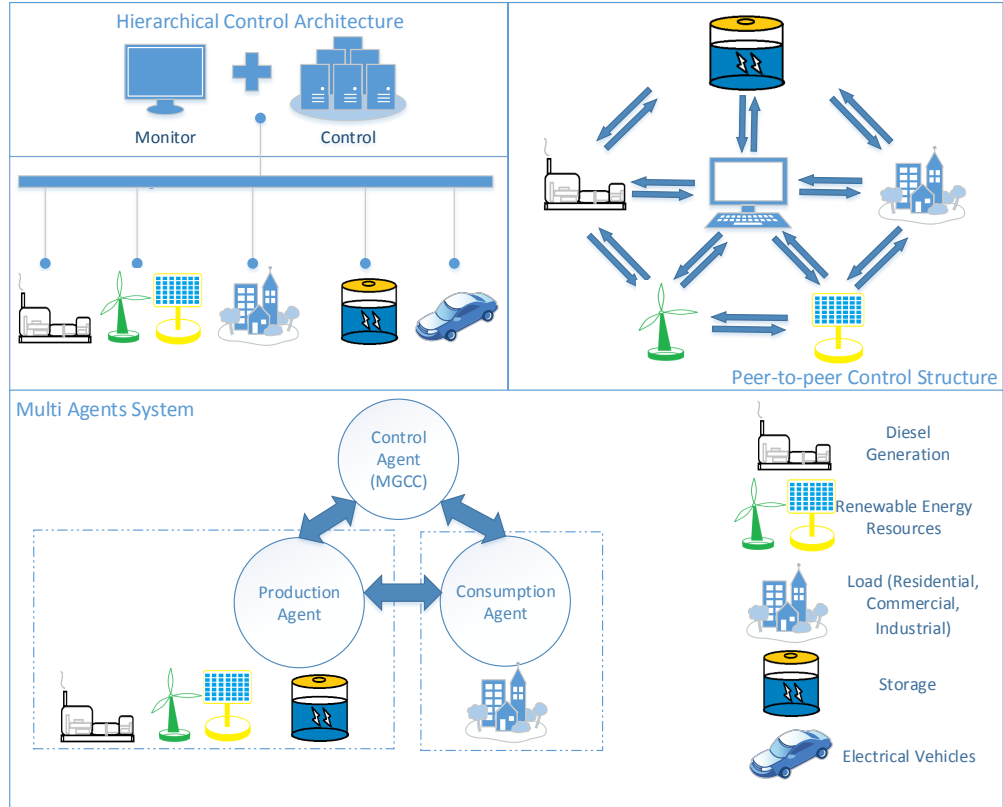
Figure 2.2: Centralized control (upper left), decentralized control (upper right) and multi agent system (bottom) [20]

2.1.2 Decentralized Control

Decentralized control, which features peer-to-peer communication, was firstly proposed by Piagi and Lasseter in [27]. In a fully decentralized control architecture, each component should be equivalent. There is no single device, like the MGCC, that is critical for the MG operation. A MGCC may exist to monitor the MG, but its presence does not influence the operation of the peer devices.

Different from the centralized control architecture, each device operates independently from the others. Hence, it can achieve the "plug and play" function. This means that MGs can continue their operation although any generation would connect to or disconnect from the grid as long as the energy requirements are still satisfied [28]. Communication infrastructure, thus, is not necessary for decentralized control. This control structure is presented on the upper-right side in Figure 2.2.

2.1.3   Multi Agents System

The implementation of a fully centralized approach can be infeasible because of the large data exchange and extensive communication. On the other hand, due to the strong link between elements in power systems, a fully decentralized cannot be achieved by only using local data [16]. A multi agents system (MAS) is a compromise between entirely centralized and fully decentralized control. Agents, which have a certain level of autonomy based on limited local information, are the main elements in a MAS. This means that they have the ability to make decisions and commands without the MGCC. Additionally they can communicate with each other to exchange information. There could also be an agent playing the role as the MGCC in the MAS, which only coordinates local tasks and records final power exchanges between the agents periodically [29].

The aim of MAS is to control complicated power systems with minimum data exchange and computational demands. Even though agents are able to communicate with each other, most of the control actions should be taken locally based on their autonomy [16, 29]. Communication infrastructure is needed in this control structure. A common communication language is normally required, since agents should be able to interact and communicate with each other to exchange information [30]. The bottom picture in Figure 2.2 shows structure of MAS.

2.1.4   Comparison of MG Projects

These surveyed projects include, for example, European Microgrids and More Microgrids projects, American CERTS Microgrid project, Canadian Hydro Boston Bar MG and Hydro-Québec, Japanese NEDO projects, and the Microgrid testbed in Hefei University of Technology (HFUT) in China [20]. The MG research activities cover a wide range from small to large scale MGs, which can be classified by their maximum load demand. For example, small scale MGs' types can vary from small single apartments to large buildings or farm houses, whereas the upper limit of the medium scale MGs reflects the maximum size of a distribution LV network. Large scale MGs can represent MV networks. Three groups of MGs classified according to the maximum load demand are as follows:

- Small Scale Microgrids: $1\,\text{VA} < P_{load} \leq 30\,\text{kVA}$

- Medium Scale Microgrids: $30\,\text{kVA} < P_{load} \leq 1\,\text{MVA}$

- Large Scale Microgrids: $P_{load} > 1\,\text{MVA}$

A comparison between the maximum load demand and total installed DG capacity of the surveyed MGs is presented logarithmically in Figure 2.3. Most of the surveyed projects
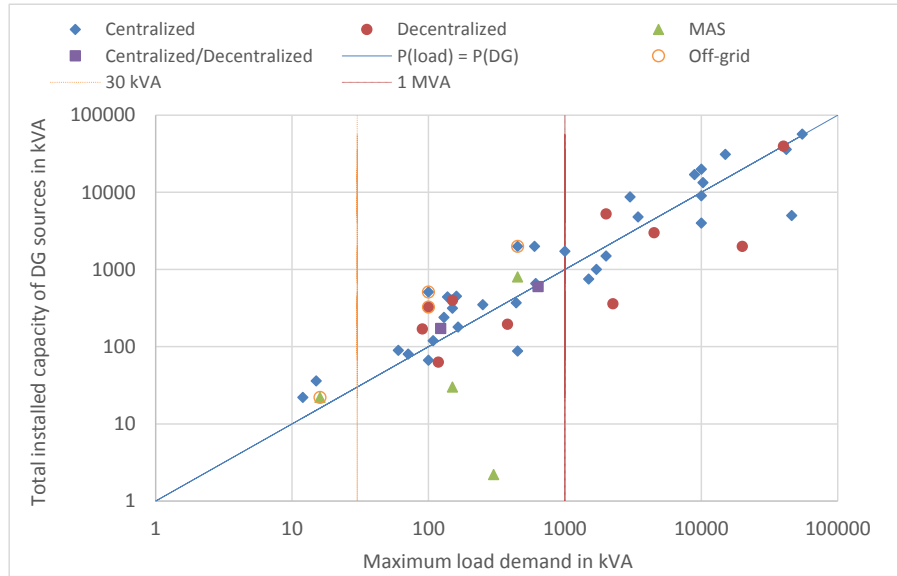
Figure 2.3: Comparison between the maximum load demand and total installed capacity of DG [20]

are on-grid MGs and some are off-grid MGs[1]. According to the picture, the majority of MGs have enough installed capacity of DG to run in islanded mode without load shedding and the rest needs to be supported by the utility network for covering the full load. Among all the investigated MG projects, the installed capacity of the DG cooperated with the backup diesel generation and batteries are sufficient for the demand of consumers in the off-grid MG projects. Most on-grid projects are able to use the DG to support their local loads, and some exceptions need to get the energy from the utility grid.

Existing control techniques have offered a lot of possibilities for the operation of MGs. Parameters like power quality and stability, installed storage capacity, requirement of a communication infrastructure and types of installed distributed generators affect the choice of control strategies. Figure 2.4 shows the percentage of the utilization of applied control strategies in the surveyed MG projects. The centralized control approach is widely adopted from small scale to large scale MGs, when there is a central storage system installed. The MAS is implemented mostly in the small and medium scale MGs, as long as there are controllable loads and generation. The decentralized control

---

[1]On-grid MGs: Microgrids are operated in grid-parallel mode; off-grid MGs: Microgrids run in islanded mode
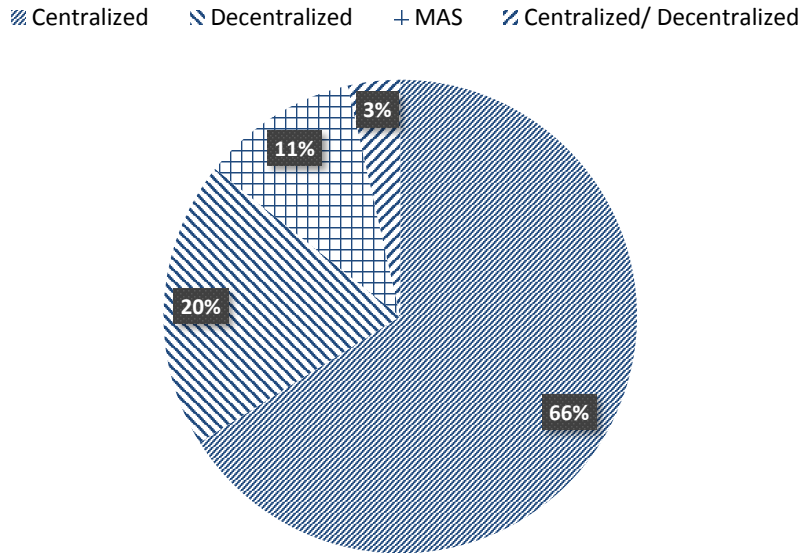
Figure 2.4: The utilization of control strategies in the surveyed MG
project [20]

technology is applied in medium and large MGs, since utilizing the decentralized control
strategy is easy to achieve the plug-and-play function of MGs and would not influence
architecture and the communication structure of energy systems. There are also test
grids, which have the ability to be reconfigured, allowing to test out both centralized
and decentralized control strategies for their systems.

The correlation between the installed capacity of volatile DG sources, like PV and wind
power plants, and the storage capacity based on the available data of the survey is given
in Figure 2.5(a). The more volatile DG sources are installed in the MGs, the larger the
used capacities of the storage systems are. Storage capacity rating related to installed
volatile DG sources is usually between 1 kWh/kW and 10 kWh/kW, which means that
storage charging duration is normally between 1 hour and 10 hours when volatile DG
sources work at their rated power. Most storages can be fully charged within 6 hours.
The correlation between the maximum load demand and the storage capacity is presented
in Figure 2.5(b). As can be seen, most MGs have enough storage to provide energy to
the customers for at least 1 hour. In the worst case, if any failure would occur during a
time period with a lack of volatile DG sources, those MGs would only last for a black-out
of several hours, but for sure not days.

Although there are differences among MG control structures, they all intend to ensure
the reliability and security of networks when a large number of DGs are integrated into
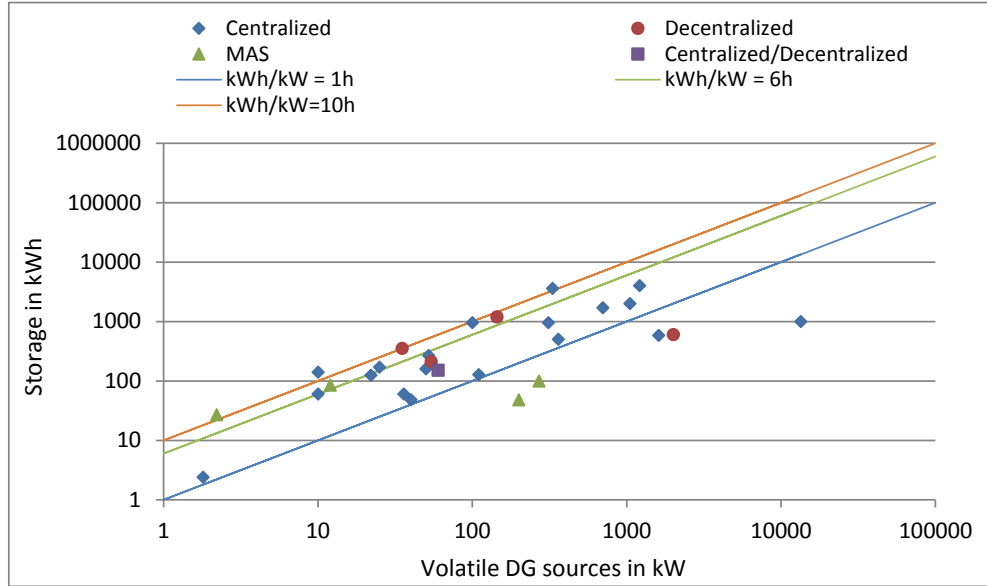
(a) The correlation between capacity of installed volatile DG sources and storage
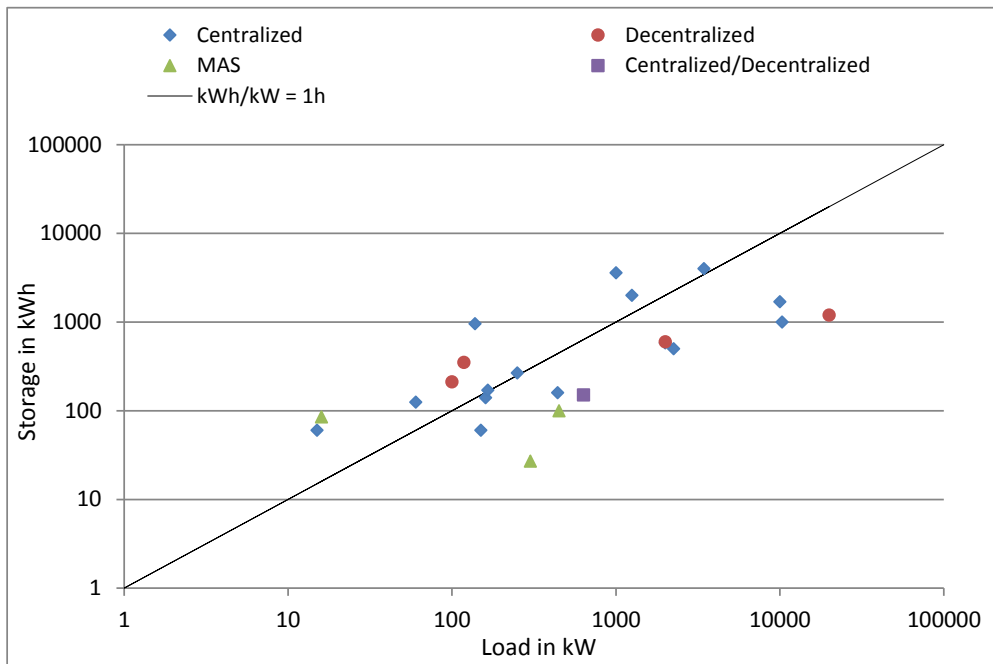
(b) The correlation between the maximum load demand and storage capacity

Figure 2.5: Data analysis [20]

utility grids. To conclude the findings of the surveyed MG projects, centralized control is currently dominant. In off-grid MGs, total installed capacity of DG sources usually exceeds maximum load demand, while in around 38% of on-grid MGs, load shedding would be necessary in a situation of reaching maximum load demand and depleted storage. Due to the use of the storage in the MGs, a long-term black-out over days can be avoided. Further information about the surveyed MG projects can be found in [20].

2.2   Swing Equation

To analyze stability of power systems with synchronous generators that are driven by prime movers, the swing equation is important. The swing equation, which relates the differential equation that describes the acceleration and deceleration of the synchronous generator and turbine (prime mover) caused by imbalance between mechanical and electrical torque, is the basis of the simulated system. In this section, a review of swing equation is given on the basis of [31, p. 9-17] and [32]. In rotational movements, the net accelerating or decelerating torque (τ_a) when there is an unbalance between torques acting on the rotor is:

$$\tau_a = J \times \frac{d\omega}{dt} \tag{2.1}$$

where J is combined moment of inertia of generator and turbine. $d\omega/dt$ is the angular acceleration of the rotor, in which ω is the angular speed of the rotor of the synchronous generator including turbine and t is the time. This applies similarly to the relation between force, mass and acceleration in linear movements. τ_a is accelerating or decelerating torque, which is equal to the difference between mechanical torque (τ_{mech}) and electrical torque (τ_{el}),

$$\tau_a = \tau_{mech} - \tau_{el} \tag{2.2}$$

For rotational generators, rotational kinetic energy (E_{rot}) is given as:

$$E_{rot} = \frac{1}{2} \times J \times \omega^2 \tag{2.3}$$

The difference between the supplied mechanical power P_{mech} (turbine) and the dissipated electrical power P_{el} (generator) is calculated by:

$$P_{mech} - P_{el} = \frac{dE_{rot}}{dt} = J \times \omega \times \frac{d\omega}{dt} \tag{2.4}$$

According to equations (2.1), (2.2) and (2.4), mechanical and electrical power difference causes torque unbalance for angular acceleration or speed change:

$$P_{mech} - P_{el} = (\tau_{mech} - \tau_{el}) \times \omega \tag{2.5}$$

The moment of inertia may vary from small to large power plants. Therefore, only the system starting time constant is often used nowadays in system analysis. The moment of inertia is thus determined by the system starting time constant (T_A). The starting time constant of a generator refers to the time, which a generator needs to reach its rated speed (ω_n) from standstill based on its rated torque (τ_n):

$$J = \frac{\tau_n \times T_A}{\omega_n} = \frac{P_n \times T_A}{\omega_n^2} \tag{2.6}$$

where P_n is the nominal power or rated power of the generator. Therefore:

$$T_A = \frac{J \times \omega_n^2}{P_n} \tag{2.7}$$

To specify the moment of inertia J in equation (2.7) if different generators are connected to the electrical power system,

$$J_{Gi} \times \omega_i^2 = \frac{J_{Gi} \times \omega_n^2}{(\omega_n/\omega_i)^2} = J_i \times \omega_n^2 \tag{2.8}$$

where J_{Gi} is the combined moment of inertia of ith generator and turbine under the angular speed of ith generator ω_i. Thus, the normalized moment of inertia (J_i) of ith generator that is connected to the electrical grid operating at the nominal angular speed can be expressed by,

$$J_i = \frac{J_{Gi}}{(\omega_n/\omega_i)^2} \tag{2.9}$$

Since generators may have different system starting time constants, the overall system starting time constant should be calculated as:

$$\sum_i J_i \times \omega_n^2 = \sum_i T_{Ai} \times P_{ni} \tag{2.10}$$

it results:

$$T_{Aoverall} = \frac{\sum_i T_{Ai} \times P_{ni}}{\sum_i P_{ni}} \tag{2.11}$$

where T_{Ai} is mechanical starting time constant of ith generator and P_{ni} is the rated power of ith generator. By substituting the difference between mechanical and electrical torque $(\tau_{mech} - \tau_{el})$ according to equation (2.5) and J from equation (2.6) into equation (2.1), it results as following:

$$\frac{P_{mech} - P_{el}}{\omega} = \frac{P_n \times T_A}{\omega_n^2} \times \frac{d\omega}{dt} \tag{2.12}$$

Frequency (f) is proportional to the angular speed:

$$\omega = 2 \times \pi \times f \tag{2.13}$$

Equation (2.12) is then:

$$\frac{df}{dt} = \frac{P_{mech} - P_{el}}{f} \times \frac{f_n^2}{P_n \times T_A} \tag{2.14}$$

where f_n is the nominal frequency. As P_{mech} presents the power which is produced by generators and P_{el} is the power that is consumed by electrical loads, swing equation can also be written as:

$$\frac{df}{dt} = \frac{\sum P_G - \sum P_L}{P_n} \times \frac{f_n^2}{f \times T_A} \tag{2.15}$$

where $\sum P_G$ is the sum of power output from all generating units and $\sum P_L$ is the sum of load demand in the electrical network.

2.3   Frequency Control

There are many reasons to keep frequency stable and not to deviate too much from nominal frequency. For example, one reason is that lots of connected devices work best at nominal frequency. In case of a non–nominal frequency situation in power systems, the power output of generation can be impaired. Besides, large frequency deviations can reduce lifespans of steam turbines or cause direct damages of them. In a worst case steam turbines need to be disconnected from the grid, which can result in a further frequency instability and end up with a black-out [33].
In islanded mode, any small change in supplied and demanded power of MGs can cause a severe frequency deviation because of the small total size of the system. Hence control of MGs is one of the main concerns for MGs operation. Frequency control is one important control method to maintain the frequency within the nominal operating conditions.

In a large power system, frequency control loops, including primary control, secondary control, tertiary and emergency control activating frequency containment reserve (FCR), frequency restoration reserve (FRR) and replacement reserve (RR), are usually available. Among the four control forms, the primary and secondary control are the two basic control loops in a power system [34, chapter 2].

2.3.1 Primary Control

Primary control provides a local droop control to generators [34, p. 65-67]. Its aim is to stabilize power systems' frequency close to the nominal value after a disturbance in a time frame of seconds [35]. Each generating unit has its own droop characteristic to respond to the frequency deviation of the power system within a few seconds without any communication with other elements or a control center. In large conventional power systems, primary control is activated in a time range from $0\,\text{s}$ to $30\,\text{s}$, however this activation time of primary control is much shorter in islanded MGs with low inertia [34, p. 36]. The active power and frequency (P/f) droop control characteristic is formulated as:

$$\frac{f - f_0}{f_n} = -\frac{1}{k} \times \frac{P - P_{0i}}{P_{ni}} \tag{2.16}$$

f_0 is the nominal set point of frequency and P_{0i} is the dispatched power of the ith generator when frequency is at the nominal set point. f_n is nominal frequency and P_{ni} is the rated active power of generator i. $\frac{1}{k}$ is the frequency droop control setting, which is the ratio of frequency deviation to the power output change of generator i. Droop settings are usually described as % droop. For instance, when k equals 25, it indicates that ith generator has a 4% frequency droop. This means that 4% frequency deviation will cause 100% change in power output [36, p. 589-594]. With a 4% droop, the power output will increase by 25% if the frequency drops by 1%.

The P/f droop characteristic is shown in Figure 2.6. If more load would be utilized in the grid, frequency would decrease according to the swing equation (2.15). When the system frequency drops from frequency set point f_0 to f_1, generators participating in primary control should increase their power output from the set point P_{01} to P_1 and from the set point P_{02} to P_2 as it is shown. f_{Min} is the grid frequency at full load. The generators, which participate in the droop control, should also reach their maximum power rating at f_{Min}, which are P_{1Max} and P_{2Max}, respectively. The droop control works the same when less load would be applied in the grid. f_{Max} is the frequency when there is no load in the grid. When the frequency limit f_{Max} is reached, active power that is produced by generators participating in droop control should be at their minimum values P_{1Min}
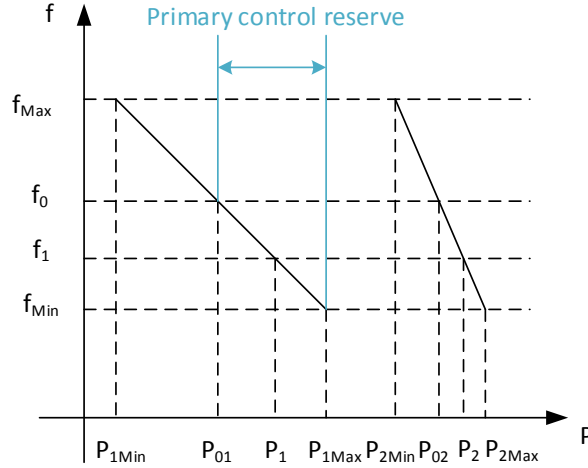
Figure 2.6: P/f droop control characteristic [34, p. 67]

and P_{2Min}. The primary control reserve shown in Figure 2.6 is the available power of generating units that can be activated from the set points up to the maximum value, in both directions, to respond to a frequency deviation.

The droop characteristic allows different generators to operate at the same frequency with different power outputs, track the load change and stabilize the frequency. It is necessary for the grid operation to have an adequate level of primary control reserve that can be activated within a few seconds in case of a frequency deviation from the nominal frequency. The system frequency stays at a certain value once a new balance between power supply and demand is achieved. However, this new steady point of frequency could be different from the nominal operating point, because of the proportional action of the generators' droop control.

2.3.2   Secondary Control

Primary control can react very fast to small frequency deviations in power systems. However, it also allows the power systems to operate at a new set point of frequency, which can be below or above the nominal value, once the balance is established between power supply and demand. Therefore, secondary control (also called as load-frequency control) [34, chapter 2] is required to replace primary control over minutes. It can modify the set point values and restore the system frequency to the nominal value. Secondary control takes place continually and parallel to primary control, however it should not affect the actions of primary control. Both primary and secondary control can react to

small disturbance under normal operation and big disturbance in case of failure of components in power systems [37, p. 243-256]. It works in a timescale of several minutes and should be completed in up to 15 mins after a disturbance at the latest [35]. In islanded MGs, its control process can be shorter than that in large traditional power systems.

The secondary control behavior over time is achieved via a simple integral or proportional-integral (PI) controller in real-world power systems [34, p. 23]. Secondary control uses the measurements of system frequency and active power flows to calculate and change the power set points of respective generators. Since system frequency and active power of generators should return to their initial set points from stationary deviation after primary control within the time duration of secondary control, an integral term is necessary [37, p. 243-256]. The proportional term of secondary control provides a fast reaction on deviation, however, it may result in a detrimental effect on the stability of interconnected operation if an overly large value is chosen for proportional gain. Appropriate values should be chosen for proportional and integral gain. In continental Europe, proportional gain has a typical value between 0% and 50% and integral time constant is normally between 50 s and 200 s [35].

2.3.3 Tertiary Control

Tertiary control is activated if frequency deviation lasts longer than the duration of secondary control that should be activated. Under normal circumstances, tertiary control is used to replace secondary control reserves, and thus, to relieve and to allocate secondary control reserves to the various generators in the most economical way [35]. Tertiary control can be either directly manually activated at any time or scheduled to be automatically activated following the exchange schedules. The activation of tertiary control is the responsibility of transmission system operators (TSOs) [35].

In a severe situation, emergency control and protection schemes, i.e. load shedding in case of under-frequency and disconnection of generation in case of over-frequency, should be considered to re-establish the nominal frequency and active power balance between generation and load [34, p. 229-232].

Since activation of tertiary control works manually or follows schedules based on economic offline optimizations automatically [33], it is not further discussed and included in this work. Automatic frequency control of the islanded MG comprises only two basic control loops, primary and secondary control.

Chapter 3

Control Method

This chapter presents the proposed method - load step pre-announcement (LSP) and bang-bang (BB) control, including the basic principles, further development of the control method, the work process, the control structure and communication requirements.

3.1 Proposed Control Method

Frequency, voltage, active and reactive power are the main parameters to determine the operation of power systems. Frequency change is closely related to active power balance between power supply and demand, while voltage is correlated with reactive power change in systems where rotating machines are present and dominate. Frequency control is the focus of this thesis.

Microgrids (MGs) have a low inertia in islanded mode in comparison to large traditional power systems, thus, frequency control of MGs is difficult to be achieved without the support from the overall network. Other control methods should be implemented to assist frequency control to keep frequency stable within islanded MGs. The proposed control method - LSP and a BB controller - was designed for an islanded MG in the earlier work [17] to anticipate active power changes which result in imbalances between load and generation, so that any dynamic effect on frequency deviations caused by power imbalances will be smoothed. Active power infeed of the conventional generation (CG)[2] based on directly coupled rotating machines can be controlled, and thus, frequency control in the MG is supported. In this chapter, the proposed control method and its further development are introduced.

---

[2]Conventional generation means that generation based on directly coupled rotating machines in this thesis

23

3.1.1 Load Step Pre-announcement

As the name implies, LSP announces possible load changes in the islanded MG. When a load requires to be switched on or off, this switch signal will be received by LSP. It will then delay the switch signal for a defined short time period[3] and maintain the previous load status to the system. Within this preset time (t_{set}) period, LSP notifies the BB controller to control the power output of the CG preemptively, so that the CG starts increasing or decreasing its power output before the load change is actually realized. The active time ranges of LSP, BB control, primary and secondary control are shown in Figure 3.1.
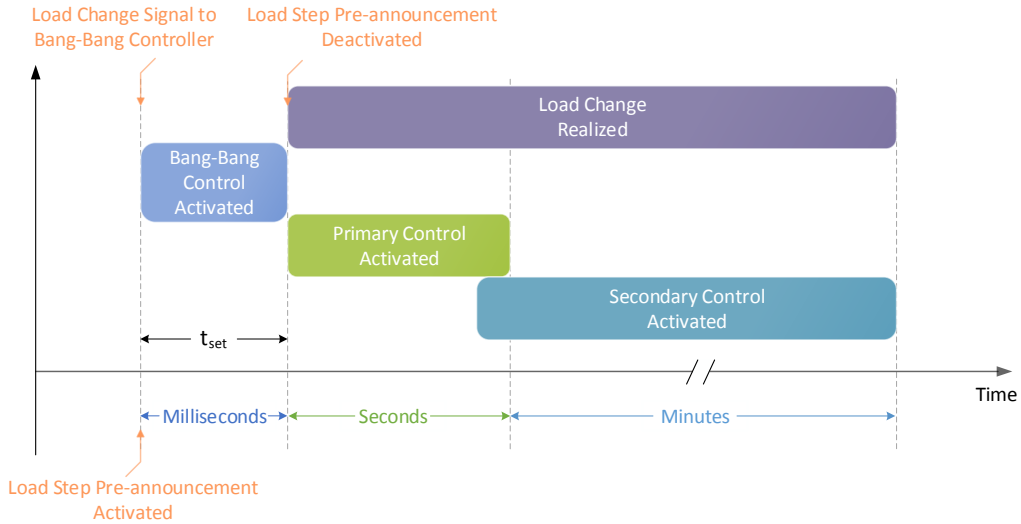
Figure 3.1: Active time ranges of LSP, BB control, primary and secondary control

This preset time is one important parameter that defines the effect of the proposed control method. In the earlier work [17], this preset time for releasing a load change is set to be 40 ms. This means that LSP will delay this load change for the next 40 ms, and meanwhile, send out the signal to the BB controller to control the power output of the CG. After these 40 ms, load change will be allowed to be released and the control action of the BB controller for the CG to ramp-up will stop. Depending on the system inertia constant, shares and dynamics of generators that participate in primary control, the preset time could be set differently.

---

[3]This defined time period of delay refers to preset time

3.1.2   Bang-Bang Control

Bang-bang control [38] is often applied in the control of non-linear systems. A BB controller can be used as a feedback controller, which switches between two states, on and off. Therefore, it is also called as on-off controller. One example of BB controllers is the common residential thermostat. It can be switched on or off automatically when the ambient temperature reaches a certain point. A BB controller for the MG to enhance the dynamic behavior has been designed based on this simple control concept [17].

Instead of the preset threshold of ambient temperature, the BB controller in the MG reacts on the signal from LSP depending on whether there is a significant load change or not. After receiving the signal from LSP, the BB controller commands the CG to change its operating point within the preset time, e.g. it increases generation at maximum rate in case of a load increase. Likewise, it requires the CG to start decreasing its power output when a load decrease is announced by LSP. If no load change signal is sent, the BB controller does not take any additional control action. However, in order to avoid any instability that may occur in MGs and not to interfere with the function of the primary and secondary control, this action of the BB controller should only be activated within a certain time period and a secure limit. In this way, the rapid change in power generation will not trigger over- or under-frequency protection of the CG, cause disconnection of the photovoltaic (PV) generation or lead to load shedding action. A detailed description of the designed BB controller can be found in [17].

3.1.3   Time Extension in Bang-Bang Controller

In the earlier designed control method [17], both LSP and BB controller work only within the preset time period. This means that the control signal will stop immediately when the load change occurs. If the initial state of the MG is assumed to show a balance between generation and load at nominal frequency, the CG will have a power difference from its initial value due to the effect of the BB controller. Thus, the MG's frequency will deviate from the nominal point. When the control signal stops and load demand is smaller than the pre-generated active power from the CG, there may be a short time that the CG tends to change its active power back to the initial value due to frequency deviation. This will be further discussed and presented in chapter 6. In order to avoid this and possibly improve the control effect of the proposed method, the time in which the control signal of the BB controller requires the CG to preemptively change its active power should be extended.

The operating time of the BB controller, which includes the preset time and an additional time period, is called total time (t_{total}) in this thesis. The active time ranges of LSP and the BB controller are shown in Figure 3.2. When the preset time runs out, load step

will be released by LSP. Due to the extension of its activation time, the BB controller stays active after the load change is realized. When the total time period is over, the BB controller will be deactivated and the CG will work again in its normal operation mode. The total time of the BB controller is the second important time parameter along with preset time. It is mainly influenced by the dynamics and share of the CG. It can vary from several up to hundreds of milliseconds. Preset and total time should be set individually as will be discussed in chapter 6.
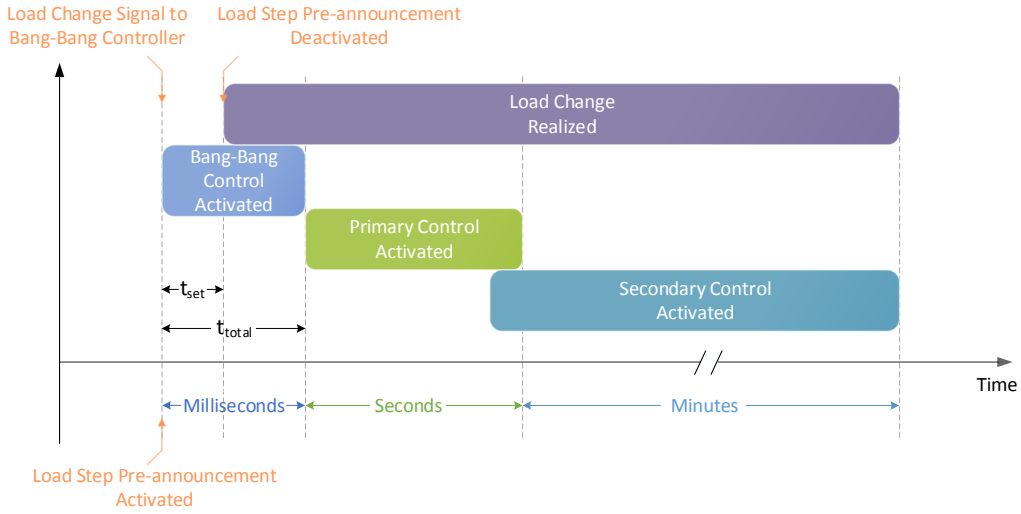

Figure 3.2: The time ranges of LSP and the BB controller with time extension

LSP and BB controller should support the frequency stability of islanded MGs while not causing other instability issues as stated above. Therefore, a secure frequency limit should be set up for activating the BB controller. The lower frequency limit is defined based on the ENTSO-E RG CE general under-frequency load shedding (UFLS) scheme [39]. The UFLS scheme is an emergency operation of a grid in case of a large frequency drop. It recommends that load shedding should be triggered in the range between 48 Hz and 49 Hz to prevent a further frequency decrease that can lead to grid collapse. According to [39], at least 5% of the total load should be disconnected at 49 Hz, while 45% ± 7% should be disconnected altogether between 48 Hz and 49 Hz. The UFLS scheme should be carried out stepwise and 10% of the total load is allowed to be disconnected at maximum for each step. Since load shedding action will be triggered at 49 Hz, the lower frequency limit of the BB controller is set to be at this value. This means that the BB controller will not be activated if the frequency would drop below 49 Hz. For the upper frequency limit, 51.5 Hz is used in line with a frequency-dependent active power

characteristic determined by the German VDE-AR-N 4105 standard [40] to avoid PV disconnection caused by over-frequency, which will be described in detail in chapter 4.

3.2   Control Architecture

As stated in chapter 2, centralized control, decentralized control and multi-agents systems are the three main control architectures of MGs. The study case, which is going to be presented in the next chapter, includes a conventional generator, a photovoltaic generator and lumped load. Since there is only one dispatchable generator in the study, a centralized control architecture is considered.

3.2.1   Centralized Control Architecture for LSP and BB control

In a fully centralized control architecture, one essential element is the microgrid central controller (MGCC), which coordinates distributed generation (DG) and manages the power balance in the MG system. It gathers data, performs calculations and determines the control actions for the operation of the MG [20]. Besides, there are also local controllers (LCs), which collect locally measured data from DG and load. They can update the local information and receive instructions from the MGCC. The LCs can be separate hardware devices or software installed in electronic meters or interfaces [41]. Communication between the MGCC and LCs is necessary. The overview of the control system of the islanded MG including LSP and BB controller is shown in Figure 3.3.
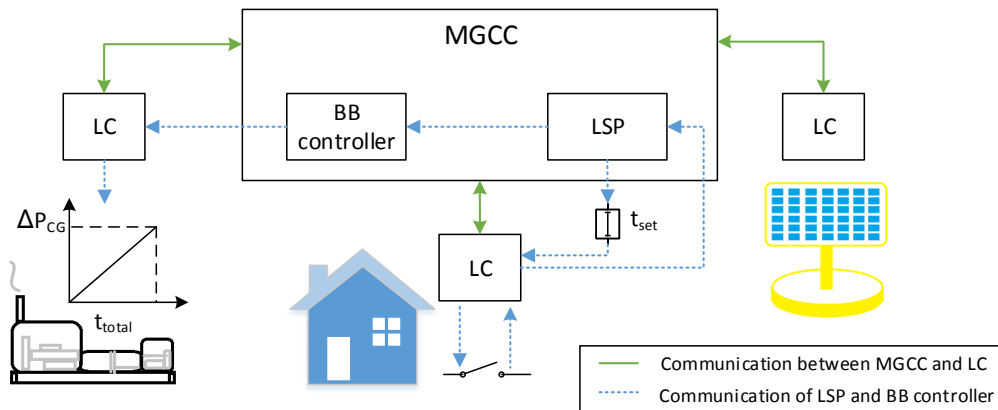

Figure 3.3: Centralized control architecture of the islanded microgrid

Both LSP and BB controller belong to the MGCC part and each element in the MG has an LC as presented in Figure 3.3. The LC of the CG provides droop settings locally.

The LC of the PV provides an active power control depending on the MG frequency change, e.g. reduction at over-frequency. The load switch should be connected to its LC that is able to collect any switch change information of the load. In the load LC, there is a predefined setting that information about the load change should be sent over to the MGCC as soon as the status of the switch button changes. An example of the predefined setting applied in the LC is given in Table 3.1.

Table 3.1: Predefined information in local controller

Cases	Actions	Communication requirement
Non-critical load change	Inform the MGCC about the change	Communication required
Critical load change	Refuse to be switched on/off	Not needed

The critical load change in Table 3.1 indicates the load step which exceeds the system possible operating limit, and hence switch-on or -off is not allowed. The non-critical load change is the load step change which can be sustained by the MG. After receiving a non-critical load change information, the MGCC performs calculations as will be described in section 5.4. It then sends out a delay request to the LC to hold the switch signal for a duration t_{set} and notifies the BB controller of the possible load change. The BB controller then gives a control command to the CG LC that requires the CG to react in advance to this potential load change for a defined operating time t_{total}. When the delay request runs out, the switch signal will be executed. After the total time that the BB control is in charge, the BB control signal will be stopped. The blue dotted line shows the communication path for LSP and BB controller to receive and send signals. The green solid line represents the communication of the MGCC to gather data from LCs and determine set points and control actions.

The work process of the control method in the centralized architecture is illustrated in Figure 3.4. As can be seen, when a load switch-on or -off button is pressed, the LC forwards this switch signal to the MGCC. The MGCC checks whether the load change signal is delivered by the load LC. If yes, it performs calculations based on the given information of the load change and starts a time counter; otherwise, it does nothing. As long as the time is within the defined preset time, LSP should hold the switch signal. The BB controller checks whether the load will rise or drop and commands the CG to increase or decrease active power with its full rate for a time period which is referred to
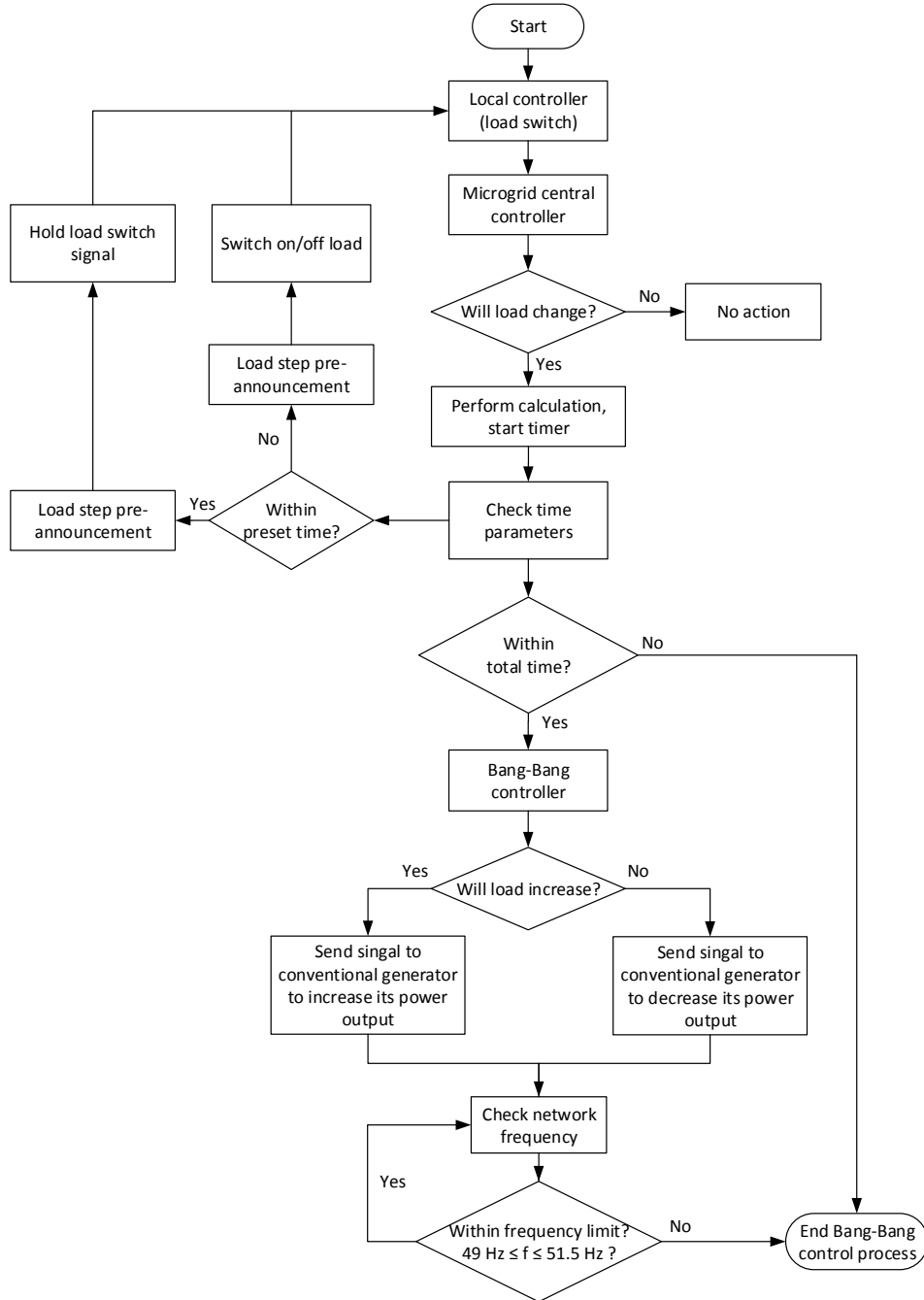
Figure 3.4: Work process of LSP and BB controller in a fully centralized control architecture

as total time in the work process flow diagram.

3.2.2　Centralized Control with Less Communication

The MGCC is the key for normal operation of the MG in a fully centralized control architecture. LCs have only limited information about the connected DG and load and do not have any level of autonomy. Their actions rely on the instruction from the MGCC. This could lead to needs of extensive communication and computation.

LCs can be predefined with more detailed information to take over some control actions from the MGCC, and thus, reduce the need of communication. For example, the load LC should determine what to do in case of a normal load change[4] fluctuation or a switch request from a critical load change[5]. The load LC receives predefined information updates from the MGCC regularly in a time range of 10 mins to 15 mins. Frequent information exchange between the LC and the MGCC can be avoided. The setting of the load LC is illustrated in Table 3.2.

Table 3.2: Predefined information in load local controller

Cases	Actions	Communication requirement
Normal load change	Continue operating under normal frequency control	Not needed
Large load change	Inform the MGCC about the change and wait for further instruction	Communication required
Critical load change	Refuse to be switched on/off	Not needed

The work process of the control method in the centralized architecture with less communication is shown in Figure 3.5. As shown in the work flow diagram, the load LC has some autonomy to determine to switch on/off a normal load, and afterwards, continue the MG operation following frequency control. It can also block a switch-on or -off action of a critical load in the MG under the predefined setting. In case that a load size belongs to the category of large load change[6], the LC will forward the switch signal and

---

[4]Load can be carried out without leading to any frequency instability issues
[5]Load exceeds the possible system steady state operating limits
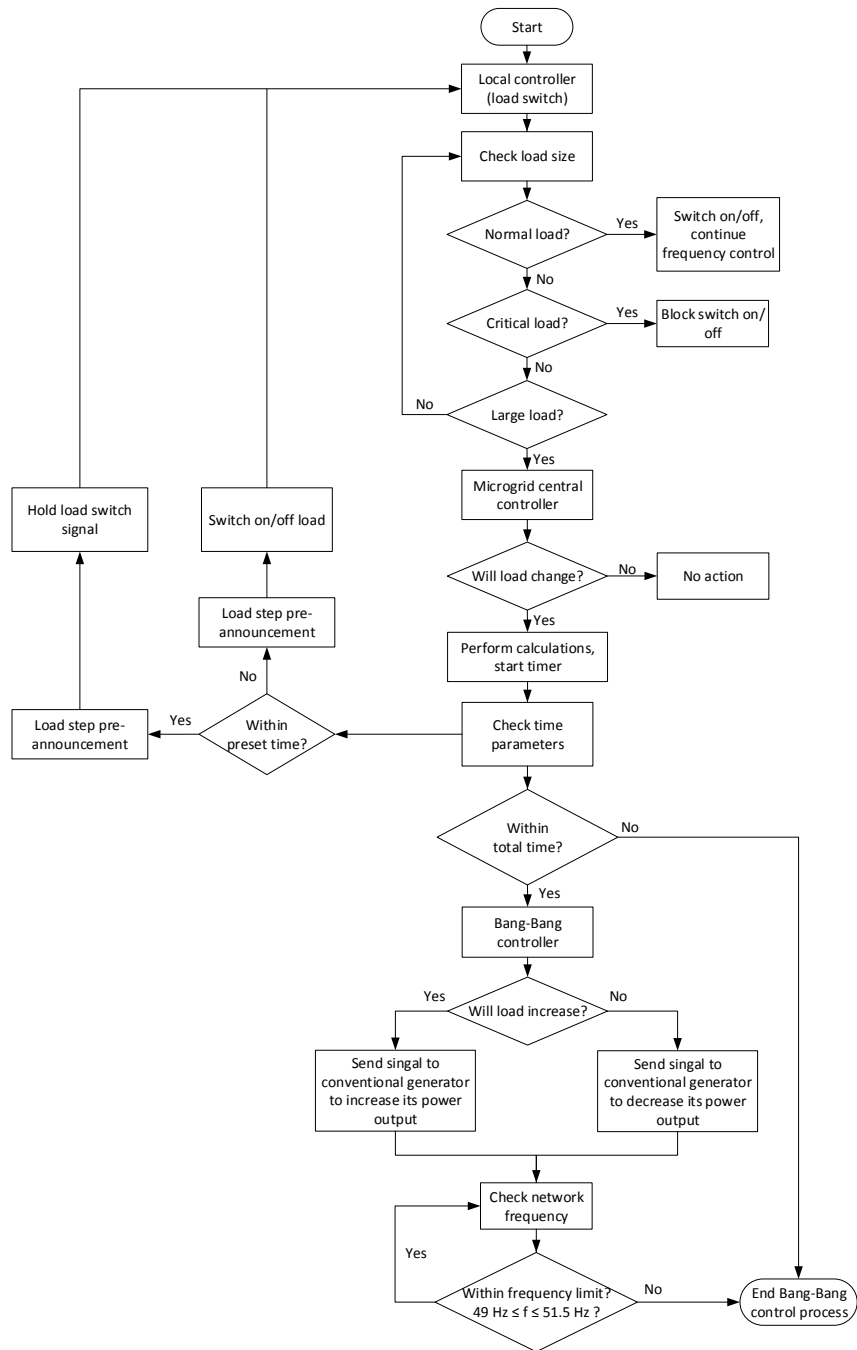[6]Load can be carried out, however cause big frequency deviations

Figure 3.5: Work process of the control method in a more decentralized control architecture

wait for further control instruction from the MGCC. Under a large load, LSP and BB controller work the same as described above.

3.2.3 Communication Requirements

The proposed method can be implemented either in a centralized or decentralized way. Different control architectures influence how much information is assigned to LCs and what an autonomy level LCs have. Depending on the control requirements, type and bandwidth of the communication as well as its cost should be taken care of.

In case of a centralized control architecture, LCs have only limited information, so they have to communicate with the MGCC regularly and get instruction from the MGCC. As stated in chapter 2, communication infrastructure plays a significant role in information exchange between MGCC and LCs in centralized control architecture. Due to the use of a centralized control architecture, reliable and fast communication between the MGCC and LCs is required. The standard IEC 61850, which was designed by the International Electrotechnical Commission (IEC) and is able to work over TCP/IP networks, can be applied to meet these requirements [16].

In a more decentralized control structure, LCs have enough predefined information about the load change so that they can make decisions by themselves to control local elements like load and DG. Communication need between MGCC and LCs can be reduced considerably and information congestion in communication network can be avoided. The reliability of the proposed control method can also be improved, since it does not strongly depend on the communication system as in the centralized way.

Chapter 4

Methodical Simulation

4.1   Overview of the Simulation Model

In order to understand frequency dynamic behavior in case of power imbalance and study the effects of the designed control method in islanded Microgrid (MG) systems, an islanded MG model with generators and load is needed. For the sake of simplicity, only two generators, one rotating machine and one inverter coupled renewable energy resource, are included. A simulation model of an islanded MG, which consists of a conventional generator (CG), a photovoltaic (PV) system and lumped load, is built up in the Matlab Simulink environment. The nominal frequency of the islanded MG is assumed to be 50 Hz as defined for continental Europe in [35].

The schematic block diagram of the islanded MG system is shown in Figure 4.1. The swing equation (2.15) described in section 2.2 is used as the fundament for the MG model to show a realistic frequency response under power deviation. Primary control is applied in the local controller (LC) of the CG with set points of active power and frequency, and thus, no communication requirement with other elements is needed. Secondary control is achieved via the microgrid central controller (MGCC) to adjust the active power set point of the CG. The Bang-Bang (BB) control signal is only sent from the MGCC to the CG LC to dispatch the active power output of the CG. For the PV generator, a frequency-dependent active power characteristic is set up following the VDE-AR-N 4105 standard [40] locally, which does not require any communication with other units. Load is assumed to be constant and has no dependency on frequency in the simulation model as is normally the case of small islanded grids [42]. The load LC communicates with the MGCC to allow load step pre-announcement (LSP) to act in case of load change. The communication paths between the MGCC and the LCs are presented in Figure 3.3 in

chapter 3. The islanded MG simulation model will be described in detail separately in
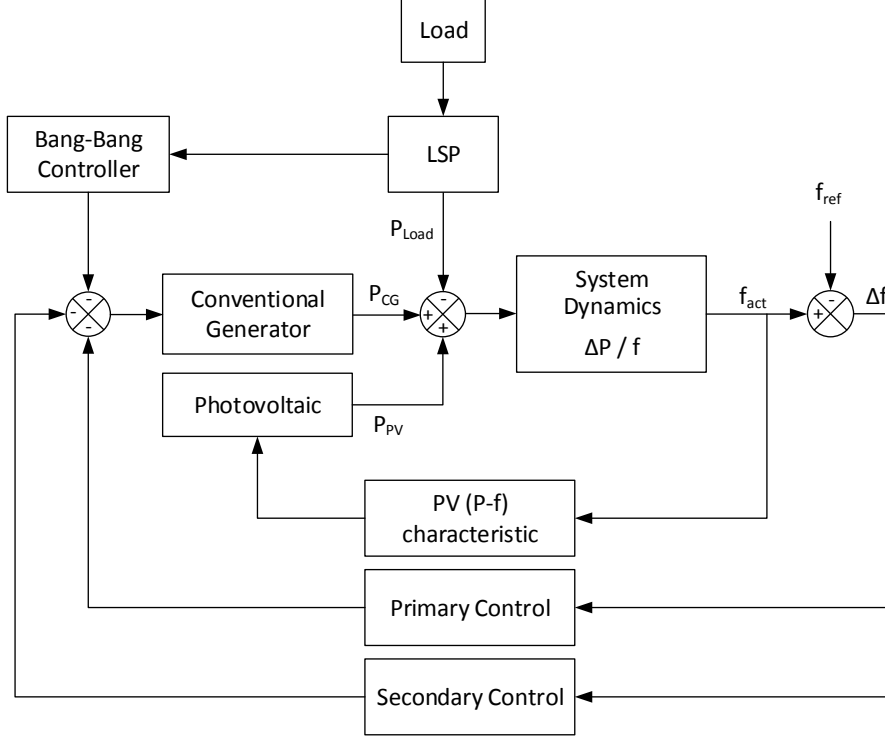the following sections in this chapter.

Figure 4.1: Schematic block diagram of islanded microgrid [7]

4.1.1   Per Unit System

The simulated MG model is set under per unit (p.u.) base. Per unit is commonly
used in the power system analysis field, because the quantities in power systems can be
normalized and calculations simplified. Per unit indicates system quantities expressed
in international system of units (SI) as fractions of a defined base value given also in the
SI units [31, p. 33], that is,

$$X_{act} \text{ (p.u.)} = \frac{X_{act} \text{ } (SI)}{X_{base} \text{ } (SI)} \tag{4.1}$$

---

[7]P_{CG}: the active power output of the conventional generator; P_{PV}: the active power output
of the PV system; P_{Load}: the active power demand of the load; ΔP: the active power deviation;
f_{act}: the current frequency; f_{ref}: the frequency set point; Δf: the frequency deviation

where X_{act} (SI) is the actual system quantity and X_{base} (SI) is the chosen base value of that quantity. A well-chosen per unit system can minimize calculation effort. The base values are normally chosen so that main variables, like frequency and voltage, are one per unit under rated conditions [31, p. 33]. For example, nominal frequency is chosen as the frequency base value (f_{base} (SI)) in the islanded MG. When system frequency is at the nominal value, frequency presented in per unit base equals 1 p.u.

4.1.2 Total Size of Islanded Microgrid

The total size of the islanded MG is defined by the maximum load demand (P_{n-L}) that can be served in the MG. This refers to P_n in equation (2.15). The rated power of the CG and PV are represented by P_{n-CG} and P_{n-PV} respectively. Hence the maximum load demand of the MG is given as:

$$P_{n-L} = P_{n-CG} + P_{n-PV} \tag{4.2}$$

The maximum load demand P_{n-L} in the SI units is chosen as the base value of active power generated or consumed in the simulated islanded MG. When load reaches its maximum value P_{n-L}, load demand in the MG equals 1 p.u. The rated power of the installed CG and PV in per unit base (p_{n-CG} and p_{n-PV})[8] are expressed as:

$$p_{n-CG} = \frac{P_{n-CG}}{P_{n-L}} \tag{4.3}$$

$$p_{n-PV} = \frac{P_{n-PV}}{P_{n-L}} \tag{4.4}$$

Shares of CG and PV (s_{CG} and s_{PV}) in the islanded MG can be calculated based on the rated power of the CG (P_{n-CG}), the rated power of the PV (P_{n-PV}) and the maximum load demand (P_{n-L}) accordingly:

$$s_{CG} = \frac{P_{n-CG}}{P_{n-L}} \tag{4.5}$$

$$s_{PV} = \frac{P_{n-PV}}{P_{n-L}} \tag{4.6}$$

---

[8]Lower case letters are used to represent the same quantities in per unit base

Because only two generators are simulated in the islanded MG to supply load, knowing either share of PV generation or share of CG in the MG, the other one can be obtained. Based on equations (4.2), (4.5) and (4.6), the shares' relation is given as:

$$s_{CG} + s_{PV} = 100\% \tag{4.7}$$

4.1.3   Starting Time Constant

In the simulation model, the CG represents a directly coupled rotating generator and the PV generator is connected to the MG via an inverter. This means that the CG with rotating mass has an inertia, whereas the PV provides no inertia to the MG. Therefore, the CG needs a certain time ($T_{CG} > 0$) to reach the synchronous speed from standstill while the PV generator does not. Since the CG and PV have different values of starting time constants, the islanded MG system starting time constant (T_{MG}) is calculated according to equation (2.11) as:

$$T_{MG} = \frac{T_{CG} \times P_{n-CG} + T_{PV} \times P_{n-PV}}{P_{n-L}} \tag{4.8}$$

where T_{CG} and T_{PV} represent the starting time constants of the CG and PV, respectively. By substituting the right sides of equations (4.5) and (4.6) into equation (4.8), it results as following:

$$T_{MG} = T_{CG} \times s_{CG} + T_{PV} \times s_{PV} \tag{4.9}$$

As the PV has no inertia without additional control scheme, its starting time constant (T_{PV}) is equal to 0. Thus, the starting time constant of the islanded MG (T_{MG}) can be simplified and obtained as:

$$T_{MG} = T_{CG} \times s_{CG} \tag{4.10}$$

With a change in the share of the CG (s_{CG}), the system starting time constant of the simulated islanded MG (T_{MG}) changes proportionally if the starting time constant of the CG (T_{CG}) is assumed constant.

4.2   Conventional Generation

As mentioned above, the term CG refers to the generation with rotating mass, which can convert mechanical energy into electrical energy. CG, such as steam turbine generators,

diesel generators and gas turbine generators, is widely used in power systems to provide energy supply. Modeling of CG plays an important role in the study of frequency control and stability. The dynamics of the CG provides the initial response in the first moment following a grid disturbance [43] as will be further described in section 5.4.1.

There are many turbine models developed for studies related to frequency stability and control in power systems [42–45]. Some of these models and a CG model used in this islanded MG frequency control study will be presented in this section.

4.2.1   Power and Frequency Regulation of Generators

Generators' mechanical torque can be controlled by turbine governors via different control modes, such as speed, power and droop control, as shown in Figure 4.2, and thus, their active power output is adjusted accordingly [37, p. 237-239].
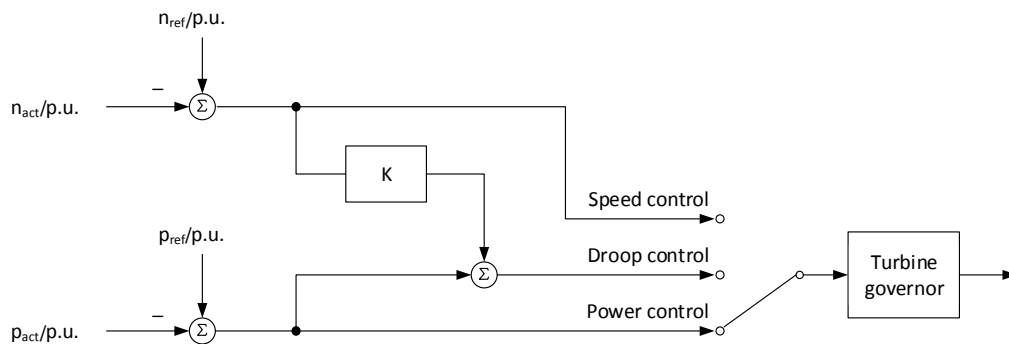

Figure 4.2: Possible power and frequency control modes of generators [37]

As can be seen, the measured actual speed of rotation of the rotor (n_{act}) of the synchronous generator, which participates in speed control, is compared with its reference value (n_{ref}) in case of speed control mode. If the actual speed of rotation is smaller than its set point, the mechanical torque of the turbine should be increased, and vice versa. This control mode is used particularly in islanded networks with single large generators, which regulate system frequency alone. If more than one generator with speed control operate jointly in a grid, they should have the exactly same speed control setting. Otherwise those generators participating in speed control try to correct the speed deviation by following their own settings and interfere with each other [36, p. 587-589]. In case of a delay or mistake in speed measurement, unique operation point is not even possible. For synchronous generators, whose mechanical torque is controlled by power control, the measured actual values of active power (p_{act}) are compared with the desired values (p_{ref}). If the active power set point is greater than the measured value, the positive

power deviation is forwarded to the turbine governor, which increases the mechanical torque. The mechanical torque is reduced correspondingly in case of a negative power deviation. For small generators and those that do not participate in frequency regulation of the network, power control is normally implemented [37, p. 237-239].

In a grid with multiple generators participating in speed control, droop control as stated in section 2.3.1 should be applied. Droop control allows different generators to find a common operating point after a frequency deviation caused by load change [36, p. 591].

4.2.2   Steam Turbine Generator

Steam turbine generators use pressurized high-temperature steam to generate mechanical energy, which is then converted into electrical energy. They are classified in two types, tandem and cross compound. All sections are on the same shaft with a single generator in a tandem compound steam turbine system, while two shafts exist in a cross compound steam turbine system and each of them is connected to a generator [33]. Models, such as TGOV1, IEEESO and IEEEG1, were developed as presented in [43–45]. Steam turbine models include speed-governors and turbine systems. Speed-governors can regulate the rotational speed of turbines to protect the turbines from over-speeding and trips the turbines in case of a critical condition [46]. The turbine systems allow steam turbine generators to adjust their active power output corresponding to load changes. A block diagram of a general speed-governor model is shown in Figure 4.3 [44].
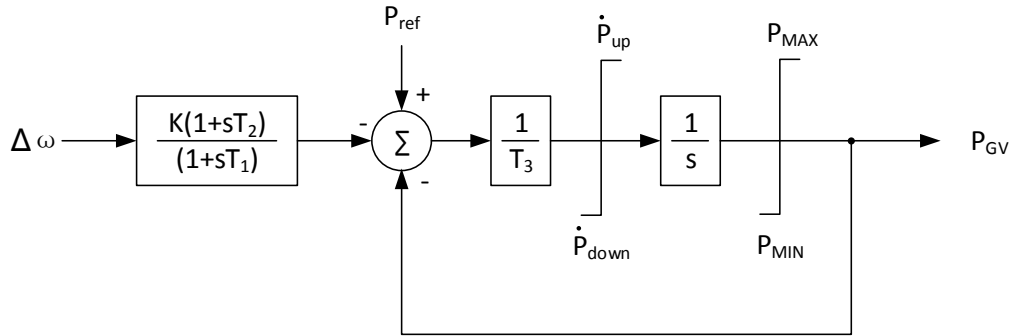

Figure 4.3: General model of speed-governor of steam turbine generator [44]

Droop control is utilized in this speed-governor model. Gain K is the reciprocal of the droop of the governor. T_1, T_2 and T_3 are time constants of the speed-governor. P_{ref} is the initial power set point of the steam turbine. P_{GV} is the total power of initial power and increments caused by speed deviation at the valve outlet depending on time lag T_3 [44]. The speed-governor of a steam turbine generator senses speed (or frequency)

Table 4.1: Parameters of speed-governor [45]

Parameter	Description	Range	Unit
K	Total effective speed-governing system gain (1/droop)	1 to 100	p.u.
T_1	Controller lag compensation	0.001 to 50	s
T_2	Controller lead compensation	0 to 100	s
T_3	Valve position time constant (servomotor mechanism)	0.01 to 5	s
$\dot{P}_{up}$	Limits of rate of change of power imposed by control valve rate limits	0.01 to 2	p.u./s
$\dot{P}_{down}$		-2 to -0.01	p.u./s
P_{MAX}	Maximum power limit imposed by valve or gate control	0.5 to 1.2	p.u.
P_{MIN}	Minimum power limit imposed by valve or gate control	0 to 0.4	p.u.

change to adjust the valve's position that influences the steam flow into the turbine. The speed-governor provides a steady-state power output setting for the turbine [34]. The speed of the valve motion is constrained by $\dot{P}_{up}$ and $\dot{P}_{down}$. Besides, the valve position is limited by P_{MAX} and P_{MIN}. A detailed information about parameters used in the block diagram is presented in Table 4.1.
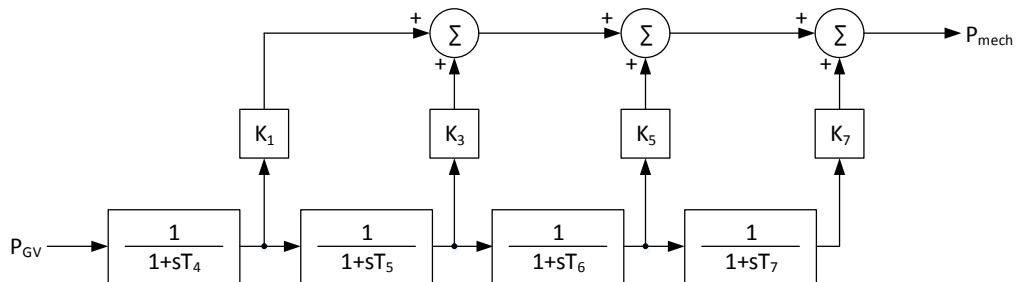

Figure 4.4: General model of steam turbine system [45]

Steam turbine systems often comprise high-pressure, intermediate-pressure and low-pressure turbines. A first-order element is usually used to model the delay between different parts of the steam turbine. The time delay gets bigger as a re-heater is installed [33]. An example of a turbine system including double reheat systems is shown in Figure

4.4. T_4, T_5, T_6, and T_7 are the time constants of the turbine system, which represent delays caused by the steam chest, two re-heaters and crossover piping, respectively. The gains K_1, K_3, K_5 and K_7 are the portions of the total power developed at various turbine stages. The sum of K_1, K_3, K_5 and K_7 is often equal to 1 [45]. The choices of these parameters can be found in [43, 45]

4.2.3   Diesel Generator

Diesel generators can convert chemical energy to mechanical energy and then electrical. They are often used to supply electricity on small or medium size islands due to their high efficiency and reliability. A diesel generator consists of three parts, speed governor, valve actuator and diesel engine [42]. A schematic diagram of a widely used diesel generator model created according to [47] is illustrated in Figure 4.5.
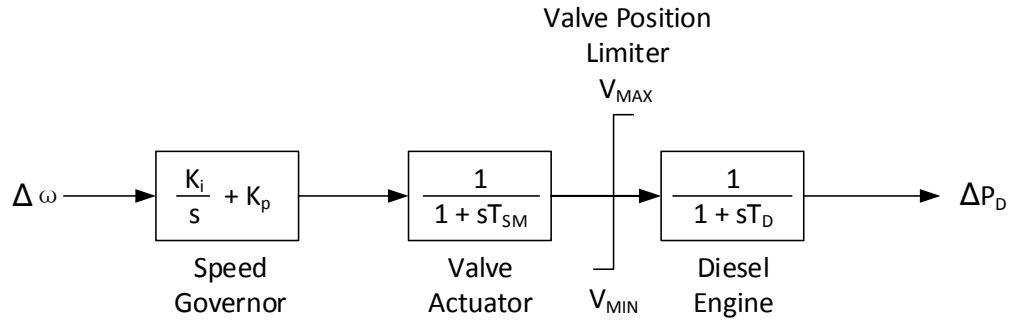

Figure 4.5: Schematic diagram of diesel generator

The input signal of the model is the speed or frequency deviation and the output is the active power change of the diesel generator. The speed control is used in the turbine governor. The speed governor implements droop and integral control, in which K_p and K_i are the proportional and integral gain. The amplified and integrated signal of the speed deviation, which is produced by the speed governor to control the valve position, can only reach a new steady state when the speed deviation equals zero due to the integral controller [36, p. 587]. In the diesel generator model, first-order lag elements represent the valve actuator servomechanism and the diesel engine. Their time constants are T_{SM} and T_D, respectively. The values of the parameters can be found in [47].

4.2.4   Simulated Conventional Generator Model

Power systems have a nature of non-linearity and time-variability [34]. It is difficult to provide an exact specification of model performance requirements for all possible systems

and study conditions [43]. In order to achieve a certain frequency response of the MG system and frequency control analysis in case of load changes, low-order elements are utilized. The simulated CG model that is created in Matlab Simulink based on the IEEEG1 model is illustrated in Figure 4.6. For a better overview, a schematic diagram of the simulated CG model is given in Figure 4.7. Settings and description of parameters of the CG model are presented in Table 4.2.
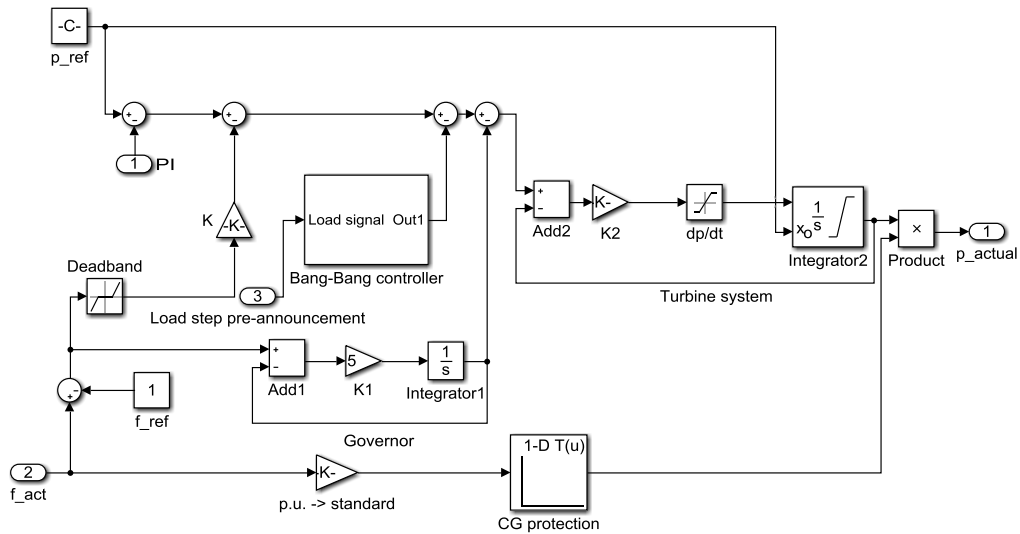

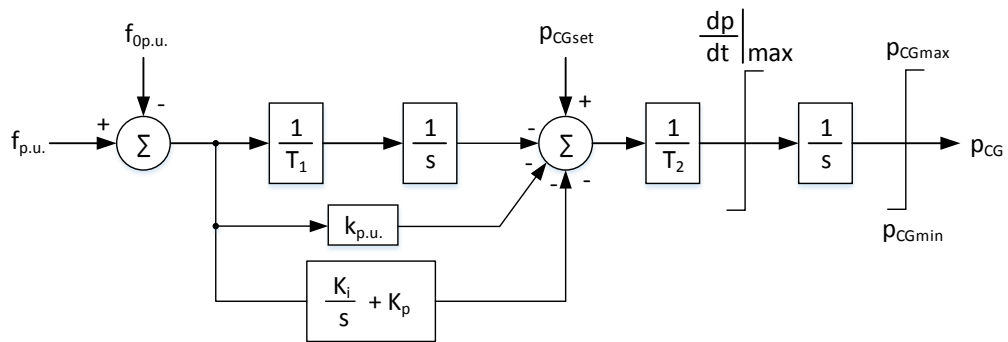Figure 4.6: Simulated model of conventional generation

Figure 4.7: A schematic diagram of CG model

As can be seen in Figure 4.6 and 4.7, simple first-order lag elements are applied for the main control valve motion and turbine system of the CG, with time constants $0.2\,\mathrm{s}$ and $0.1\,\mathrm{s}$ as indicated in [44]. According to the measurements of a diesel generator, which

Table 4.2: Parameters of CG model

Parameter	Description	Value	Unit
p_{CGset}	Power set point of CG in per unit base	50% p_{n-CG}	p.u.
p_{CG}	Actual power output of CG in per unit base	Variable	p.u.
$f_{p.u.}$	Actual system frequency in per unit base	Variable	p.u.
$f_{0p.u.}$	Frequency set point in per unit base	1	p.u.
T_1	Time constant of governor	0.2	s
T_2	Time constant of turbine system	0.1	s
$\frac{dp}{dt}\big|_{max}$	Limits of rate of change of power imposed by control valve rate limits	s_{CG}	p.u./s
		$-s_{CG}$	p.u./s
p_{CGmax}	Maximum power limit imposed by valve or gate control	p_{n-CG}	p.u.
p_{CGmin}	Minimum power limit imposed by valve or gate control	0	p.u.
$k_{p.u.}$	Primary frequency control droop in per unit system on the base of P_{n-L}	$25 \times s_{CG}$	-
K_p	Proportional gain of PI control	1	p.u.
K_i	Integral gain of PI control	0.2	p.u.

had a capacity of 620 kVA, in the "SORGLOS" project[9] [48], the rate limits of change of power imposed by control valve rate limits of the CG, which are represented by $\frac{dP}{dt}\big|_{max}$, were -100% and 100% of its rated power (P_{n-CG}) per one second, respectively. This means,

$$\frac{dP}{dt}\bigg|_{max} = \begin{cases} 100\% \times \dfrac{P_{n-CG}}{1\,\mathrm{s}} & \text{, for power increase,} \\[4mm] -100\% \times \dfrac{P_{n-CG}}{1\,\mathrm{s}} & \text{, for power decrease.} \end{cases} \tag{4.11}$$

---

[9]SORGLOS: Smarte Robuste Regenerativ Gespeiste Blackout-feste Netzabschnitte. It is a project funded by the Austrian Klima- und Energiesfonds (KLIEN) and led by the Institute of Energy System and Electrical Drives, TU Wien

Converting equation (4.11) into per unit base by dividing through the base values P_{n-L} leads to

$$\left.\frac{dp}{dt}\right|_{max} = \begin{cases} 100\% \times \dfrac{P_{n-CG}}{P_{n-L} \times 1\,\text{s}} & \text{, for power increase,} \\ \\ -100\% \times \dfrac{P_{n-CG}}{P_{n-L} \times 1\,\text{s}} & \text{, for power decrease.} \end{cases} \tag{4.12}$$

By substituting the right side of equation (4.5) into equation (4.12), the rate limit of change of power of the CG in per unit base is then expressed as

$$\left.\frac{dp}{dt}\right|_{max} = \begin{cases} \dfrac{s_{CG}}{1\,\text{s}} & \text{, for power increase,} \\ \\ -\dfrac{s_{CG}}{1\,\text{s}} & \text{, for power decrease.} \end{cases} \tag{4.13}$$

As share of CG (s_{CG}) is between 0 and 1, the value of $\left.\frac{dp}{dt}\right|_{max}$ is within the acceptable setting range as presented in Table 4.1. Therefore, equation (4.13) is considered to be reasonable to represent the rate limits of change of power of the CG. The power limits imposed by valve or gate control of the CG (p_{CGmax} and p_{CGmin}) are included in the integrator 2 to avoid wind-up, which can cause unnecessary overshoot and oscillations. Since the CG is the only controllable unit in both directions at nominal frequency in the islanded MG, frequency control and the proposed control method are implemented in the CG. The primary control has a 4% droop setting ($k = 25$ on machine base) with a $\pm 0.0004\,\text{p.u.}$ ($\pm 20\,\text{mHz}$) deadband. Within the deadband, very small frequency deviations should not activate the primary control. When the frequency deviation exceeds the deadband, the primary control responds to the deviation within a few seconds. Converting the droop setting into per unit system on the base of the maximum load demand P_{n-L} according to equation (2.16) results in

$$k_{p.u.} = -\frac{p - p_0}{f_{p.u.} - f_{0_{p.u.}}} = -\frac{\dfrac{P - P_0}{P_{n-CG}} \times \dfrac{P_{n-CG}}{P_{n-L}}}{\dfrac{f - f_0}{f_n}} = k \times s_{CG} = 25 \times s_{CG}$$

In order to eliminate the steady state frequency error of the primary control, the secondary control loop uses a proportional-integral controller. As discussed in section 2.3.2, a large proportional term may have a detrimental effect on the system stability and the integral term must be limited in order to react immediately in case of large changes. A typical value of proportional gain is between 0% and 50% and the integral time constant

is normally between 50 s and 200 s [35]. Based on the given range, the proportional and integral gains of secondary control applied in the MG are adjusted to be 1 and 0.2, respectively. With these settings, the secondary control takes approximately 6 to 7 minutes to bring back the frequency to its nominal value if reserve capacity is sufficient. LSP and BB controller are added into the feedback loop of the CG model. Activation time duration of LSP and BB controller are t_{set} and t_{total}, which can be further optimized for different incidents.

Except for the control system described above, protection schemes are also included to avoid damage to the CG under emergency conditions. Over-frequency or under-frequency issues can result in too fast or too low rotational speed of turbines, which decreases the turbines' lifespan or directly damages them. Thus, under-frequency protection (UFP) and over-frequency protection (OFP) are necessary for the CG. The settings of UFP and OFP of the CG are those values also used in grid-connected mode, e.g. 47.5 Hz for UFP and 52 Hz for OFP [49]. When frequency is between 47.5 Hz and 52 Hz, the CG operates following frequency control and provides active power that is demanded by loads. As long as the MG frequency is above 52 Hz or below 47.5 Hz, the CG should be tripped. UFP and OFP are configured in the look-up table in Figure 4.6.

4.3   Photovoltaic Generation

Regarding the grid instability issues that can be brought by increasing amount of PV generation, specific technical standards for the grid connection, which differ from country to country, are established [50]. The German regulations for PV operation are described, discussed and implemented in this thesis.

4.3.1   VDE 0126-1-1 Standard

In May 2005, the DIN VDE 0126-1-1 industry standard has been introduced to provide regulations for integrated PV generation in distribution networks [51]. This standard regulated all PV generation in the grid against unacceptable frequencies, and thus, the threat of unwanted islands could be mitigated. The regulation of infeed active power of PV depending on the system frequency is illustrated in Figure 4.8.

As shown in Figure 4.8, the allowable frequency operating range for PV generation was defined between 47.5 Hz and 50.2 Hz. When frequency is within the limits, integrated PV generation feeds 100% of its currently available active power into the grid. PV generation should disconnect automatically once the frequency is below 47.5 Hz or above 50.2 Hz. It is only possible to reconnect to the grid, when the frequency is and has been within the allowable operating range for at least 30 s. The actual active power infeed of a PV
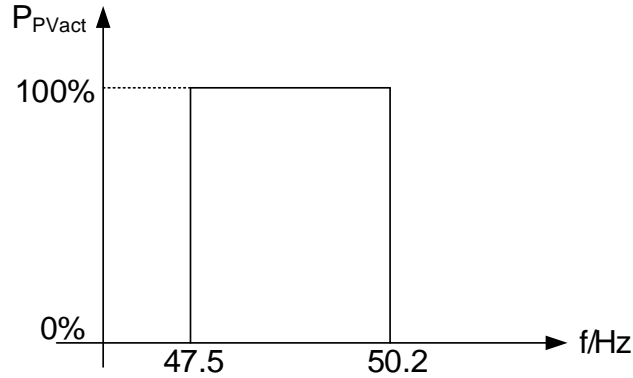
Figure 4.8: VDE 0126-1-1 frequency-dependent active power (P-f) characteristic curve [10]

generator based on the P-f characteristic defined by the VDE 0126-1-1 standard can be expressed as:

$$P_{PV} = \begin{cases} 100\% \times P_{PVact} & , 47.5\,\text{Hz} \leq f \leq 50.2\,\text{Hz}, \\ 0 & , f < 47.5\,\text{Hz or } f > 50.2\,\text{Hz}. \end{cases} \tag{4.14}$$

VDE 0126-1-1 standard prevents unintentional islanding by disconnecting PV generation in the grid once frequency exceeds 50.2 Hz. In traditional power systems, frequency deviation above 0.2 Hz is unlikely to happen under normal operations, however, it is possible to happen under unexpected big disturbances because of oversupply of electrical power in the grid [52]. For islanded MGs, frequency changes fast due to their low inertia when there is a mismatch between power supply and demand, thus frequency deviation above 0.2 Hz can easily appear.

Installed capacity of PV generation in Germany already reached around 41.3 GWp until 2016 [14]. If such a large amount of PV generation would suddenly disconnect from the overall grid at 50.2 Hz, this could lead to a significant decrease of the system frequency, and thus cause load shedding actions; on the other side, if lots of PV generation simultaneously connects to the grid, frequency would increase substantially, which could result in disconnection of other generating units or even cause a black-out. Except for the mentioned problems that can occur, there could be another stability issue - frequency swing - caused by disconnection and reconnection of PV generation at 50.2 Hz. These issues regarding frequency stability are known as "50.2 Hz problem" [12].

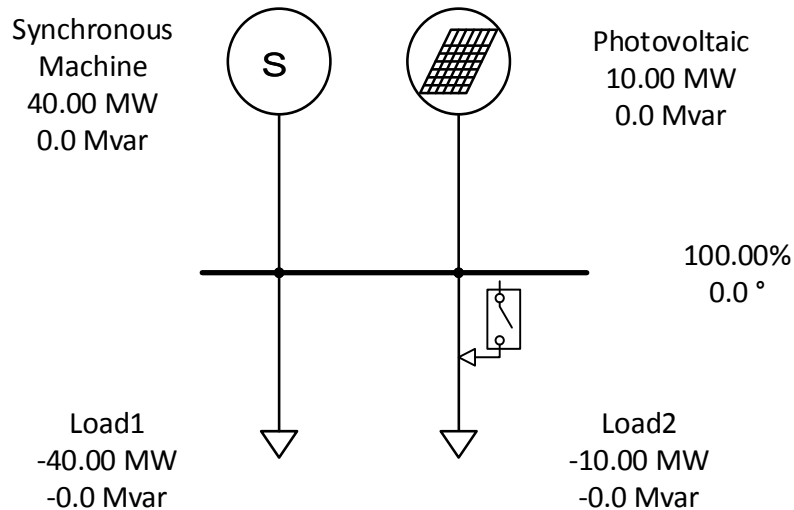[10] P_{PVact}: currently available active power of photovoltaic generator

Example

Figure 4.9: A test microgrid

A MG test case, including a synchronous generator, a PV generator and two loads, is presented in Figure 4.9 in order to understand the impact of applying the VDE 0126-1-1 standard. The synchronous generator utilizes a speed controller "TGOV1" [43] to adjust its active power output depending on system frequency and the PV generator is regulated following the VDE 0126-1-1 standard. The test MG has a balance between power production of 40 MW from the synchronous generator and 10 MW from the connected PV generator and power consumption of 50 MW total load initially. The initial frequency of the test MG is 50 Hz. When $t = 1$ s, the switch connected with the 10 MW load is switched off. Frequency response on this event in the test MG, including frequency swing caused by repeated PV reconnection, is illustrated in Figure 4.10.

As can be seen, when 10 MW of load is disconnected at $t = 1$ s, MG's frequency starts to increase because power generation is greater than load demand. When frequency reaches 50.2 Hz, the 10 MW PV generation is disconnected from the MG according to the VDE 0126-1-1 standard. MG's frequency is then decreased and stabilized by frequency control of the synchronous generator after disconnection of the PV generator. If MG's frequency is stable between 47.5 Hz and 50.2 Hz for at least 30 s, the disconnected PV generation starts to reconnect to the MG. However, this leads to the disconnect of PV generation from the grid again because the frequency exceeds 50.2 Hz. Thus, PV generation disconnects and reconnects repeatedly, which causes frequency oscillation.
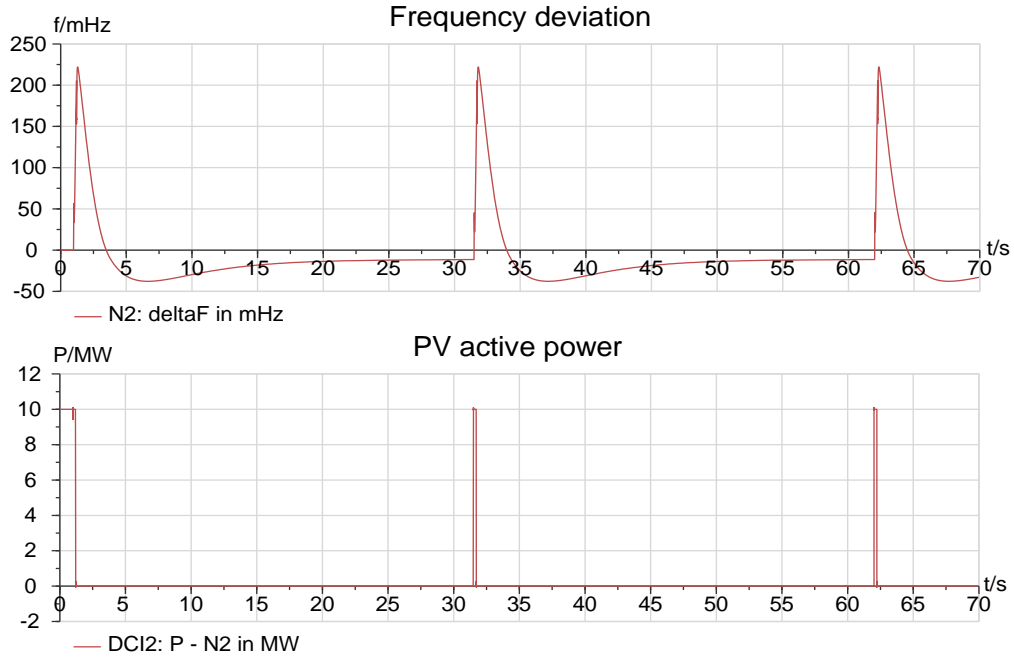
Figure 4.10: Frequency swing caused by repeated disconnection and reconnection of PV generation

4.3.2   VDE-AR-N 4105 Standard

With concern of the instability that may happen due to the VDE 0126-1-1 standard, an updated German VDE-AR-N 4105 standard has been implemented since 2011 [40]. It provides guidance for PVs in medium and low voltage networks to respond smoothly to frequency deviations when the system frequency exceeds certain limits [12, 52]. Instead of sudden disconnection of PV generation at $50.2\,\mathrm{Hz}$ according to the VDE 0126-1-1 standard, it provides a frequency-dependent active power control once frequency is above $50.2\,\mathrm{Hz}$. The frequency-dependent active power infeed (P-f) characteristic curve of PV generation is presented in Figure 4.11.

According to the VDE-AR-N 4105 guide, the PV frequency-dependent active power infeed characteristic is defined as following:

- when grid frequency is between $47.5\,\mathrm{Hz}$ and $50.2\,\mathrm{Hz}$, PV generation feeds 100% of its currently available active power (P_{PVact}) into the grid;

- when frequency is between $50.2\,\mathrm{Hz}$ and $51.5\,\mathrm{Hz}$, the active power infeed of PV generation should be reduced by 40% per $1\,\mathrm{Hz}$;
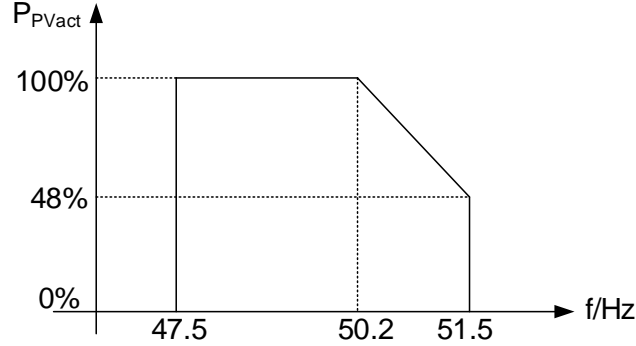
Figure 4.11: VDE-AR-N 4105 PV frequency-dependent active power
infeed characteristic curve [40]

- PV generation should disconnect from the grid when frequency is below $47.5\,\text{Hz}$ or above $51.5\,\text{Hz}$ to avoid unwanted islands;

- after a disconnection, PV reconnection is allowed if the system frequency is between $47.5\,\text{Hz}$ and $50.05\,\text{Hz}$ for at least $60\,\text{s}$;

- the increase of active power infeed of PV generation after the reconnection should not exceed 10% of its maximum active power per minute.

The formula of P-f characteristic defined by the VDE-AR-N 4105 standard is given as:

$$P_{PV} = \begin{cases} 100\% \times P_{PVact} & , 47.5\,\text{Hz} \leq f \leq 50.2\,\text{Hz}, \\ P_{PVact} \times (1 - \dfrac{40\%}{\text{Hz}} \times \Delta f_{PV}) & , 50.2\,\text{Hz} < f \leq 51.5\,\text{Hz}, \\ 0 & , f < 47.5\,\text{Hz} \text{ or } f > 51.5\,\text{Hz}. \end{cases} \tag{4.15}$$

where

$$\Delta f_{PV} = f - 50.2\,\text{Hz} \tag{4.16}$$

The same example of the MG, in which frequency swing occurs due to the repeated disconnection and reconnection of the PV generation, as shown in Figure 4.9 is used to present the frequency behavior after applying the VDE-AR-N 4105 standard. The grid frequency behavior is improved as shown in Figure 4.12.

MG's frequency starts to increase, when $10\,\text{MW}$ of load is disconnected from the MG at $1\,\text{s}$. In comparison to the sudden PV disconnection happening at $50.2\,\text{Hz}$ in the MG
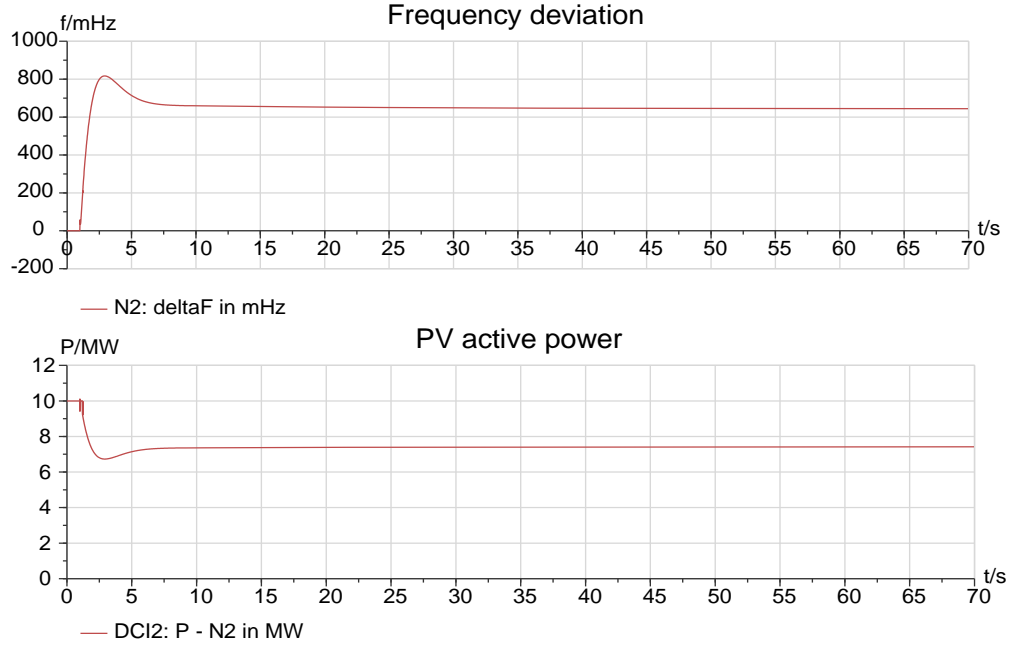
Figure 4.12: Improved frequency behavior in test islanded microgrid by applying VDE-AR-N 4105

test case, in which the VDE 0126-1-1 standard is applied for the PV generation, the active power infeed of PV generation shown in Figure 4.12 starts to decline smoothly by implementing the defined P-f characteristic curve of the VDE-AR-N 4105 standard in the PV generator when frequency is above 50.2 Hz. It only gets disconnected from the grid if frequency exceeds 51.5 Hz. Hence the grid avoids such a sudden cutoff of PV generation at 50.2 Hz, and afterward the system frequency is stabilized by frequency control of the synchronous generator and the frequency-dependent active power regulation of the PV generator.

4.3.3 Simulated Photovoltaic Generator Model

The VDE-AR-N 4105 standard is applied in the PV generation model in the simulated islanded MG because of the improvement of frequency stability as described in section 4.3.2. The detailed simulation model of the PV generation is presented in Figure 4.13. Figure 4.14 shows the schematic diagram of the PV model.

In Figure 4.14, p_{PVact} is the power set point of the PV generation, which indicates how much active power is currently available, e.g. in the simulation $p_{PVact} = 50\% \ p_{n-PV}$
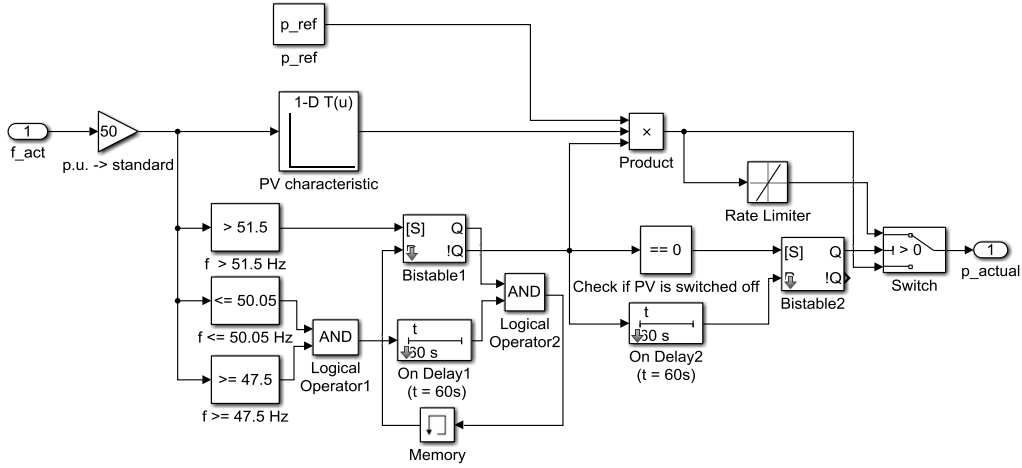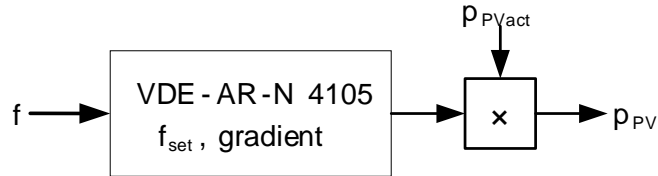
Figure 4.13: PV simulation model

Figure 4.14: A schematic diagram of PV model

means that 50% of the rated active power of the PV is available. The actual active power infeed of the PV is represented by p_{PV}. As can be seen in Figure 4.13, the VDE-AR-N 4105 standard is built into the look-up table and implemented as a factor to be multiplied with the available active power p_{PVact} to obtain the actual power infeed of the PV. The logic blocks and rate limiter in Figure 4.13 define the reconnection conditions and maximum reconnection rate of the PV generation in the simulated model. The

Table 4.3: Parameters of PV generation model

Parameter	Description	Value	Unit
p_{PVact}	Power set point of PV generation (available active power of PV)	50% p_{n-PV}	p.u.
p_{PV}	Actual active power infeed of PV generation	Variable	p.u.
f	Actual system frequency	Variable	Hz

maximum reconnection rate is 10% of the rated active power p_{n-PV} per one minute according to the VDE-AR-N 4105 standard. The description of parameters of the PV generation is illustrated in Table 4.3.

4.4 Load

Step response can be used to measure the dynamic behavior of a system, since a step signal as input is generally considered to be a severe dynamic requirement for the system. As long as the dynamic behavior of the system under a step signal input can fulfill the expectation, the dynamic behavior would also be satisfactory under slower kinds of input. Therefore, load change is presented by a step signal in the islanded MG model. As shown in Figure 3.3, loads are connected with an intelligent switch and controlled by its LC that can communicate with the LSP in the MGCC. When the load switch-on or -off signal is given by the LC, the MGCC performs calculations and may activate the BB control to support system frequency under active power disturbances.

In order to reduce extensive communication and computation in the MG control system as described in section 3.2.2, the load step change can be classified into three categories, including normal, large and critical load change. These types of load steps are classified by frequency nadir during dynamic responses after power deviations that occur in the MG.

4.4.1 Normal Load Step

Normal load step indicates those small load changes that can be carried out without leading to any frequency instability issues. Frequency disturbances caused by this kind of load step can be covered by frequency control directly. Under a change of normal load step, LSP and the BB controller are not required.

Frequency deviation caused by the normal load step change in the islanded MG should stay within a certain limit, e.g. the frequency drop nadir would not exceed 49 Hz in case of load increase or the frequency increase nadir would not exceed 51.5 Hz in case of load decrease. In this way, neither load shedding action would be triggered because of under-frequency nor PV generation would be disconnected due to over-frequency.

4.4.2 Large Load Step

Large load steps, unlike normal load steps, are defined as load changes that can cause severe frequency disturbance after occurring in the MG. The severe frequency disturbance means that the frequency nadir is below 49 Hz or above 51.5 Hz. Under a large

load step in the MG, system frequency would not be stable any more without emergency control, like activating load shedding if frequency is below 49 Hz or cutting off the PV generation if frequency is above 51.5 Hz.

Despite causing severe frequency disturbance, large load steps may be conducted in the MG with frequency control and, in addition, the proposed control method. By introducing LSP and BB control into the control system is possible to limit the peak frequency, and hence the dynamic behavior and frequency stability of the MG system can be improved.

4.4.3   Critical Load Step

Critical load steps refer to the load changes which exceed the possible system steady state operating limits. Therefore, no matter which kinds of control schemes are applied, the load cannot be executed in the islanded MG under a stable condition. In case of a change request from a critical load step, the control system refuses its switch action directly. A more detailed description of the possible steady state operating limits will be given in chapter 5.

Table 4.4 summarizes the three kinds of load steps.

Table 4.4: Definition of different sizes of load

Cases	Definition
Normal load step	Load step causes frequency deviations in the range of $49\,\text{Hz} \leq f \leq 51.5\,\text{Hz}$
Large load step	Load step causes frequency deviations $f < 49\,\text{Hz}$, or $f > 51.5\,\text{Hz}$
Critical load step	Load step is greater than steady state limit that is defined by the system settings

Chapter 5

Analytical Contemplation

In this chapter, the possible operating range, steady state limit and dynamic operating limit of the islanded microgrid (MG) are presented.

5.1 Definition of Parameters in Islanded MG

Steady state limit, which is determined by the settings of the MG, defines the maximum and minimum possible operating points of the islanded MG. Dynamic operating limit represents a system's ability to return to its steady state after a change occurs. Dynamic operating limit is within steady state limit. In order to analyze the steady state and dynamic operating limits of the MG system, some essential parameters are introduced in this section.

As mentioned in chapter 4, the maximum load demand (P_{n-L}) indicates the total size of the islanded MG. The rated power of the conventional generation (CG) and the photovoltaic (PV) generation are P_{n-CG} and P_{n-PV}. The maximum active power of the CG is P_{CGmax}, which is the same as the CG rated power (P_{n-CG}) in the study. Its minimum power is P_{CGmin}, which is assumed to be 0 in the simulation model. P_{CGset} indicates the set point of the active power of the CG at initial state. The dispatchable active power of the CG is between P_{CGset} and P_{CGmin} or between P_{CGset} and P_{CGmax}. The loading status of the CG (l_{CG}) is represented by the ratio of the CG's current active power generation (P_{CG}) to its rated power (P_{n-CG}), which is given as

$$l_{CG} = \frac{P_{CG}}{P_{n-CG}} \qquad (5.1)$$

P_{PVact} presents the currently available active power of the simulated PV model as described in section 4.3. Since the base value of active power is taken from the maximum load demand, defined parameters as mentioned above in per unit base vary depending on different shares of CG and PV, except for the maximum load demand P_{n-L}. These parameters decide the steady state limit of the MG as will be described in section 5.3. Two time parameters - preset time (t_{set}) and total time (t_{total}) - have been introduced in chapter 3. The preset time indicates the time delay period that LSP holds an individual load switch-on or -off signal. The total time represents the time duration that the BB controller is activated and changes the operating point of the CG to let it generate or reduce power as fast as possible after receiving a signal from LSP. These time parameters can be different depending on the settings of the islanded MG, e.g. system inertia constant and dynamics of the generators participating in primary control. Different settings of the time parameters influence the dynamic operating limit of the MG.

5.2   Possible Operating Points of the Islanded MG

In non-linear power systems, stability depends on type and magnitude of the input and their initial states [53, p. 181]. It is important to discuss about possible initial load that can be supplied by the islanded MG before analyzing the steady state limit. In this section, the possible operating points of initial load that can be handled by the MG are presented.

5.2.1   Possible Initial Load Under PV Fully Available

Possible initial load (P_{L-in}) implies the possible load states under initial steady conditions. In other words, it reflects possible steady state operating points of the islanded MG. It only depends on initial available active power of the CG and the PV generation, namely the CG and PV power set points (P_{CGset} and P_{PVact}), as well as the initial system frequency. The P-f characteristic curve according to the VDE-AR-N 4105 standard is implemented in the simulated PV as described in chapter 4. If the initial frequency is 50 Hz, the PV generation provides 100% of its currently available active power to load. Thus, the possible initial load can be formulated as following:

$$P_{L-in} = P_{CGset} + 100\% \times P_{PVact} \qquad (5.2)$$

If the possible initial load changes, the two parameters P_{CGset} and P_{PVact} should be adjusted depending on the share of CG and PV in the islanded MG. In the simulated

model, the maximum load demand P_{n-L} that can be supplied by the islanded MG is used as the base value for the whole system. Hence equation (5.2) can also be presented in per unit base by dividing through the base value P_{n-L},

$$p_{L-in} = p_{CGset} + 100\% \times p_{PVact} \tag{5.3}$$

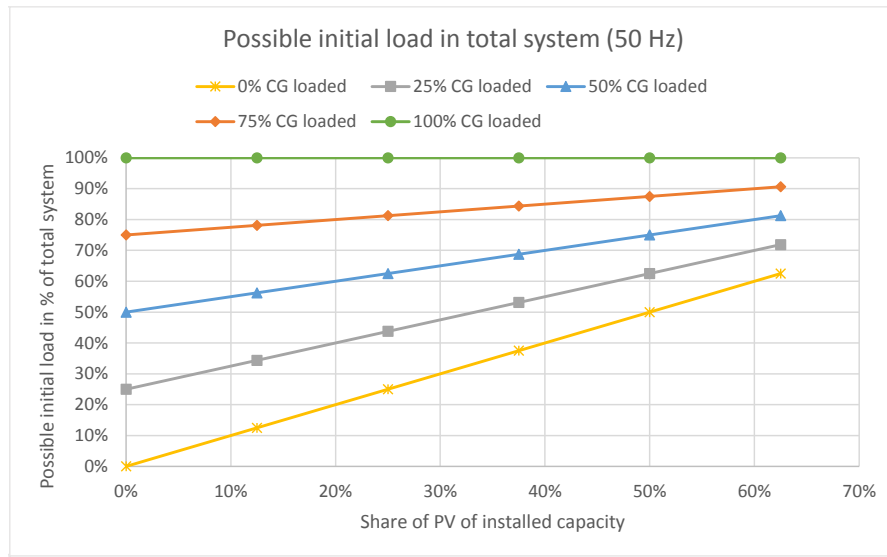The relation between the possible initial load and share of PV is shown in Figure 5.1.

Figure 5.1: Possible initial load in % of total system in the islanded MG when frequency at $50\,\mathrm{Hz}$ (PV fully available: $P_{PVact} = P_{n-PV}$)

For example, the maximum load demand P_{n-L} is assumed to be $40\,\mathrm{MW}$. If the share of CG and PV generation (s_{CG} and s_{PV}) are 50%, respectively, the rated power of them are $20\,\mathrm{MW}$ each. This means that both p_{n-CG} (or p_{CGmax}) and p_{n-PV} are $0.5\,\mathrm{p.u.}$ If the CG is 50% loaded initially, its power set point (p_{CGset}) is calculated following equation (5.1) as

$$p_{CGset} = l_{CG} \times p_{n-CG} = 50\% \times 0.5\,\mathrm{p.u.} = 0.25\,\mathrm{p.u.}$$

This means that the CG provides $10\,\mathrm{MW}$ active power to the load under the initial state. If the PV generation is fully available, then p_{PVact} should be equal to the PV rated power ($p_{n-PV} = 0.5\,\mathrm{p.u.}$). As mentioned above, the PV generation feeds 100% of its available $20\,\mathrm{MW}$ active power into the grid when frequency is $50\,\mathrm{Hz}$. Hence the

islanded MG is able to supply 30 MW (0.75 p.u.) load initially. Therefore, the possible initial load is 75% of the total system loading capacity as can be seen in Figure 5.1. Under the same conditions, in case that the CG is 100% loaded initially, the possible initial load would have to be 1 p.u. So the MG can supply 40 MW load, which is 100% of the total system size.

If the initial system frequency is not 50 Hz, the possible initial load that can be supplied by the MG can be different than described above due to the PV P-f characteristic curve presented in Figure 4.11. An extreme case occurs if initial frequency would be at 51.5 Hz. When the system frequency is 51.5 Hz, the PV generation would feed 48% of its currently available active power into the grid following the VDE-AR-N 4105 standard. Thus, the possible initial load that can be supplied is as following:

$$P_{L-in} = P_{CGset} + 48\% \times P_{PVact} \tag{5.4}$$

Converting equation (5.4) into per unit base leads to,

$$p_{L-in} = p_{CGset} + 48\% \times p_{PVact} \tag{5.5}$$

A detailed relation between the percentage of the possible initial load in the total system and share of PV, when the initial frequency is 51.5 Hz, is illustrated in Figure 5.2.
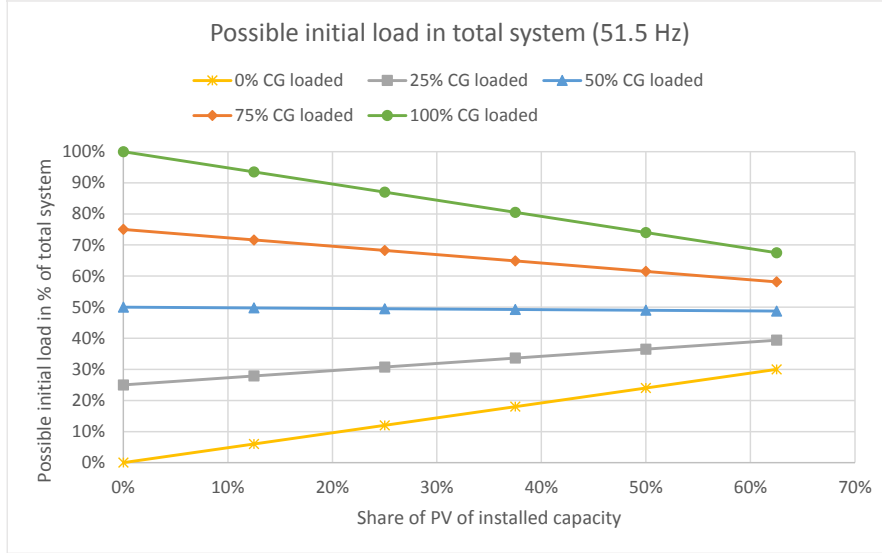

Figure 5.2: Possible initial load in % of total system in the islanded MG when frequency at 51.5 Hz (PV fully available: $P_{PVact} = P_{n-PV}$)

5.2.2 Possible Initial Load Under PV Partially Available

The simulated MG with partially available PV (i.e. 50% of its rated power) is given in this section to compare the size of the possible initial load under different circumstances. Except for a different set point of PV generation (P_{PVact}) which is half of the set point as described in section 5.2.1, the other parameters are the same as the islanded MG with fully available PV. The size of the possible initial load is smaller in the islanded MG with partially available PV than that with fully available PV, however, the possible initial load is calculated just like in case of fully available PV. The calculation of the operable initial load is as stated in equation (5.2) when system initial frequency is $50\,\mathrm{Hz}$ and as in equation (5.4) when initial frequency is $51.5\,\mathrm{Hz}$. A correlation between the possible operating points of the initial load and shares of PV under the conditions that PV is partially available and initial frequency is $50\,\mathrm{Hz}$ is presented in Figure 5.3.
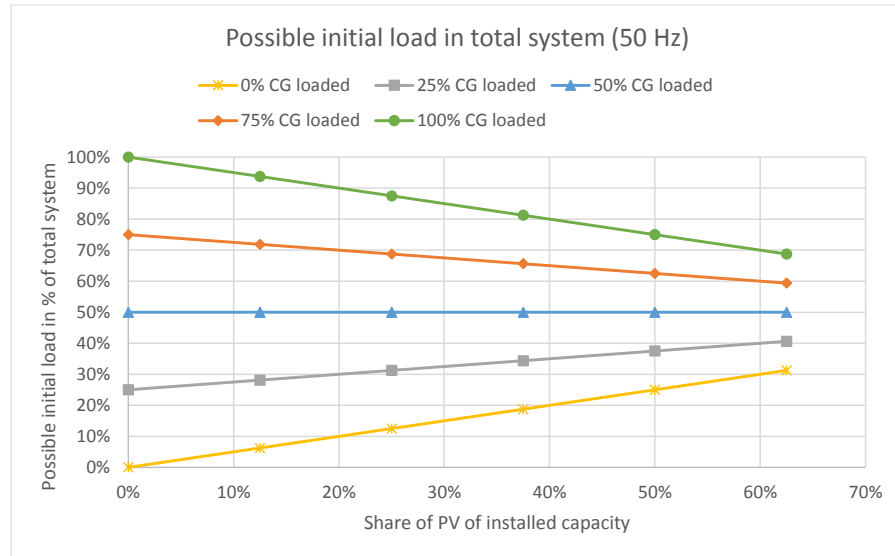

Figure 5.3: Possible initial load in % of the total system in the islanded MG when frequency at $50\,\mathrm{Hz}$ (PV partially available:
$$P_{PVact} = 50\% \ P_{n-PV})$$

As an example, the base value is the $40\,\mathrm{MW}$ maximum load demand just as for the MG with fully available PV. In case that both shares of CG and PV (s_{CG} and s_{PV}) are 50%, p_{n-CG} (or p_{CGmax}) and p_{n-PV} are equal to 0.5 p.u. When the CG is 50% loaded initially, meaning $p_{CGset} = 0.25$ p.u., it feeds $10\,\mathrm{MW}$ active power into the islanded MG. Meanwhile, as the PV generation is 50% partially available ($p_{PVact} = 0.25$ p.u.), the

PV generation can only provide 10 MW active power instead of its rated 20 MW active power into the MG when frequency is at 50 Hz. The islanded MG, therefore, is able to supply 20 MW load initially, which is 50% of the total system as shown in Figure 5.3. Under the same conditions, if the CG is 100% loaded initially, the possible initial load would be 0.75 p.u. So the MG can supply the 30 MW load, which is 75% of the total system size.

If the system frequency is 51.5 Hz initially, possible initial load operating points based on different shares of PV are presented in Figure 5.4.
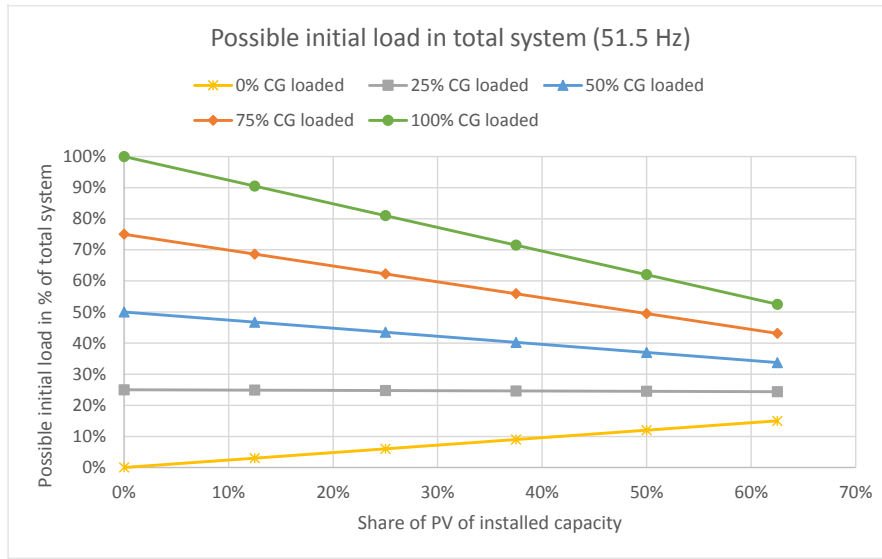

Figure 5.4: Possible initial load in % of the total system in the islanded MG when frequency at 51.5 Hz (PV partially available: $P_{PVact} = 50\% \ P_{n-PV}$)

5.3   Steady State Limit

The steady state limit indicates the maximum and minimum load limit that can be supplied by the islanded MG system.

5.3.1   Possible Steady State Operating Range

As mentioned in section 5.2, the possible initial load is closely related to the operating points of the CG and PV as well as the P-f characteristic curve of the PV generation.

The possible initial load is defined by the settings and parameters of the MG system itself, thus, it determines possible operating points, i.e. how much load can be supplied under different circumstances. By combining these operating points of the initial load when grid frequency is at nominal value and, in an extreme case, at $51.5\,\mathrm{Hz}$, an absolute operating range of possible load in the MG can be obtained. This operating range indicates the steady state operating limit of the MG.

Possible operating points of the MG are calculated taking into account the availability of PV generation as discussed in section 5.2. 50% partially available PV generation (this means $P_{PVact} = 50\% \, P_{n-PV}$) in the MG is chosen as the study case for the following discussion and simulation in the later sections in this chapter and chapter 6. The possible steady state operating range of the islanded MG with 50% partially available PV is presented in Figure 5.5.
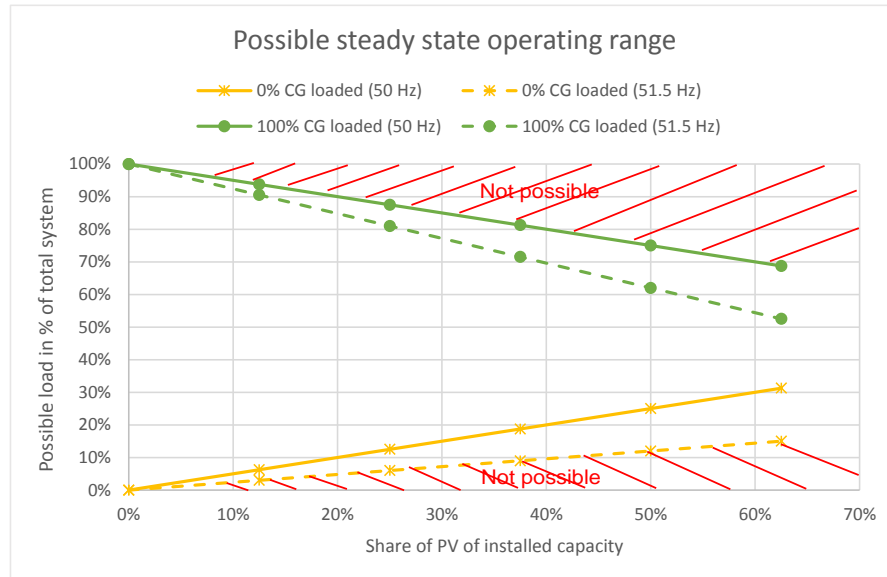

Figure 5.5: Possible steady state operating points of islanded MG with partially available PV

As can be seen, the possible steady state operating range shows the maximum and minimum load that can be handled by the MG. The upper limit of the possible steady state operating range is defined by the possible load when the CG generates its maximum power (P_{CGmax}) and the PV generator is able to feed 100% of its available active power (P_{PVact}) into the MG, namely, the CG is 100% loaded and frequency is at nominal value. The minimum load to be supplied by the MG system is related to the minimum active

power of the CG (P_{CGmin}) and the lowest steady state point along the P-f characteristic curve. Hence the lower possible steady state operating points are limited by the possible load when the CG is 0% loaded and the PV generation feeds in 48% of its currently available active power at 51.5 Hz. The possible steady state operating range, thus, can be formulated as:

$$
\begin{aligned}
P_{Lmax} &= P_{CGmax} + 100\% \times P_{PVact} \\
P_{Lmin} &= P_{CGmin} + 48\% \times P_{PVact}
\end{aligned}
\tag{5.6}
$$

where P_{Lmax} and P_{Lmin} are maximum and minimum load that can be handled by the islanded MG, respectively. The loads that are bigger than P_{Lmax} or smaller than P_{Lmin} cannot be allowed to be operated in the MG. The possible steady state operating range in per unit base is given as

$$
\begin{aligned}
p_{Lmax} &= p_{CGmax} + 100\% \times p_{PVact} \\
p_{Lmin} &= p_{CGmin} + 48\% \times p_{PVact}
\end{aligned}
\tag{5.7}
$$

5.3.2   Steady State Positive Load Change Limit

In this section steady state limits are investigated. For simplicity, any change (increase or decrease) is referred to as "step" compared to the initial condition.

Another way to present the steady state limit is to use load change limits, including steady state positive and negative load change limits. Steady state positive and negative load change limits represent the maximum possible positive and negative load change that can be realized from the initial load. Both of them depend on the initial state of the MG system, the CG operating points and the PV P-f characteristic curve. Since power mismatch due to the load change causes frequency disturbance, the size of possible load changes can be influenced. Steady state positive and negative load change limits, which define a baseline for the MG's dynamic operating limit as will be described in section 5.4 and chapter 6, are introduced under ideal circumstances by neglecting frequency instability problems that can be caused by the inability of the MG to reach a possible stable operating point due to dynamical limitations.

The steady state positive load change limit (P_{Lsmax}), which is related to the maximum load to be supplied in the MG, indicates how large a stepwise load increase can be tolerated by the MG. In case of load increase, increase of power generation is required in the MG. According to the swing equation (2.15) in chapter 2, load increase can cause the grid frequency to drop. A more detailed description about the system's dynamic behavior will be given in section 5.4. If the system frequency is assumed to be at nominal value

initially, the PV generation feeds 100% of its currently available active power (P_{PVact}) into the MG, and thus, cannot increase its active power infeed any further. This means that the steady state positive load change limit is only influenced by the amount of dispatchable active power of the CG. The dispatchable active power of the CG is calculated from its power set point (P_{CGset}) and the maximum active power (P_{CGmax}) that can be produced. Thus, the steady state positive load change limit is given as follows:

$$P_{Lsmax} \mid_{50\,\text{Hz}} = P_{CGmax} - P_{CGset} \tag{5.8}$$

To convert equation (5.8) into per unit base by dividing through P_{n-L} leads to,

$$p_{Lsmax} \mid_{50\,\text{Hz}} = p_{CGmax} - p_{CGset} \tag{5.9}$$

If the initial system frequency is $51.5\,\text{Hz}$, the PV generation provides 48% of its available active power to the grid. It then has the possibility to increase its infeed up to 100% of the available active power. Besides, the active power supplied by the CG is fully controllable and can be increased between P_{CGset} and P_{CGmax}. The steady state positive load change limit in case of non-nominal initial frequency can be formulated as:

$$P_{Lsmax} \mid_{51.5\,\text{Hz}} = P_{CGmax} - P_{CGset} + P_{PVact} \times (1 - 48\%) \tag{5.10}$$

Equation (5.10) is expressed in per unit base as follows,

$$p_{Lsmax} \mid_{51.5\,\text{Hz}} = p_{CGmax} - p_{CGset} + p_{PVact} \times (1 - 48\%) \tag{5.11}$$

Example

As an example, an islanded MG with 50% shares of installed capacity for the CG and PV is used here to explain the steady state positive load change limit. The maximum load demand P_{n-L} of $40\,\text{MW}$ defines the total size of the MG and is used as the base value. The MG can supply a $14.8\,\text{MW}$ load initially. Some assumed values of the test MG are given in Table 5.1.

The assumed values, including P_{n-CG}, P_{n-PV}, P_{L-in} and P_{PVact}, are converted into per unit system by dividing through the base value P_{n-L} as presented in Table 5.2.

Case 1: steady state positive load change limit in the MG under initial state of nominal frequency

According to Table 5.1 and 5.2, the rated power of the CG and PV in per unit base

Table 5.1: Assumed values of an test microgrid

Parameter	Description	Value
P_{n-L}	Maximum load demand in the MG, which is the base value of active power	40 MW
s_{CG}	Share of CG	50%
s_{PV}	Share of PV	50%
P_{n-CG}	Rated active power of CG	20 MW
P_{n-PV}	Rated active power of PV	20 MW
P_{L-in}	Initial load supplied by MG	14.8 MW
P_{PVact}	PV's currently available active power	10 MW

Table 5.2: Assumed values of test microgrid in per unit base

Parameter	Description	Value
p_{n-CG} or p_{CGmax}	Rated active power of CG in per unit base	0.5 p.u.
p_{n-PV}	Rated active power of PV in per unit base	0.5 p.u.
p_{L-in}	Initial load supplied by MG in per unit base	0.37 p.u.
p_{PVact}	PV's currently available active power in per unit base	0.25 p.u.

(p_{CGmax} and p_{n-PV}) are both 0.5 p.u. Besides, $p_{PVact} = 50\%\ p_{n-PV}$, which means that 50% of the rated power of the PV generator is assumed to be available currently. If a load of 0.37 p.u. is supposed to be supplied in the MG at nominal frequency initially, the power set point of the CG can be calculated according to equation (5.3) as

$$p_{CGset} = p_{L-in} - 100\% \times p_{PVact} = 0.37\,\text{p.u.} - 0.25\,\text{p.u.} = 0.12\,\text{p.u.}$$

Hence from equation (5.1), the loading status of the CG is given as

$$l_{CG} = \frac{p_{CGset}}{p_{CGmax}} = \frac{0.12\,\text{p.u.}}{0.5\,\text{p.u.}} = 24\%$$

This means that the CG is 24% loaded. The CG can increase its power generation from the set point ($p_{CGset} = 0.12$ p.u.) up to the rated power ($p_{CGmax} = 0.5$ p.u.), therefore, it allows a load increase of 0.38 p.u. Under the assumption of nominal frequency as the initial condition, the PV generator feeds in 100% of its currently available active power as described in section 4.3.2 and cannot contribute to balancing a load increase. Based on equation (4.15), the initial active power infeed of the PV (p_{PV-in}) is

$$p_{PV-in} = 100\% \times p_{PVact} = 0.25 \text{ p.u.}$$

The load (p_{Lmax}) that can be supplied by the MG at most is, thus, calculated following equation (5.7)

$$p_{Lmax} = p_{CGmax} + 100\% \times p_{PVact} = 0.5 \text{ p.u.} + 0.25 \text{ p.u.} = 0.75 \text{ p.u.}$$

Based on equation (5.9), the maximum possible positive load change ($p_{Lsmax}\ |_{50\,\text{Hz}}$) that can be realized is given as

$$p_{Lsmax}\ |_{50\,\text{Hz}} = p_{CGmax} - p_{CGset} = 0.5 \text{ p.u.} - 0.12 \text{ p.u.} = 0.38 \text{ p.u.}$$

Table 5.3 summarizes the calculated values of the test case under the initial conditions with nominal frequency.

Table 5.3: Summary of calculated values of test microgrid under initial conditions with nominal frequency based on given assumption

Parameter	Description	Value
p_{PV-in}	The initial active power infeed of PV in per unit base	0.25 p.u.
p_{CGset}	The initial set point of active power of CG in per unit base	0.12 p.u.
l_{CG}	The loading status of CG	24%
p_{Lmax}	The maximum load to be supplied by the MG in per unit base	0.75 p.u.
$p_{Lsmax}\ |_{50\,\text{Hz}}$	The steady state positive load change limit in per unit base	0.38 p.u.

Case 2: steady state positive load change limit in the MG under initial state of non-nominal frequency

The same assumed values from Table 5.1 and 5.2 are taken for the test MG under initial state of non-nominal frequency. If the initial frequency is $51.5\,\mathrm{Hz}$, only 48% of the currently available active power of the PV generator is fed into the MG according to equation (4.15)

$$
\begin{aligned}
p_{PV-in} &= p_{PVact} \times (1 - \frac{40\%}{\mathrm{Hz}} \times \Delta f_{PV}) \\
&= 0.25\,\mathrm{p.u.} \times [1 - \frac{40\%}{1\,\mathrm{Hz}} \times (51.5\,\mathrm{Hz} - 50.2\,\mathrm{Hz})] \\
&= 0.25\,\mathrm{p.u.} \times 48\% \\
&= 0.12\,\mathrm{p.u.}
\end{aligned}
$$

Following equation (5.5), more active power is required from the CG to supply the supposed $0.37\,\mathrm{p.u.}$ initial load in the MG if the initial frequency is $51.5\,\mathrm{Hz}$, while the initial active power infeed of the PV generator (p_{PV-in}) is $0.12\,\mathrm{p.u.}$

$$
p_{CGset} = p_{L-in} - 48\% \times p_{PVact} = 0.37\,\mathrm{p.u.} - 0.12\,\mathrm{p.u.} = 0.25\,\mathrm{p.u.}
$$

Hence the loading status of the CG is calculated according to equation (5.1) as,

$$
l_{CG} = \frac{p_{CGset}}{p_{CGmax}} = \frac{0.25\,\mathrm{p.u.}}{0.5\,\mathrm{p.u.}} = 50\%
$$

which means that 50% of the total capacity of the CG is used initially. The CG can allow an increase of generation from the $0.25\,\mathrm{p.u.}$ power set point p_{CGset} to the rated power p_{CGmax} of $0.5\,\mathrm{p.u.}$ In addition, the power infeed of the PV generator is able to be changed from 48% to 100% of the currently available active power. In this case, according to equation (5.7), the maximum load can be supplied by the MG is given as

$$
p_{Lmax} = p_{CGmax} + 100\% \times p_{PVact} = 0.5\,\mathrm{p.u.} + 0.25\,\mathrm{p.u.} = 0.75\,\mathrm{p.u.}
$$

From equation (5.11),

$$
\begin{aligned}
p_{Lsmax} \mid_{51.5\,\mathrm{Hz}} &= p_{CGmax} - p_{CGset} + p_{PVact} \times (1 - 48\%) \\
&= 0.5\,\mathrm{p.u.} - 0.12\,\mathrm{p.u.} + 0.25\,\mathrm{p.u.} \times (1 - 48\%) \\
&= 0.38\,\mathrm{p.u.}
\end{aligned}
$$

meaning a maximum of $0.38\,\mathrm{p.u.}$ positive load change ($p_{Lsmax} \mid_{51.5\,\mathrm{Hz}}$) can be realized. Table 5.4 lists out all the parameters that are mentioned above in this test case under initial conditions with non-nominal frequency.

Table 5.4: Summary of calculated values of test microgrid under initial conditions with non-nominal frequency based on given assumption

Parameter	Description	Value
p_{PV-in}	The initial active power infeed of PV in per unit base	0.12 p.u.
p_{CGset}	The initial set point of active power of CG in per unit base	0.25 p.u.
l_{CG}	The loading status of CG	50%
p_{Lmax}	The maximum load to be supplied by the MG in per unit base	0.75 p.u.
$p_{Lsmax} \mid_{51.5\,\text{Hz}}$	The steady state positive load change limit in per unit base	0.38 p.u.

Figure 5.6 presents initial load, maximum load and possible positive load changes in the exemplary MG under different shares of PV based on the assumption of the total size of the MG being $P_{n-L} = 40\,\text{MW}$. In both case 1 and 2, in order to supply the same initial load, the power set point of the CG is adjusted depending on the different possible power infeeds of the PV under the initial conditions of 50 Hz and 51.5 Hz while the availability of the PV is assumed to be 50% of the rated power. Additionally, as discussed in section 5.3.1, the maximum load to be supplied by the MG can be defined following the installed capacity of the CG and PV and possible power infeed of the PV. The initial frequency determines the initial share of load between CG and PV but not the maximum load size, therefore, the maximum load that can be supplied by the MG in the study cases under both initial conditions of 50 Hz and 51.5 Hz is 0.75 p.u. as shown in Figure 5.6. The difference between initial load and maximum load represents the possible positive load change. In both cases, the maximum possible positive load changes that can be realized in the MG are 0.38 p.u.

The maximum possible positive load change of the test cases, shown in Figure 5.6, refers to the steady state positive load change limit of the MG. If initial load, shares of PV and CG are fixed in the MG, the steady state positive load change limits are independent from initial frequency. This is also valid for steady state negative load change limit as be will described in section 5.3.3. However, the frequency dynamic behavior of the MG when there is a power mismatch due to a load step is dependent on the initial frequency. Dynamic operating limits of a MG system are determined in a way that no violations of frequency are caused during the frequency response on a load change as will be discussed
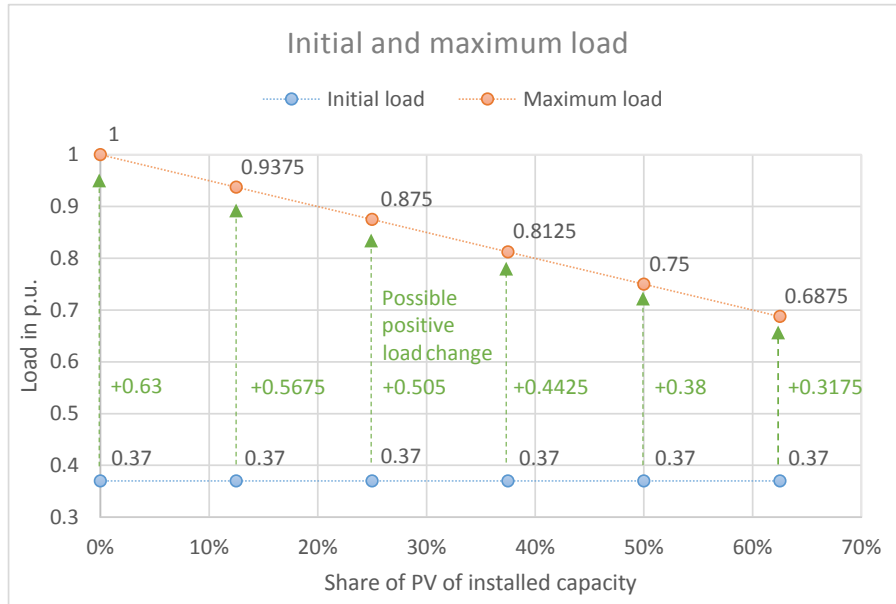
Figure 5.6: Initial load and maximum load in the test MG

in section 5.4 and chapter 6. Hence the dynamic operating limits of the MG can vary depending on different initial frequency conditions.

Figure 5.7 presents the steady state positive load change limits, including both initial frequency being 50 Hz and 51.5 Hz, of the islanded MG with fixed 50% partially available PV generation under different situations of shares of PV and CG loading. If the CG constantly generates a certain percentage of its rated power and the available active power of the PV generator to be fed into the MG is fixed, the initial load is different under nominal and 51.5 Hz initial frequency for non-zero share of PV. The difference in initial load is the reason for the increased possible positive load change of the MG under 51.5 Hz in comparison to nominal initial frequency. The steady state positive load change limits of test case 1 and 2 are presented by the squared point on the gray solid line[11] when the CG is 24% loaded at nominal frequency initially and the triangular point on the blue dashed line when 50% of the CG power is used at 51.5 Hz in the exemplary MG with a 50% share of PV in Figure 5.7.

---

[11] As the curve of 24% loading of the CG can be approximated by the 25% loading of the CG, for the sake of clarity, the gray lines are used to show the approximate steady state positive load change limit of the MG when CG is 24% loaded.
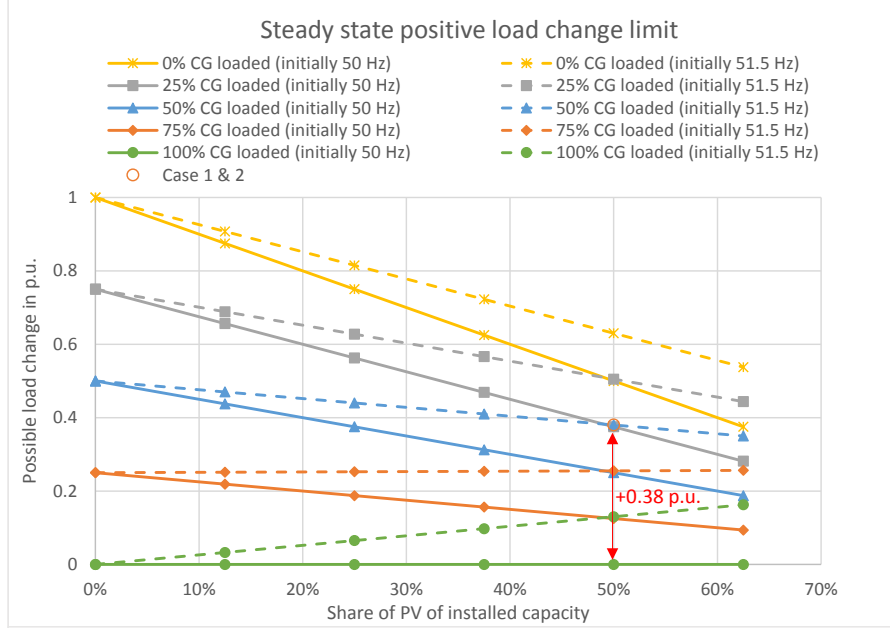
Figure 5.7: Steady state positive load change limit

5.3.3 Steady State Negative Load Change Limit

The steady state negative load change limit (P_{Lsmin}) is related to the MG minimum load operating points. It represents the maximum load decrease that is acceptable in the MG. Load decrease requires a power decrease from generation and results in a frequency rise at first according to the swing equation (2.15). The active power of the CG is fully controllable and can be decreased between the initial power set point (P_{CGset}) and minimum active power (P_{CGmin}). If the initial frequency is 50 Hz, the PV generation feeds 100% of its currently available active power (P_{PVact}) into the grid. The active power infeed of the PV generation would be constant at 100% of its currently available active power (P_{PVact}) if the frequency stays below 50.2 Hz; otherwise, it would decrease its active power infeed by 40% per 1 Hz and disconnect once frequency exceeds 51.5 Hz according to the VDE-AR-N 4105 standard [40]. The lowest active power steady point along the PV P-f curve is 48% of its available active power when frequency is 51.5 Hz. Hence the steady state negative load change limit is determined by the dispatchable active power of the CG and the changeable active power of the PV generation along its P-f characteristic curve. The steady state negative load change limit can be expressed as:

$$P_{Lsmin} \mid_{50\,\text{Hz}} = P_{CGmin} - P_{CGset} + P_{PVact} \times (48\% - 1) < 0 \qquad (5.12)$$

Negative values are used to represent load change decrease. As for the per unit system, equation (5.12) is given as,

$$p_{Lsmin} \mid_{50\,\text{Hz}} = p_{CGmin} - p_{CGset} + p_{PVact} \times (48\% - 1) < 0 \qquad (5.13)$$

If the initial system frequency is 51.5 Hz, above which the PV generator would be disconnected, the MG could only receive 48% of the PV's available active power. This is the lowest active power steady point along the PV P-f characteristic curve, so the active power infeed of the PV generation cannot be reduced even more. Only the CG in the islanded MG is able to decrease its power to react on a negative load change. The steady state negative load change limit then is calculated as:

$$P_{Lsmin} \mid_{51.5\,\text{Hz}} = P_{CGmin} - P_{CGset} < 0 \qquad (5.14)$$

Converting equation (5.14) into per unit base results in,

$$p_{Lsmin} \mid_{51.5\,\text{Hz}} = p_{CGmin} - p_{CGset} < 0 \qquad (5.15)$$

Example

The same MG test case with assumption as given in Table 5.1 and 5.2 in section 5.3.2 is used again to explain the steady state negative load change limit.

Case 3: steady state negative load change limit in the MG under initial state of nominal frequency

In order to supply the supposed 0.37 p.u. load at nominal frequency initially, the power set point of the CG (p_{CGset}) is calculated just as case 1 in section 5.3.2 based on equation (5.3), while p_{PVact} equals 0.25 p.u. Hence

$$p_{CGset} = p_{L-in} - 100\% \times p_{PVact} = 0.37\,\text{p.u.} - 0.25\,\text{p.u.} = 0.12\,\text{p.u.}$$

The CG has the potential to decrease its active power from the power set point ($p_{CGset} = 0.12\,\text{p.u.}$) to the minimum active power ($p_{CGmin} = 0$), namely a power decrease of 0.12 p.u. As regulated by the VDE-AR-N 4105 standard, the PV generator feeds 100% of its available active power into the MG if the initial frequency is at nominal value. From equation (4.15),

$$p_{PV-in} = 100\% \times p_{PVact} = 0.25\,\text{p.u.}$$

Hence the active power infeed of the PV generator can be reduced to 48% at most to contribute in case of a load decrease. In this case, the possible negative load change can be calculated following equation (5.13) as

$$
\begin{aligned}
p_{Lsmin} \mid_{50\,\text{Hz}} &= p_{CGmin} - p_{CGset} + p_{PVact} \times (48\% - 1) \\
&= 0 - 0.12\,\text{p.u.} + 0.25\,\text{p.u.} \times (48\% - 1) \\
&= -0.25\,\text{p.u.}
\end{aligned}
$$

According to equation (5.7), the minimum load (p_{Lmin}) that can be supplied by the MG is given as

$$
p_{Lmin} = p_{CGmin} + 48\% \times p_{PVact} = 0 + 48\% \times 0.25\,\text{p.u.} = 0.12\,\text{p.u.}
$$

Table 5.5 presents the calculated data of the test MG under initial conditions with nominal frequency based on the same assumption as in Table 5.1 and 5.2.

Table 5.5: Summary of calculated values of test microgrid under initial conditions with nominal frequency based on given assumption

Parameter	Description	Value
p_{PV-in}	The initial active power infeed of PV in per unit base	0.25 p.u.
p_{CGset}	The initial set point of active power of CG in per unit base	0.12 p.u.
l_{CG}	The loading status of CG	24%
p_{Lmin}	The minimum load to be supplied by the MG in per unit base	0.12 p.u.
$p_{Lsmin} \mid_{50\,\text{Hz}}$	The maximum negative load change in per unit base	−0.25 p.u.

Case 4: steady state negative load change limit in the MG under initial state of non-nominal frequency

If the MG runs at 51.5 Hz initially, the PV provides an infeed of 48% of its currently available active power to the grid based on equation (4.15), meaning

$$
p_{PV-in} = 48\% p_{PVact} = 48\% \times 0.25\,\text{p.u.} = 0.12\,\text{p.u.}
$$

According to equation (5.5), to supply the supposed 0.37 p.u. load at 51.5 Hz while p_{PVact} = 0.25 p.u., p_{CGset} results in

$$p_{CGset} = p_{L-in} - 48\% \times p_{PVact} = 0.37 \,\text{p.u.} - 48\% \times 0.25 \,\text{p.u.} = 0.25 \,\text{p.u.}$$

Since 48% of the available power to be fed into the MG at 51.5 Hz is the lowest steady state point along the P-f characteristic curve defined by the VDE-AR-N 4105 standard, further decrease is not possible and can cause unwanted repeated PV reconnection issues as will be discussed in section 6.4.3. Based on equation (5.15),

$$p_{Lsmin} \mid_{51.5 \,\text{Hz}} = p_{CGmin} - p_{CGset} = 0 - 0.25 \,\text{p.u.} = -0.25 \,\text{p.u.}$$

Therefore, a maximum load change of -0.25 p.u. can be realized as a result of the dispatchable active power of the CG between its set point 0.25 p.u. and the minimum power. The minimum load of this MG test case is calculated following equation (5.7),

$$p_{Lmin} = p_{CGmin} + 48\% \times p_{PVact} = 0 + 48\% \times 0.25 \,\text{p.u.} = 0.12 \,\text{p.u.}$$

The calculated values of the test case under the initial conditions with non-nominal frequency are presented in Table 5.6.

Table 5.6: Summary of calculated values of test microgrid under initial conditions with non-nominal frequency based on given assumption

Parameter	Description	Value
p_{PV-in}	The initial active power infeed of PV in per unit base	0.12 p.u.
p_{CGset}	The initial set point of active power of CG in per unit base	0.25 p.u.
l_{CG}	The loading status of CG	50%
p_{Lmin}	The minimum load to be supplied by the MG in per unit base	0.12 p.u.
$p_{Lsmin} \mid_{51.5 \,\text{Hz}}$	The maximum negative load change in per unit base	-0.25 p.u.

Initial and minimum load of the exemplary MG under different shares of PV are presented in Figure 5.8. The active power generation of the CG (p_{CGset}) can be adapted to the 0.37 p.u. initial load in case of the different infeed power of the PV under the

initial conditions of 50 Hz and 51.5 Hz while 50% of the rated power the PV is assumed to be available. Besides, the minimum load to be supplied by the MG in the study cases with the assumption given in Table 5.1 and 5.2 is 0.12 p.u. under both initial conditions of 50 Hz and 51.5 Hz. The difference between the initial load and the minimum load indicates the possible negative load change. The possible negative load change limits of the both test cases are −0.25 p.u. as marked in Figure 5.8.
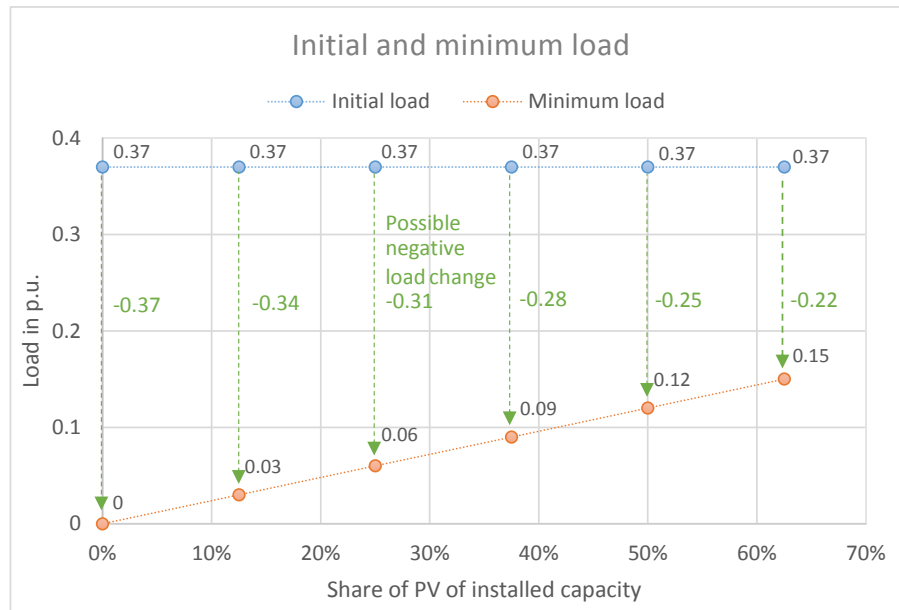

Figure 5.8: Initial load and minimum load

The steady state negative load change limits of the simulated islanded MG with fixed 50% partially available PV generation under different situations of shares of PV and CG loading are shown in Figure 5.9. The values of the steady state negative load change limits on the left-hand side y-axis are negative because they represent load decrease. If both the CG loading and the available active power of the PV generator are fixed, the initial load is different for the MG with non-zero share of PV under nominal and 51.5 Hz initial frequency. The difference in initial load results in the decreased possible negative load change of the MG under 51.5 Hz in comparison to nominal initial frequency. The marked possible negative load change of the test cases in Figure 5.8 refers to the steady state negative load change limit of the MG. In the MG with a 50% share of PV, it is presented by the squared point on the gray solid line when the CG is 24% loaded at nominal frequency initially and the triangular point on the blue dashed line when 50% of the CG power is used at 51.5 Hz in Figure 5.9.
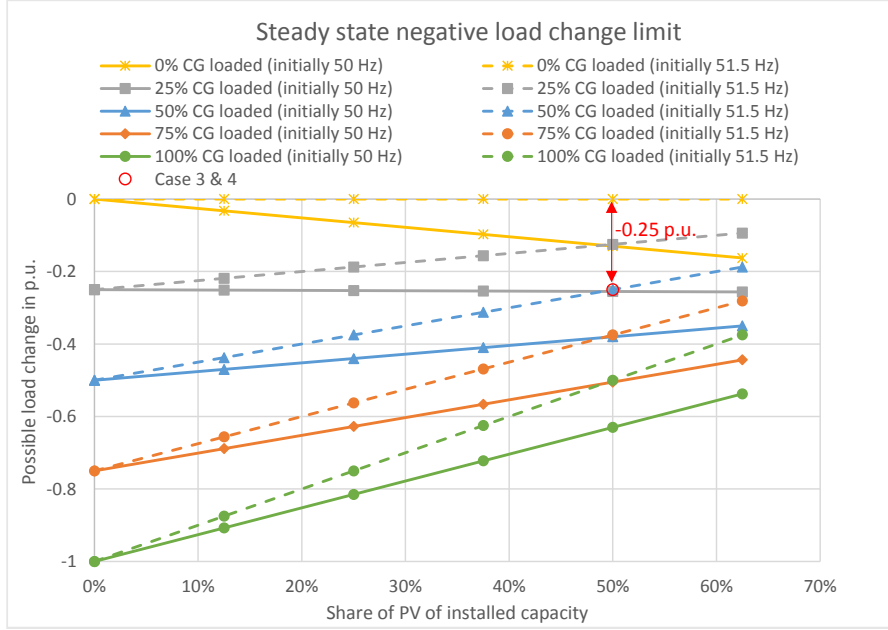
Figure 5.9: Steady state negative load change limit

5.3.4   Steady State Load Change Limit

Steady state positive and negative load change limits together represent steady state load change limit. The steady state load change limit introduced in section 5.3.2 and section 5.3.3 only includes cases that the MG frequency will be stable at final states and does not take into account which value the final stable frequency has. If there is sufficient secondary control reserve, the final frequency can be regulated back to 50 Hz. In that case, the steady state load change limit can be different from the ones described in section 5.3.2 and section 5.3.3. This is because the change of the PV power infeed that contributes to the load increase or decrease can vary if the final frequency is not the same as the nominal value. Thus, following the PV P-f characteristic curve, the PV generation provides 100% of its available active power when the MG frequency is stabilized at 50 Hz after a load change. The initial frequency could be between 47.5 Hz and 51.5 Hz, in which the PV infeed power varies within the range of 48% to 100% of its available active power.

In case of a load increase, the system would requires a higher power generation. The active power produced by the CG is fully dispatchable from its set point (P_{CGset}) to the maximum active power (P_{CGmax}). To satisfy a maximum load demand, the CG

increases its active power to the maximum and the PV feeds in 100% of its available active power. The steady state positive load change limit is the same as in equations (5.8) and (5.10) when initial system frequency is 50 Hz and 51.5 Hz, respectively. The steady state positive load change limit would not be influenced by the secondary control to restore the nominal frequency.

If load decreases, the generators in the MG need to reduce their power infeed correspondingly. Considering that if the system frequency should be brought back to 50 Hz after secondary control, the final active power infeed of PV should be 100% of its current possible active power. The CG is fully controllable between its power set point and minimum active power (P_{CGmin}). If the initial frequency is 50 Hz, the steady state negative load change limit only depends on the dispatchable active power of the CG. It is calculated following equation (5.14). In case of a situation at a non-nominal initial frequency, the PV generator may provide less than 100% of its actual active power. The dispatchable active power of the CG includes the share that is needed to be reduced because of load decrease and the one that can be decreased to ensure that the PV generator is able to feed in 100% of its active power eventually. The steady state negative load change limit under this condition is given as:

$$P_{Lsmin} = (P_{CGmin} - P_{CGset}) + P_{PVact} \times (1 - 48\%) \qquad (5.16)$$

For the interest of this study, the steady state load change limit in the SI units is represented by equations (5.8) and (5.12) under the condition of the initial nominal frequency, and equations (5.9) and (5.13) are valid for the steady state load change limit in the per unit base.

5.4   Dynamic Operating Limit

The dynamic behavior of a system shows the effects of the interaction of its elements. It describes how a system reacts over time to a change that breaks the initial steady state balance. Dynamic stability indicates a system's ability to return to a steady state after a change occurs without violation of the limits [54].

In case of a power mismatch between power generation and load demand in the MG, frequency changes. If frequency deviations are within a certain range, e.g. between 47.5 Hz and 52 Hz for the simulated MG, frequency can be regulated and stabilized by its control system; otherwise the MG undergoes frequency instability and this may result in a black-out. In this thesis, the dynamic operating limit indicates the maximum dynamically allowable positive and negative load steps that can be dealt with by the islanded MG at one time. It is influenced by factors like initial loading status, shares of

generators, system inertia and the MG's control system. The dynamic operating limit is restricted to the baseline defined by the steady state load change limit that is determined by the MG settings under ideal conditions ignoring frequency deviations as described in section 5.3. In other words, a load step must be supported dynamically and in steady state, but system dynamics limits the path the steady state limits can be realized. In this thesis, the stepwise change of load is investigated as most dynamically challenging change to reach a new steady state operation. Introducing the proposed control method that anticipates active power changes between power generation and demand can improve the MG's dynamic stability, and thus, can bring the dynamic operating limit closer to its steady state limit as will be discussed in chapter 6. It is important to study the system frequency dynamic behavior before analyzing control effects of LSP and the BB controller in the MG.

5.4.1   System Frequency Dynamic Behavior - Frequency Response

Frequency response is an important aspect of power system performance [43]. In electrical power systems, power generation and demand should be constantly in equilibrium. If this balance is interrupted, frequency will deviate due to the power disturbance. Frequency deviations in power systems, where rotating machines are present and dominate, are closely related to active power changes according to the swing equation (2.15) in chapter 2. Only two generators are used to supply load in the simulated islanded MG, hence the active power that is produced by generators ($\sum P_G(t)$) is calculated as:

$$\sum P_G(t) = P_{CG}(t) + P_{PV}(t) \tag{5.17}$$

where $P_{CG}(t)$ and $P_{PV}(t)$ are the actual active power infeeds of the CG and PV, respectively. Besides, since the control system of the MG continuously tries to match the power generation to the load demand, if a stable point can be reached, the load change is equal to the sum of the active power change of CG and PV (ΔP_{CG} and ΔP_{PV}) as given below,

$$\Delta P_L = \Delta P_{CG} + \Delta P_{PV} \tag{5.18}$$

By placing $\sum P_G(t)$ from equation (5.17), the system starting time constant of the MG (T_{MG}) and the base value (P_{n-L}) into the swing equation (2.15), the MG swing equation is then formulated as:

$$\frac{df(t)}{dt} = \frac{[P_{CG}(t) + P_{PV}(t) - P_L(t)] \times f_n^2}{P_{n-L} \times f(t) \times T_{MG}} \tag{5.19}$$

where P_{n-L} is the maximum load demand that can be supplied by the MG and f_n is the nominal frequency, which is 50 Hz. Converting all parameters except for T_{MG} in equation (5.19) into per unit base by dividing through the base values P_{n-L} and f_n results in

$$\frac{df_{p.u.}(t)}{dt} = \frac{p_{CG}(t) + p_{PV}(t) - p_L(t)}{f_{p.u.}(t) \times T_{MG}} \tag{5.20}$$

where $f_{p.u.}(t)$ is the actual system frequency of the microgrid in per unit base. $p_{CG}(t)$, $p_{PV}(t)$ and $p_L(t)$ are active power outputs of the CG and PV, and load consumption in per unit base, respectively. This means,

$$f_{p.u.}(t) = \frac{f(t)}{f_n} \tag{5.21}$$

$$p_{CG}(t) = \frac{P_{CG}(t)}{P_{n-L}} \tag{5.22}$$

$$p_{PV}(t) = \frac{P_{PV}(t)}{P_{n-L}} \tag{5.23}$$

$$p_L(t) = \frac{P_L(t)}{P_{n-L}} \tag{5.24}$$

From now on, all power and frequency parameters in this section formulas are stated in p.u. base. The islanded MG is assumed to have a balance between power generation and load demand at the nominal frequency initially. So,

$$p_{CG}(t) + p_{PV}(t) - p_L(t) = 0, \ for \ t = 0^- \tag{5.25}$$

There is no change in frequency, since rate of change of frequency (ROCOF, df/dt) is zero under initial conditions. A load change (Δp_L), which breaks the initial power balance, occurs in the islanded MG when t equals 0, meaning

$$p_{CG}(t) + p_{PV}(t) - p_L(t) = -\Delta p_L, \ for \ t = 0^+ \tag{5.26}$$

For instance, ROCOF becomes negative in case of a load increase, which means that frequency drops, hence more power generation is required. The PV generation feeds in 100% of its available active power if frequency is between 47.5 Hz and 50.2 Hz according to the VDE-AR-N 4105 standard. So, the power infeed of the PV generation is already at the maximum at the initial state and cannot be increased further. Therefore, this disturbance can only be compensated by the CG, first by injection of kinetic energy

and then by adapting the operating point. For a better understanding, a test MG
with no share of PV is given for the calculation of ROCOF. When the active power
output of the CG becomes equal to the load demand, ROCOF becomes zero. At this
point, the system frequency reaches its minimum, which is the nadir of the frequency
deviation. This behavior is the so-called inertia response [43, 55]. The initial rate of
frequency decline is influenced by the system inertia, e.g. cumulative inertia response
of all generators and loads. The higher this initial rate of frequency change is, the
bigger the frequency dip will be after the inertia response. In case of the initial state
of nominal frequency, which means $f_{p.u.}(\text{t=0}) = 1\,\text{p.u.}$, with the load change Δp_L the
initial ROCOF can be calculated:

$$\frac{df_{p.u.}(t)}{dt}\,\bigg|_{t=0} = \frac{-\Delta p_L}{T_{MG}} \tag{5.27}$$

The initial ROCOF is taken as the ROCOF over the whole inertia response period to
approximate the frequency nadir. Rearranging equation (5.27) and integrating with
respect to time gives

$$f_{p.u.}(t) \approx -\frac{\Delta p_L}{T_{MG}} \times t + C \tag{5.28}$$

Inserting initial conditions leads to $C = 1$,

$$f_{p.u.}(t) \approx -\frac{\Delta p_L}{T_{MG}} \times t + 1 \tag{5.29}$$

The time that the CG needs to increase its mechanical power with full rate until it
provides the same amount of power as the increased load demand for the first time is
assumed as time (t) in equation (5.29). An approximation for the frequency nadir that
is reached at the end of the inertia response is thereby given by equation (5.29). The
real ROCOF is smaller than the initial rate of change but the real increase of the CG is
slower or equal to the maximum one assumed here. The adapting time (t_{adp}) that the
CG needs to change its power to reach a certain value can be estimated based on power
deviation and rate of power change of the CG. The adapting time of the CG with full
rate, thus, is expressed as,

$$t_{adp} = \frac{\Delta p_{CG}}{\dfrac{dp}{dt}\bigg|_{max}} \tag{5.30}$$

where Δp_{CG} is the power change of the CG. For $t = t_{adp}$ in equation (5.29), Δp_{CG}
equals the expected load change Δp_L. Therefore, equation (5.29) results in,

$$f_{p.u.}(t = t_{adp}) \approx -\frac{\Delta p_L^2}{T_{MG} \times \left.\frac{dp}{dt}\right|_{max}} + 1 \tag{5.31}$$

Without considering additional governor action of generators within inertia response, the frequency deviation nadir can be approximated following equation (5.31).

Example

For example, a test MG with a 0.6 s system starting time constant (T_{MG}) and 0% share of PV is operated at nominal frequency initially. Table 5.7 lists out some parameters of the test MG.

Table 5.7: Parameters of an test microgrid

Parameter	Description	Value
s_{CG}	Share of CG	100%
s_{PV}	Share of PV	0%
Δp_L	Expected load change in per unit base	0.1 p.u.
T_{MG}	System starting time constant of the MG	0.6 s
f_0	Initial frequency of the MG	50 Hz

From equation (4.13) in section 4.2.4, the full rate of power change of the CG in the exemplary MG is given as

$$\left.\frac{dp}{dt}\right|_{max} = \begin{cases} \frac{s_{CG}}{1\,\text{s}} = 1\,\text{p.u./s} & \text{, for power increase,} \\[2ex] -\frac{s_{CG}}{1\,\text{s}} = -1\,\text{p.u./s} & \text{, for power decrease.} \end{cases}$$

According to equation (5.30), if load increases by 0.1 p.u., the duration of inertia response can be approximated as

$$t_{adp} = \frac{\Delta p_{CG}}{\left.\frac{dp}{dt}\right|_{max}} = \frac{\Delta p_L}{\left.\frac{dp}{dt}\right|_{max}} = \frac{0.1\,\text{p.u.}}{1\,\text{p.u./s}} = 100\,\text{ms}$$

Then the frequency nadir is calculated following equation (5.31) as

$$f_{p.u.}(t = 100\,\text{ms}) \approx -\frac{\Delta p_L^2}{T_{MG} \times \left.\frac{dp}{dt}\right|_{max}} + 1$$

$$= -\frac{(0.1\,\text{p.u.})^2}{0.6\,\text{s} \times 1\,\text{p.u./s}} + 1$$

$$= 0.9833\,\text{p.u.}$$

Hence the approximated frequency nadir is equal to $0.9833\,\text{p.u.}$ ($49.17\,\text{Hz}$). Table 5.8 gives a summary of the calculated values.

Table 5.8: Summary of calculated values of test microgrid based on given parameters

Parameter	Description	Value
$\left.\frac{dp}{dt}\right\|_{max}$	Full rate of change of active power of CG	$\pm\,1\,\text{p.u./s}$
t_{adp}	Adapting time of the CG with full rate, which is used to approximate the duration of inertia response	$100\,\text{ms}$
$f_{p.u.}(t = t_{adp})$	Approximated frequency nadir at end of inertia response	$0.9833\,\text{p.u.}$

The simulated frequency response under the mentioned conditions is presented in Figure 5.10. As can be seen, the approximated nadir is lower than the actual value because the CG's governor action is disregarded in the frequency time characteristic after the load change. As long as the approximated frequency decrease or increase caused by load change does not exceed the limit, e.g. where load shedding is required or PV generation is required to be cut off, the MG continues to be operated under normal frequency control. If estimated frequency deviation is out of the acceptable range of normal load step as presented in Table 4.4 in section 4.4, the proposed control method - LSP and BB control - should be implemented additionally. Since the given approximation of the frequency nadir according to equation (5.31) is not a worst case scenario, a slow rate of active power change of the CG may lead to that the actual frequency deviation is beyond the estimated frequency nadir. However, in case of a large load change in islanded MGs, the full rate of power change of the CG can be triggered due to control reaction on a big frequency deviation.
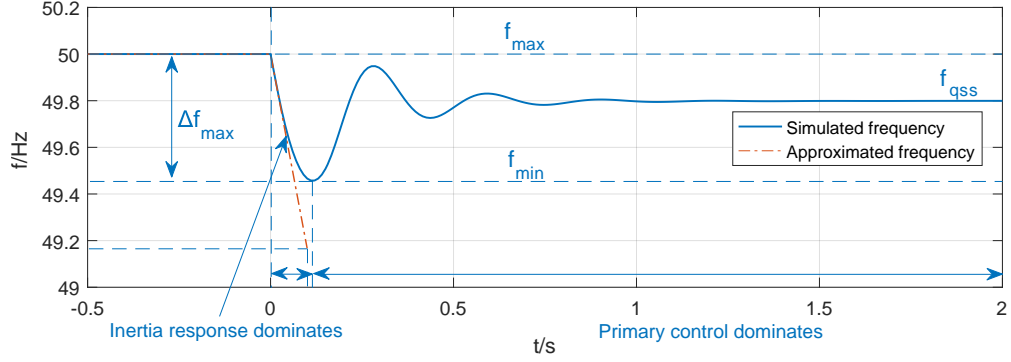
Figure 5.10: Simulated frequency response and approximated frequency
nadir following a frequency disturbance

For traditional large power systems the typical frequency deviation is below $\pm 1\%$ with
an initial rate of change usually below $\pm 0.3\,\mathrm{Hz/s}$. For islanded MGs, frequency deviation
may be as high as $\pm 5\%$ with an initial rate of frequency change in the area of $\pm 1\,\mathrm{Hz/s}$
to $1.5\,\mathrm{Hz/s}$ [43]. The inertia response dominates for a few seconds in large conventional
grids. In the simulated MG, it only covers some hundreds of milliseconds due to its
relative low system starting time constant. In parallel, primary control of the CG is
activated. It would continue to adjust the CG's active power infeed until the frequency
reaches a new stable point and active power is again balanced between generation and
demand, which is defined by the droop setting of primary control. The new frequency
steady point at quasi-steady state[12] (f_{qss}) can be calculated based on the droop setting
of primary control of the CG and the regulation of the active power infeed of the PV
generation.
Converting equation (5.18) into per unit base by dividing through the base values P_{n-L}
on both sides gives

$$\Delta p_L = \Delta p_{CG} + \Delta p_{PV} \tag{5.32}$$

Based on the droop characteristic following equation (2.16), the relation between the
new frequency steady point at quasi-steady-state and the active power change of the CG
is given in per unit system as:

---

[12]In this thesis, quasi-steady state designates the state of the system after the required droop
reaction has been fully activated.

$$f_{qss_{p.u.}} = f_{0_{p.u.}} - \frac{1}{k_{p.u.}} \times \Delta p_{CG} \tag{5.33}$$

where $f_{0_{p.u.}}$ is the frequency set point at initial state and Δp_{CG} is the active power change in the CG between initial state and quasi-steady-state. Hence the active power change of the CG can be expressed as

$$\Delta p_{CG} = -k_{p.u.} \times \Delta f_{p.u.} \tag{5.34}$$

where

$$\Delta f_{p.u.} = f_{qss_{p.u.}} - f_{0_{p.u.}} \tag{5.35}$$

As for the PV generation, its active power can be regulated following the frequency change as described in the VDE-AR-N 4105 standard and its P-f characteristic curve is presented in Figure 4.11 in section 4.3. Therefore, according to equations (4.15) and (4.16), the change of active power infeed of the PV generator between initial state and quasi-steady-state is given as

$$\Delta p_{PV} = \begin{cases} 0 & , 47.5\,\text{Hz} \leq f_0 \leq 50.2\,\text{Hz} \\ & \cap 47.5\,\text{Hz} \leq f_{qss} \leq 50.2\,\text{Hz} \\ -k_{Pf} \times \Delta f_{PV0_{p.u.}} \times p_{PVact} & , 50.2\,\text{Hz} < f_0 \leq 51.5\,\text{Hz} \\ & \cap 47.5\,\text{Hz} \leq f_{qss} \leq 50.2\,\text{Hz} \\ -k_{Pf} \times \Delta f_{PV_{p.u.}} \times p_{PVact} & , 47.5\,\text{Hz} \leq f_0 \leq 50.2\,\text{Hz} \\ & \cap 50.2\,\text{Hz} < f_{qss} \leq 51.5\,\text{Hz} \\ -k_{Pf} \times \Delta f_{p.u.} \times p_{PVact} & , 50.2\,\text{Hz} < f_0 \leq 51.5\,\text{Hz} \\ & \cap 50.2\,\text{Hz} < f_{qss} \leq 51.5\,\text{Hz} \end{cases} \tag{5.36}$$

where

$$\Delta f_{PV0_{p.u.}} = 1.004\,\text{p.u.} - f_{0_{p.u.}}$$

$$\Delta f_{PV_{p.u.}} = f_{qss_{p.u.}} - 1.004\,\text{p.u.}$$

In equation (5.36), k_{Pf} represents the active power reduction rate following frequency change, which is 40% per 0.02 p.u. (1 Hz) as defined by the VDE-AR-N 4105 standard, and p_{PVact} is the currently available active power of the PV generator. Under initial

conditions of nominal frequency, 100% of the available active power of the PV is fed
into the MG. If the frequency at quasi-steady-state f_{qss} is between $47.5\,\text{Hz}$ and $50.2\,\text{Hz}$,
there is no change in the active power infeed. If f_{qss} exceeds $50.2\,\text{Hz}$ and stays below
$51.5\,\text{Hz}$, the active power infeed decreases with a slope of $-k_{Pf}$. By substituting Δp_{CG}
following equation (5.34) and Δp_{PV} according to equation (5.36) in equation (5.32), the
load change under initial conditions with nominal frequency is calculated as

$$\Delta p_L = \begin{cases} -k_{p.u.} \times \Delta f_{p.u.} & , 47.5\,\text{Hz} \leq f_{qss} \leq 50.2\,\text{Hz} \\ -k_{p.u.} \times \Delta f_{p.u.} - k_{Pf} \times \Delta f_{PV\,p.u.} \times p_{PVact} & , 50.2\,\text{Hz} < f_{qss} \leq 51.5\,\text{Hz} \end{cases}$$
$$(5.37)$$

Example

For a better understanding, the MG with given parameters in Table 5.7 is used as an
example to present the calculation of the frequency at quasi-steady state (f_{qss}). For
$f_{0\,p.u.}$ being set to be $1\,\text{p.u.}$ and share of PV being 0%, only the droop setting of the
primary control of the CG influences f_{qss}. This means that equation (5.33) is valid
for the frequency calculation. The CG's power change (Δp_{CG}) is the same as the load
change (Δp_L), which is

$$\Delta p_{CG} = \Delta p_L = 0.1\,\text{p.u.}$$

The CG is assumed to have a droop of 4% on machine base in the islanded MG model
as mentioned in chapter 2 and chapter 4. According to equation (2.16), when the share
of CG is 100% in the MG, droop setting in per unit system ($k_{p.u.}$) taking P_{n-L} as the
base value is given as

$$k_{p.u.} = -\frac{\Delta p_{CG}}{\Delta f_{p.u.}} = -\frac{\dfrac{\Delta P_{CG}}{P_{n-CG}} \times \dfrac{P_{n-CG}}{P_{n-L}}}{\dfrac{\Delta f}{f_n}} = k \times s_{CG} = \frac{1}{4\%} \times 100\% = 25$$

Therefore, the MG frequency at quasi-steady-state can be calculated following equation
(5.33) as

$$f_{qss\,p.u.} = f_{0\,p.u.} - \frac{1}{k_{p.u.}} \times \Delta p_{CG} = 1 - \frac{1}{25} \times 0.1\,\text{p.u.} = 0.996\,\text{p.u.}$$

The frequency at quasi-steady state (f_{qss}) of the exemplary MG being $49.8\,\text{Hz}$ is illustrated in Figure 5.10. As shown in the investigated test case, the primary frequency control needs approximately 2 to $3\,\text{s}$ to settle frequency to a new steady state. The primary control will usually result in that frequency is stable at a value different to the nominal frequency. Therefore, secondary control takes over to mitigate frequency deviation and restores the nominal frequency after 6 to 7 minutes in the test MG.

In case of initial conditions with non-nominal frequency, the PV generation may not provide 100% of its available power to the grid according to equation (4.15). If the frequency at quasi-steady-state f_{qss} is between $47.5\,\text{Hz}$ and $50.2\,\text{Hz}$, the active power infeed of the PV changes from its initial value up to or stays at 100% of the available active power depending on the initial frequency f_0. If f_{qss} is in the range of $50.2\,\text{Hz}$ to $51.5\,\text{Hz}$, the active power infeed changes according to the VDE-AR-N 4105 standard. The active power change of the PV under initial conditions of non-nominal frequency can be expressed by equation (5.36).

Example

If the initial frequency is $51.2\,\text{Hz}$, the PV generation feeds in 60% of its actual power following equation (4.15) if it is operated according to the VDE-AR-N 4105 standard. This means that if frequency decreases due to a load increase in the MG, the PV generation is able to increase its power infeed up to 100% of the available power. The nadir of frequency deviation including the effect of active power change of PV generation is more difficult to be calculated. However, the initial rate of frequency change can be calculated following equation (5.31) as well as the frequency at quasi-steady-state. Parameters of one test MG is presented in Table 5.9.

Table 5.9: Parameters of an test microgrid

Parameter	Description	Value
s_{CG}	Share of CG	50%
s_{PV}	Share of PV	50%
Δp_L	Expected load change in per unit base	$0.1\,\text{p.u.}$
p_{PVact}	PV's currently available active power in per unit base	$0.25\,\text{p.u.}$
p_{CGset}	The initial set point of active power of CG in per unit base	$0.25\,\text{p.u.}$
f_0	Initial frequency of the MG	$51.2\,\text{Hz}$

According to the parameters given in Table 5.9, p_{PVact} and p_{CGset} are both 0.25 p.u.
This means that the PV is 50% partially available and the CG is initially 50% loaded
in the MG with a 50% share of PV. Under initial conditions when frequency is stable
at 51.2 Hz, the load that can be supplied is calculated according to equations (4.15) and
(5.25) as follows

$$
\begin{aligned}
p_L(t=0) &= p_{CG}(t=0) + p_{PV}(t=0) \\
&= 0.25 \text{ p.u.} + [1 - \frac{40\%}{1\,\text{Hz}} \times (51.2\,\text{Hz} - 50.2\,\text{Hz})] \times 0.25\,\text{p.u.} \\
&= 0.4\,\text{p.u.}
\end{aligned}
$$

In the test MG model, the droop setting of the primary control of the CG is assumed to
be 4%. Thus, in equation (5.33), $k_{p.u.} = 25 \times s_{CG}$ in per unit system having P_{n-L} as the
base value, where s_{CG} represents the share of the CG. By substituting $k_{p.u.} = 25 \times s_{CG}$
in equation (5.34), the active power change of CG is then calculated as,

$$
\Delta p_{CG} = -25 \times s_{CG} \times \Delta f_{p.u.}
$$

If the quasi-steady-state frequency f_{qss} after primary control is assumed to stay between
50.2 Hz and 51.5 Hz, according to equations (4.15) and (5.36), the change of the active
power infeed of the PV generation is given as

$$
\Delta p_{PV} = -\frac{40\%}{0.02\,\text{p.u.}} \times \Delta f_{p.u.} \times p_{PVact}
$$

By substituting Δp_{CG} and Δp_{PV} following equations (5.34) and (5.36) in equation
(5.32), the load change can be calculated. As for the test case,

$$
\begin{aligned}
\Delta p_L &= -25 \times s_{CG} \times \Delta f_{p.u.} - \frac{40\%}{0.02\,\text{p.u.}} \times \Delta f_{p.u.} \times p_{PVact} \\
&= -25 \times 50\% \times \Delta f_{p.u.} - \frac{40\%}{0.02\,\text{p.u.}} \times \Delta f_{p.u.} \times 0.25\,\text{p.u.} \\
&= -17.5 \times \Delta f_{p.u.}
\end{aligned}
$$

As given in Table 5.9, the load is assumed to increase by 0.1 p.u. in the MG. Therefore,

$$
\Delta f_{p.u.} = -\frac{\Delta p_L}{17.5} = -\frac{0.1\,\text{p.u.}}{17.5} = -0.006\,\text{p.u.}
$$

According to equation (5.35), the quasi-steady-state frequency in per unit base is calcu-
lated as

$$f_{qss_{p.u.}} = \Delta f_{p.u.} + f_{0_{p.u.}} = -0.006 \, \text{p.u.} + 1.024 \, \text{p.u.} = 1.018 \, \text{p.u.}$$

Hence the frequency at quasi-steady state f_{qss} is equal to $50.92 \, \text{Hz}$. This frequency response behavior is shown in Figure 5.11.
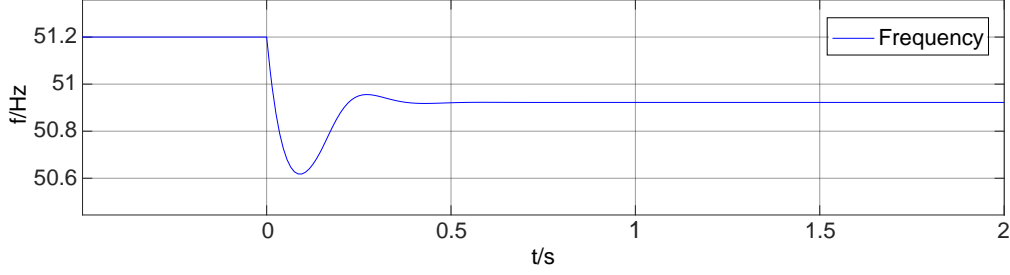
Figure 5.11: Frequency response when initial frequency is not at its nominal value

In the rest of this thesis, initial frequency is considered to be $50 \, \text{Hz}$, as the aim is to analyze frequency stability that is expected to be improved by the introduced control method. With an initial system frequency not at the nominal value, the proposed method could cause a series of problems. For instance, when the initial frequency is at $51.5 \, \text{Hz}$ and the load is about to increase, LSP will send a signal to the BB controller to let the CG generate more power and feed it into the grid, which would lead to a further frequency increase. This could, then, result in the PV generation to be cut off. On the other side, if frequency is $49 \, \text{Hz}$ and the load is about to decrease, active power of CG reduces due to the BB controller, which can cause a frequency drop below $49 \, \text{Hz}$ and result in unnecessary load-shedding. The proposed control method could then disturb the frequency stability instead of benefits that it can bring. Besides, frequency would be stabilized at a value elsewhere than its nominal value after primary control, and afterwards, frequency can actually be regulated to $50 \, \text{Hz}$ by secondary control. The proposed method can increase the time for secondary control to re-establish the nominal frequency. Therefore, as discussed earlier in section 5.3, the steady state load change limit is expressed by equations (5.8) and (5.12). The dynamic operating limit under the initial condition of nominal frequency will be investigated and discussed in chapter 6.

5.4.2   Relation between System Frequency and Preset Time

As mentioned in chapter 3, preset time is one important parameter in the proposed control method. It determines how long LSP delays the load switch signal and how

much active power of the CG can be changed in advance corresponding to the potential load change. Therefore, preset time influences the magnitude of the frequency deviation caused by the active power change of the CG at the end of LSP delaying the load switch signal. The relation between frequency and preset time is discussed in this section.

In the simulated islanded MG model, the CG is fully dispatchable between $47.5\,\mathrm{Hz}$ and $52\,\mathrm{Hz}$ as described in chapter 4. If frequency stays between $47.5\,\mathrm{Hz}$ and $50.2\,\mathrm{Hz}$, the PV generator remains steady at 100% of its generated active power. Hence if frequency drops from the nominal value, the infeed of the PV generator is not influenced. In case of frequency being between $50.2\,\mathrm{Hz}$ and $51.5\,\mathrm{Hz}$, the PV generator decreases its power infeed according to the VDE-AR-N 4105 standard. Taking this P-f characteristic of the PV generation in to consideration increases the difficulty to calculate the system frequency change in the non-linear islanded MG model caused by the active power change of the CG during the time interval determined by the preset time. To make the calculation simpler, the change of active power infeed of the PV generation is ignored. By doing this, calculation of the frequency decrease from the nominal value caused by the power reduction of the CG in advance is not influenced, because the infeed of the PV generation does not change. Due to the PV active power regulation when frequency raises above $50.2\,\mathrm{Hz}$, the calculated frequency increase is equal to or bigger than the simulated value. However, acceptable preset time parameters can be determined in a safe way by limiting the calculated frequency to a certain range. The system swing equation during the preset time interval is calculated according to equation (2.15) in SI units as:

$$\frac{df(t)}{dt} = \frac{P_{CG}(t) + P_{PV}(t) - P_L(t)}{P_{n-L}} \times \frac{f_n^2}{f(t) \times T_{MG}} \qquad (5.38)$$

According to equation (5.20), equation (5.38) can be expressed in per unit base as:

$$\frac{df_{p.u.}(t)}{dt} = \frac{p_{CG}(t) + p_{PV}(t) - p_L(t)}{f_{p.u.}(t) \times T_{MG}} \qquad (5.39)$$

At the initial state, power generation and load demand are equal as described by equation (5.25). During the preset time interval, LSP holds the load switch signal and the CG receives a signal from the BB controller to change the active power output with its full rate ($\frac{dP}{dt}\big|_{max}$) before the load is released. During this time period, there is only an active power change of the CG, as change of active power infeed of the PV generation is neglected for simplicity, and no change in load demand, meaning[13]

---

[13]t = 0 means initial state, which is beginning of preset time interval here, in contrast to earlier section, where t = 0 refers to the moment when load change, meaning the end of the preset time interval

$$p_{CG}(t) + p_{PV}(t) - p_L(t) = \Delta p_{CG}(t), \ 0 \leq t \leq t_{set} \tag{5.40}$$

where $\Delta p_{CG}(t)$ is the active power output change of CG. Therefore,

$$\frac{df_{p.u.}(t)}{dt} = \frac{\Delta p_{CG}(t)}{f_{p.u.}(t) \times T_{MG}} \tag{5.41}$$

The active power change of CG with full rate increase or decrease over the time span is given as:

$$\Delta p_{CG}(t) = t \times \left. \frac{dp}{dt} \right|_{max} \tag{5.42}$$

As described in section 4.2, the limit of rate of change of power $\left(\left. \frac{dp}{dt} \right|_{max} \right)$ imposed by the control valve of the CG model in the islanded MG can have a positive or negative algebraic sign as given by equation (4.13). Thus, $\Delta p_{CG}(t)$ being positive indicates a power increase of the CG and a negative $\Delta p_{CG}(t)$ means a power decrease. Substituting $\Delta p_{CG}(t)$ according to equation (5.42) in equation (5.41) leads to:

$$\frac{df_{p.u.}(t)}{dt} = \frac{t \times \left. \frac{dp}{dt} \right|_{max}}{f_{p.u.}(t) \times T_{MG}} \tag{5.43}$$

Based on the assumption of the simulated MG model described in section 4.2, s_{CG}/s and $-s_{CG}/s$ represent the rate limits of power increase and decrease, respectively. When the CG is required to increase its active power at full rate, rearranging equation (5.43) and integrating with respect to time gives

$$\frac{f_{p.u.}^2(t)}{2} = \frac{s_{CG} \times t^2}{2\,\mathrm{s} \times T_{MG}} + C_1 \tag{5.44}$$

and when the CG is required to decrease, equation (5.43) is expressed as:

$$\frac{f_{p.u.}^2(t)}{2} = -\frac{s_{CG} \times t^2}{2\,\mathrm{s} \times T_{MG}} + C_1 \tag{5.45}$$

For this consideration, at initial state $t = 0$, system frequency is 1 p.u. (50 Hz). Therefore, C_1 is equal to $\frac{1}{2}$. Thus, the system frequency time dependent function is:

$$f_{p.u.}(t) = \sqrt{1 \pm \frac{s_{CG} \times t^2}{1\,\mathrm{s} \times T_{MG}}} \tag{5.46}$$

Inserting t_{set}, equation (5.46) is given as:

$$f_{p.u.}(t_{set}) = \sqrt{1 \pm \frac{s_{CG} \times t_{set}^2}{1\,\text{s} \times T_{MG}}} \tag{5.47}$$

This approximation of frequency at the end of the preset time interval is only valid for such cases that the preset time period is equal to or longer than 0 and total time is equal to or longer than preset time. Substituting T_{MG} of equation (4.10) into equation (5.48) leads to

$$f_{p.u.}(t_{set}) = \sqrt{1 \pm \frac{t_{set}^2}{1\,\text{s} \times T_{CG}}} \tag{5.48}$$

System frequency at preset time can be approximated by equation (5.48).

Example

For the simulated MG having a 100% share of CG, which has a starting time constant of 0.6 s, the important parameters for approximating frequency at preset time are given in Table 5.10.

Table 5.10: Parameters of exemplary islanded microgrid

Parameter	Description	Value
s_{CG}	Share of CG	100%
T_{CG}	CG's starting time constant	0.6 s
$f_{0_{p.u.}}$	MG's initial frequency in per unit base	1 p.u.
t_{set}	The time that LSP delays an individual load switch-on or -off signal	70 ms
t_{total}	The time that BB controller is activated	$\geq$ 70 ms

If preset time is set to be 70 ms and the CG increases its power with full rate during this time, system frequency is calculated according to equation (5.48) as

$$f_{p.u.}(t_{set}) = \sqrt{1 + \frac{t_{set}^2}{1\,\text{s} \times T_{CG}}} = \sqrt{1 + \frac{(0.07\,\text{s})^2}{0.6\,\text{s}^2}} = 1.004\,\text{p.u.}$$

Hence system frequency is approximately 1.004 p.u. (50.2 Hz) after the 70 ms preset time. As there is no change in PV active power infeed if frequency is below 50.2 Hz, this calculation is valid for all shares of PV.

Figure 5.12 shows the frequency limitations during the time interval determined by the

preset time. As LSP and BB controller are introduced to provide dynamic support to the islanded MG, their most important feature is that the frequency disturbance caused by them does not create an instability issue. The frequency deviation resulting from the BB control effect should be within a certain range similar to the one defined in Table 4.4. At the end of the preset time interval, system frequency should not rise higher than 51.5 Hz or drop below 49 Hz due to the active power change of the CG, so that no cutting-off of the PV generation or load shedding happens. Since the calculated system frequency should be limited within 49 Hz to 51.5 Hz, possible settings of the preset time in which LSP holds the load switch signal and the CG changes its active power output following the BB control in advance can be determined.
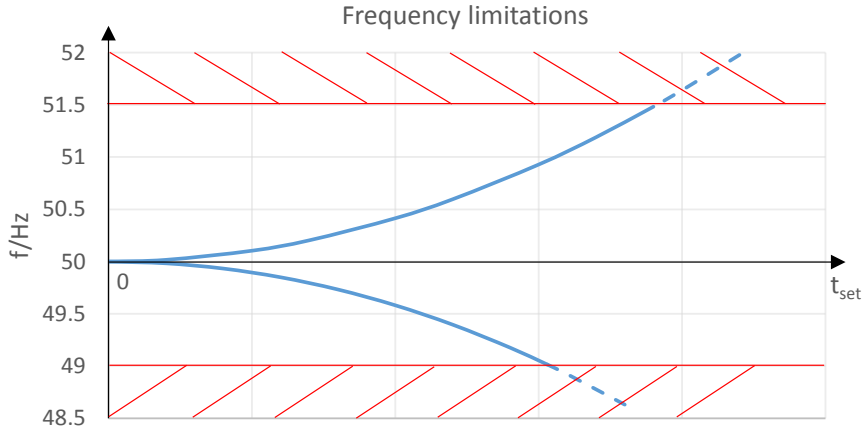
Figure 5.12: Frequency limitations during time interval determined by preset time

Example

As an example, the MG with s_{CG}, T_{CG} and f_0 as given in Table 5.10 is used to calculate the preset time limits regarding frequency boundaries. The approximated frequency at preset time is limited within 49 Hz (0.98 p.u.) and 51.5 Hz (1.03 p.u.), thus, equation (5.48) is as follows,

$$f_{p.u.}(t_{set}) = \sqrt{1 + \frac{t_{set}^2}{1\,\text{s} \times T_{CG}}} \leq 1.03\,\text{p.u., for power increase of CG}$$

$$f_{p.u.}(t_{set}) = \sqrt{1 - \frac{t_{set}^2}{1\,\text{s} \times T_{CG}}} \geq 0.98\,\text{p.u., for power decrease of CG}$$

Substituting $T_{CG} = 0.6\,\mathrm{s}$ leads to

$$0 \leq t_{set} \leq 191\,\mathrm{ms}, \text{ for power increase of CG}$$

$$0 \leq t_{set} \leq 154\,\mathrm{ms}, \text{ for power decrease of CG}$$

Hence the maximum preset time that is allowed for delaying the load switch signal and changing the power of the CG in advance in case of load increase is $191\,\mathrm{ms}$ in the MG without PV. In the MG including PV generation, the amount of the active power generation of the CG during the time interval determined by the preset time can be increased, because the PV reduces its active power infeed if frequency raises above $50.2\,\mathrm{Hz}$ following the VDE-AR-N 4105 standard. Therefore, a preset time longer than $191\,\mathrm{ms}$ is possible in the MG with non-zero share of PV. As for a load decrease in the MG without PV, the maximum preset time of delaying the load signal is $154\,\mathrm{ms}$. Since active power infeed of PV remains constant at 100% of its currently available power if frequency drops from the nominal value, the power reduction of the CG in advance is not affected in the MG including PV. The maximum preset time that can be used in the simulated MG is $154\,\mathrm{ms}$ regardless of share of PV.

5.4.3   Optimization Criteria

LSP and BB controller allow the CG to generate or reduce the power in advance. This means that the balance between power generation and demand at the initial steady state can be interrupted, and thus, frequency can deviate from the nominal value. As mentioned in section 5.4.2, it is important to keep the frequency deviation caused by LSP and BB controller within $49\,\mathrm{Hz}$ and $51.5\,\mathrm{Hz}$.

The two time parameters of LSP and BB controller, preset and total time, determine when the load step is about to be released, how much the CG active power is increased or decreased before the load change, how much active power change of the CG is realized during the entire total time, and the magnitude of frequency deviation. The selection of these two time parameters influences the control effect of the proposed control method. Determining optimal time parameters for the proposed control method is achieved through three different criteria.

Criterion 1: The dynamic simulation of the islanded MG implementing LSP and BB controller with different combinations of time parameters is run. The frequency response of each load step under different shares of PV is observed. Among each sample of frequency response, the maximum and minimum frequency (f_{max} and f_{min}) that occurred in the whole dynamic frequency response is recorded. A frequency deviation band, thus, can be calculated,

$$f_{band} = f_{max} - f_{min} \tag{5.49}$$

For the first criterion, the smallest value of the frequency deviation band (f_{band}), while limits are not exceeded, is sought-after. The frequency deviation band is shown in Figure 5.13. The smaller this frequency band between the maximum and minimum frequency is, the better the dynamic behavior of the islanded MG is in case of a load change. Since the minimum and maximum frequency have been limited between 49 Hz and 51.5 Hz as described above, the maximum possibly admissible frequency band would be limited to 2.5 Hz.
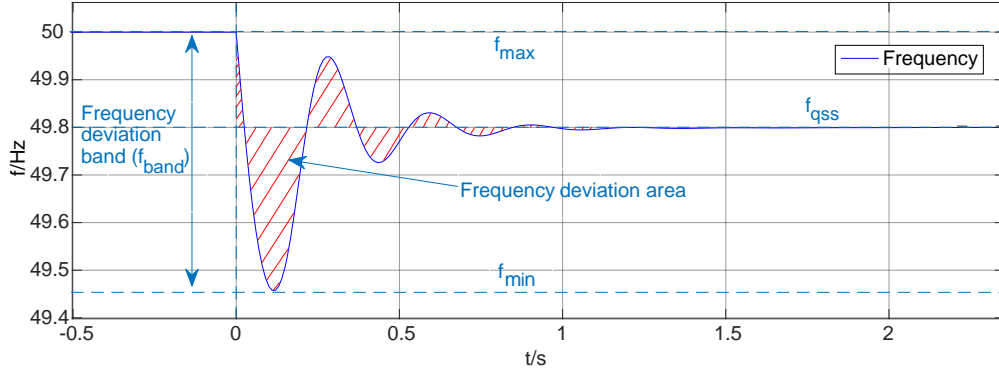
Figure 5.13: Time parameters optimization criteria

Criterion 2: The area between final frequency at quasi-steady state after primary control and actual frequency in the time interval from when the load change occurs until the end of primary control is calculated. This frequency deviation area is marked as the red shaded regions in Figure 5.13. Since negative regions could cancel out positive regions in the integral, the square of the frequency difference between system frequency and frequency at quasi-steady state is integrated. This also ensures a high sensitivity to large frequency deviations. So,

$$c_{area} = \int_{t_0}^{t_{qss}} [f(t) - f_{qss}]^2 dt \tag{5.50}$$

where c_{area} represents the size of the frequency deviation area after a load change. $f(t)$ is the actual frequency of the islanded MG and f_{qss}, which can be calculated following the droop setting according to equation (5.37), is the final frequency at the quasi-steady

state. t_0 is the time when the load change happens in the MG, which is $0\,\mathrm{s}$ in the example shown in Figure 5.13. t_{qss} is the end time of the primary control of the islanded MG, which is approximately $2\,\mathrm{s}$ in the simulated model as shown in Figure 5.13.

A smaller value of the frequency deviation area index c_{area} indicates a better dynamic behavior of the MG system after a load change. The optimal setting of time parameters regarding criterion 2 is, thus, determined by the smallest frequency deviation area index.

Criterion 3: The third criterion combines criteria 1 and 2 and searches for the smallest sum of frequency deviation band and frequency deviation area index. Since the units of frequency deviation band and frequency deviation area index are different, it is necessary to use a reference value. Hence,

$$c_{sum} = \frac{f_{band}}{f_{band-ref}} + \frac{c_{area}}{c_{area-ref}} \tag{5.51}$$

where $f_{band-ref}$ and $c_{area-ref}$ are the frequency deviation band and the frequency deviation area recorded in simulations of the islanded MG without LSP and BB controller, which is equivalent to that the preset and total time are 0. They are used as references for the frequency deviation values of a MG with controller as presented in equation (5.51). All the recorded values of frequency deviation band and frequency deviation area index should be divided through their individual reference. For example, the reference point of sum index $(c_{sum-ref})$ is given as

$$c_{sum-ref} = \frac{f_{band-ref}}{f_{band-ref}} + \frac{c_{area-ref}}{c_{area-ref}} = 2$$

In criterion 3, c_{sum} is the sum index of these two relative values and, corresponding to criterion 1 and 2, its minimum value indicates the optimal time parameters of the proposed control method.

Chapter 6

Simulation Evaluation

In this chapter, the islanded MG model described in chapter 4 is used as a study case to simulate, analyze and evaluate the dynamic behavior of the system in case of a load change and frequency disturbances. In addition, the impact of time delay on the proposed control method is viewed in section 6.4.2. A discussion regarding repeated PV reconnection issues is given in section 6.4.3.

6.1 Dynamic Simulations

In order to find out what impact the proposed control method has on the microgrid (MG) system and how the two time parameters - preset and total time - influence the control effect of load step pre-announcement (LSP) and bang-bang (BB) controller, dynamic simulation results of the MG system with only frequency control and the system including LSP and BB controller with different time parameter settings additionally are compared in this section.

Example

The simulated islanded MG consisting of 75% share of conventional generation (CG) and 25% share of photovoltaic (PV) generation is used as a study case. The parameters of the exemplary MG are given in Table 6.1.
As mentioned in section 4.1.2, the total size of the islanded MG is defined by the maximum load demand (P_{n-L}) that can be supplied by its installed capacity. If P_{n-L} is assumed to be 40 MW in this example, P_{n-CG} and P_{n-PV} can be calculated following equations (4.5) and (4.6) as

Table 6.1: Settings of exemplary islanded microgrid in per unit base

Parameter	Description	Value
s_{CG}	Share of CG	75%
s_{PV}	Share of PV	25%
p_{n-CG}	Rated active power of CG in per unit base	0.75 p.u.
p_{n-PV}	Rated active power of PV in per unit base	0.25 p.u.
p_{L-in}	Initial load supplied by MG in per unit base	0.5 p.u.
p_{PVact}	PV's currently available active power in per unit base	0.125 p.u.
p_{CGset}	Initial set point of active power of CG in per unit base	0.375 p.u.
Δp_L	Expected load change in MG in per unit base	0.15 p.u.
f_0	MG's initial frequency	50 Hz

$$P_{n-CG} = P_{n-L} \times s_{CG} = 40\,\text{MW} \times 75\% = 30\,\text{MW}$$
$$P_{n-PV} = P_{n-L} \times s_{PV} = 40\,\text{MW} \times 25\% = 10\,\text{MW}$$

From equations (4.3) and (4.4), the rated power of CG and PV in per unit base (p_{n-CG} and p_{n-PV}) are given as

$$p_{n-CG} = \frac{P_{n-CG}}{P_{n-L}} = \frac{30\,\text{MW}}{40\,\text{MW}} = 0.75\,\text{p.u.}$$
$$p_{n-PV} = \frac{P_{n-PV}}{P_{n-L}} = \frac{10\,\text{MW}}{40\,\text{MW}} = 0.25\,\text{p.u.}$$

50% of the rated power of the PV generation is assumed to be currently generated and available, meaning

$$p_{PVact} = 50\% \times p_{n-PV} = 50\% \times 0.25\,\text{p.u.} = 0.125\,\text{p.u.}$$

When the initial frequency is 50 Hz, the PV generator feeds 100% of its currently available active power into the grid, namely $p_{PV-in} = 100\% \times p_{PVact} = 0.125$ p.u. The CG, having a 0.6 s starting time constant, is 50% loaded initially, which means $p_{CGset} = 0.375$ p.u. According to equation (5.3), the load to be supplied by the MG under the initial conditions is calculated as

$$p_{L-in} = p_{CGset} + 100\% \times p_{PVact} = 0.375 \, \text{p.u.} + 100\% \times 0.125 \, \text{p.u.} = 0.5 \, \text{p.u.}$$

The load is assumed to increase to 0.65 p.u. at $t = 0$, meaning a positive load change of $\Delta p_L = 0.15$ p.u.

Dynamic simulation results are shown in Figure 6.1[14]. The blue dashed line in the diagram presents the frequency response of the islanded MG only with frequency control. Since LSP and the BB controller are not involved, the CG starts to change its active power under primary and then secondary control to stabilize the system frequency and the PV generation provides active power following the P-f characteristic curve based on the VDE-AR-N 4105 standard when frequency deviates. The red dash-dotted, purple dotted and yellow solid lines illustrate the frequency response of the MG implementing not only frequency control but also LSP and the BB controller. The red and purple lines indicate the frequency responses of the MG with the additional proposed control method, in which both LSP and BB controller are activated before the load change actually happens. This means that the preset time (t_{set}) equals to the total time (t_{total}). The yellow line[15] represents the dynamic behavior of the MG, whose BB controller still continues to work for an additional defined time ($t_{total} - t_{set}$) after LSP releases the load increase.

As shown in Figure 6.1, a frequency drop to approximately 48.2 Hz in the islanded MG with only frequency control can be caused by a 0.15 p.u. positive load step (blue dashed line). This can result in load shedding action to support the frequency stability. If LSP and BB controller are implemented together with frequency control in the MG, the frequency response of the MG can be improved. In case that the MG includes LSP and BB controller, and besides, the preset time and total time are both set to be 40 ms (red dash-dotted line), the CG is controlled by the BB controller to start to ramp up 40 ms before the load is released. After 40 ms, the BB controller signal stops, so the CG operates again in its normal operation mode[16]. The system frequency increases and reaches approximately 50.07 Hz at the end of the preset time and the CG already started increasing its output, and therefore, the frequency decreases by approximately 0.5 Hz less than the frequency change in the MG without LSP and BB controller at the minimum after the load change happens.

According to the dynamic behavior illustrated by the red dash-dotted line, the CG at the

---

[14]Under the same circumstances, simulation results over 800 s are presented in Figure A1 in Appendix.

[15]The optimal settings of the preset and total time for the exemplary islanded MG are used in dynamic frequency response illustrated by the yellow line.

[16]Normal operation mode means that the CG is only coordinated by frequency control.
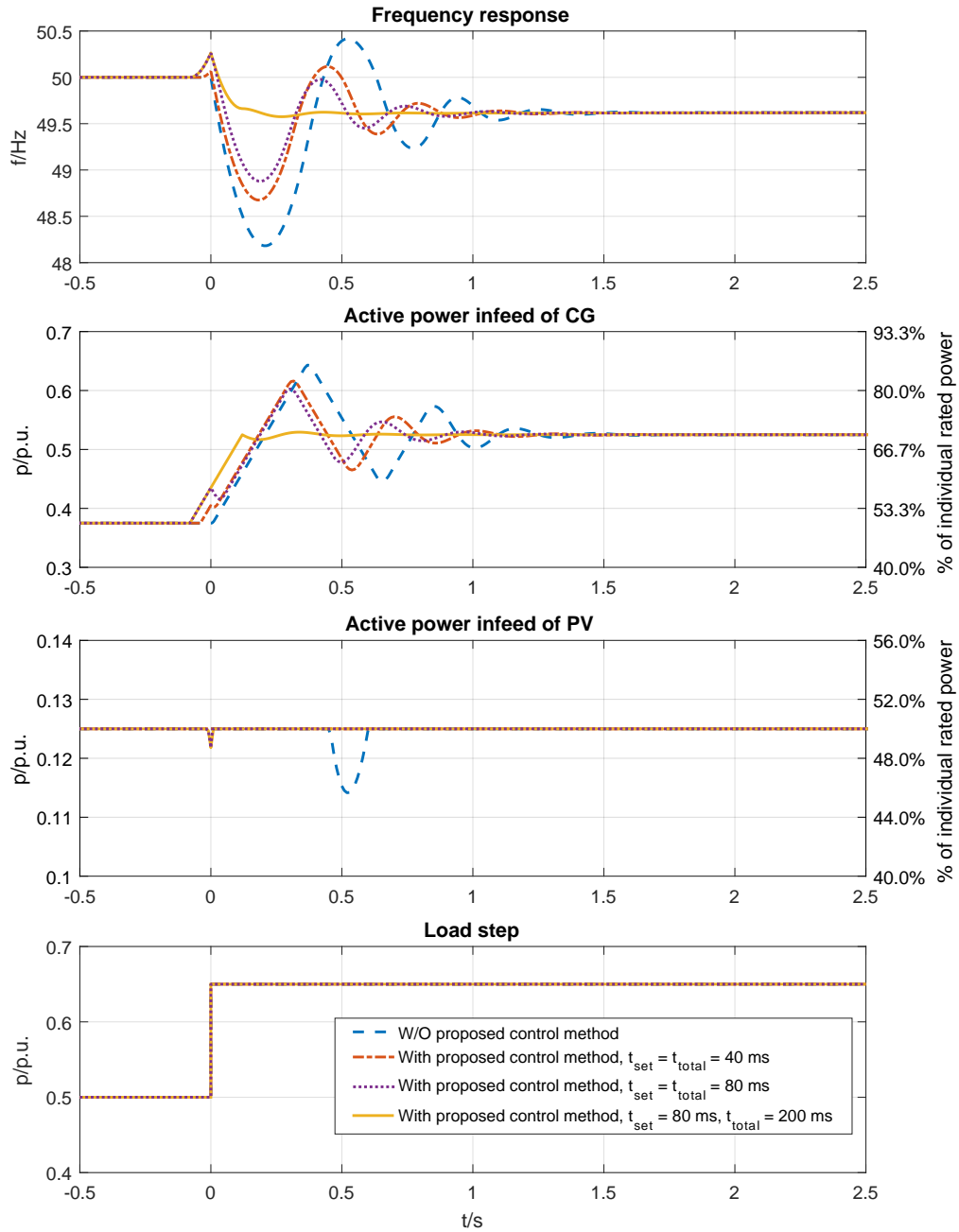
Figure 6.1: Dynamic simulations of the islanded microgrid without and
with implementation of the proposed control method under three
different settings of time parameters

moment of actual load increase ($t = 0$) only generates a small percentage of the active power that is required in quasi-steady state after droop control is fully activated. In order to see the influence of more active power generated in advance at the end of the preset time interval on the frequency dynamic behavior, longer activation time period for LSP and BB controller are tested. For the purple dotted line, both LSP and BB controller are activated for 80 ms, namely $t_{set} = t_{total} = 80$ ms. Within this period, the load switch signal is delayed by LSP and the CG increases its active power at full rate under BB control. After 80 ms, frequency raises and reaches approximately 50.25 Hz. Afterwards, the load change is realized and the CG is again regulated by normal frequency control since the BB control is deactivated. Following frequency droop control as described in section 2.3.1, when the frequency raises from its nominal value, the active power of the CG should decrease, and vice versa. However, the CG's active power is increased while the BB control dominates the active power regulation of the CG. Therefore, once the BB control stops and the CG is operated under frequency control, the CG reduces its active power until the active power meets the requirement of the frequency droop control. Then the CG changes the power output following the droop setting. This is also observed for the MG with LSP and BB controller having 40 ms preset and total time. In the MG with the proposed control method having preset and total time of 80 ms (purple dotted line), the system dynamic behavior is slightly improved compared to that with 40 ms preset and total time (red dash-dotted line).

As illustrated by both the red dash-dotted and purple dotted lines in Figure 6.1, the frequency nadirs are still below 49 Hz. This requires further optimization of the time parameters of LSP and BB controller. The power reductions of the CG that occur after the BB control signal stops during the dynamic process diminish the control effect of LSP and BB controller because more active power than supplied at $t = 0$ is expected to be required at quasi-steady state. Hence, based on the case that the purple dotted line represents, the total time is extended. For the yellow solid line, the preset time for LSP to hold the load switch signal is 80 ms and the total time for the BB controller to be activated is 200 ms. Therefore, the CG is able to increase its active power at the full rate for 80 ms before the load is actually changed. The load change is realized after the 80 ms preset time. Since the BB controller is still activated after the load change, it will continue to command the CG to increase power at the full rate. When the total time of the BB controller, namely 200 ms, is elapsed, it stops to override the control of the CG, which then returns to the normal operation mode. Because of the CG's preemptively generated power controlled by the BB controller and the effect of LSP, the frequency increases to approximately 50.25 Hz at the end of 80 ms preset time, which is the same as that presented by the purple dotted line. After the load increase, the CG continues to ramp up, which allows it to reach the amount of active power required by the load

earlier than the MG without LSP and BB controller as well as the one with LSP and BB controller but not optimal preset and total time settings. Frequency dip in the yellow line is about 49.6 Hz, which does not exceed 49 Hz. Hence possible under-frequency load shedding can be avoided. The CG keeps increasing its active power as long as the total time of the BB controller does not run out. This avoids the power drops that occur in the cases presented by the red dash-dotted and purple dotted lines after the 40 ms and 80 ms total time, respectively.

The exemplary islanded MG implementing LSP and BB controller (both red dash-dotted and yellow solid lines) features a better reaction on power disturbances and show lower frequency deviations than the one without LSP and BB controller (blue dashed line). The designed LSP and BB controller, thus, enhance the performance of the MG control system. In addition, the settings of two important time parameters – preset time and total time – can influence the control effect of LSP and BB controller in the islanded MG. A further investigation of the effect of LSP and BB controller and their time parameters is given in sections 6.2, 6.3 and 6.4.

6.2   Dynamic Operating Limits with Fixed Time Parameters

In earlier work [17], the maximum dynamically allowable load step in the islanded MG solely with frequency control is compared to the MG in which the proposed control method is implemented additionally. In this section, the dynamic behavior of the islanded MG model in case of load changes with different shares of PV is simulated further.

Example

The size of the islanded MG is defined by the maximum load demand P_{n-L}, which is assumed to be constant at 40 MW. A load of 0.5 p.u. is supposed to be supplied at 50 Hz by the islanded MG initially regardless of shares of CG and PV. The initial frequency determines the initial share of load between CG and PV as discussed in chapter 5. If 50% of the rated power of the PV generation is assumed to be available, the CG is 50% loaded initially according to Figure 5.3 in section 5.2.2. For those cases that LSP and BB controller are applied, both preset and total time are fixed at 40 ms. The assumptions of the islanded MG are given in Table 6.2.

The dynamic operating limits resulting from further simulations of the islanded MG

under different system settings as well as a comparison between the steady state and dynamic operating limits are shown in Figure 6.2.

Table 6.2: Assumptions of exemplary islanded microgrid

Parameter	Description	Value
P_{n-L}	Maximum load demand in the MG, which is the base value of active power	40 MW
p_{L-in}	Initial load supplied by the MG in per unit base	0.5 p.u.
p_{PVact}	Currently available active power of PV in per unit base	50% p_{n-PV}
p_{CGset}	Initial set point of active power of CG in per unit base	50% p_{n-CG}
$f_{0_{p.u.}}$	Initial frequency of the MG in per unit base	1 p.u.
t_{set}	The time that LSP delays an individual load switch-on or -off signal while starting BB controller	40 ms
t_{total}	The time that the BB controller is activated in total	40 ms

As discussed in section 5.3, the steady state load change limit of the MG under ideal conditions is mainly defined by the settings of the MG, e.g. the installed capacity of CG and PV, initial power set points, the PV P-f characteristic curve and initial frequency. For the investigated test cases under initial conditions with nominal frequency in this chapter, the steady state load change limit can be calculated according to equation (5.8) and (5.12) and is represented by the red solid lines in Figure 6.2. For example, if the exemplary islanded MG has 0% share of PV, its steady state positive and negative load change limits then are 0.5 p.u. and -0.5 p.u., respectively (points A in Figure 6.2).

The other curves in Figure 6.2 show the maximum dynamically allowable positive and negative load steps in the MG system with different control conditions, starting time constants and shares of PV generation under the circumstances of dynamic frequency disturbances due to load changes. Among these, the solid curves represent the MG with implementation of LSP and BB controller and the dashed lines stand for the MG without them. For instance, when only frequency control is implemented and the system starting time constant (T_{MG}) is 0.6 s, the MG without LSP and BB controller has a maximum allowable positive load step of 0.236 p.u. (point B in Figure 6.2). This means that the
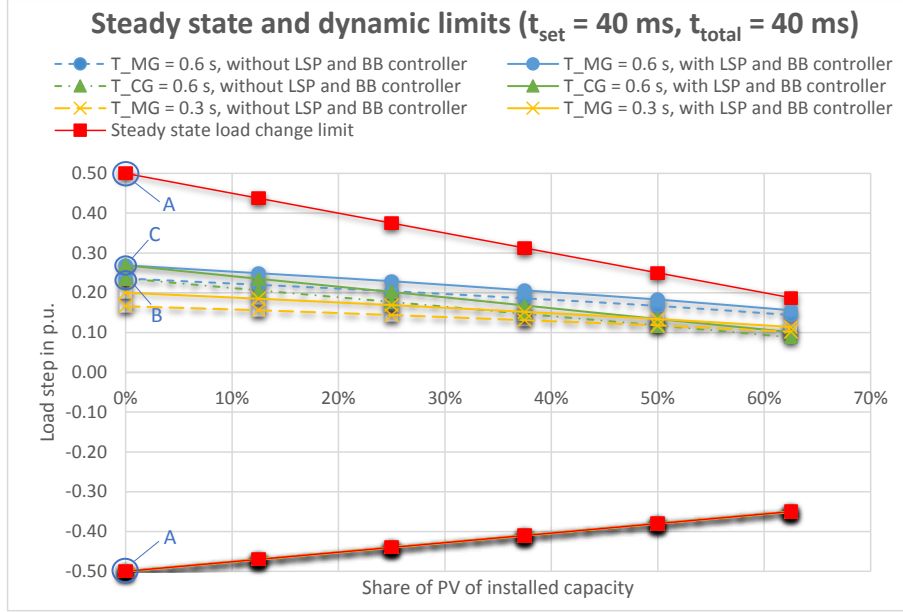
Figure 6.2: Steady state and dynamic operating limits

load can raise from 0.5 p.u. up to 0.736 p.u. If the MG includes LSP and BB controller
with 40 ms of both preset and total time additionally, the maximum allowable positive
load step is 0.269 p.u. (point C in Figure 6.2) As can be seen, all the dynamic operating
limits of the MG are within the steady state load change limits. The dynamic positive
load step limit is closer to the steady state positive load change limit in the MG with
LSP and BB controller than the one without under the same conditions. In addition, a
higher share of PV leads to a decrease in both the steady state and dynamic operating
limits, because the PV generation has low control possibility and no inertia. The results
of the islanded MG with shares of PV up to 62.5% were gathered.

Based on equation (4.10), the MG system starting time constant can easily be calculated
when the starting time constant and share of CG are given. When T_{CG} is fixed, the
higher the share of PV is, the smaller the MG system starting time constant will be.
As can be seen in Figure 6.2, the maximum allowable load step of the MG with $T_{MG} =$
0.6 s and $T_{CG} = 0.6$ s are the same in case of no PV generation. This is because

$$T_{MG} = T_{CG} \times s_{CG} = 0.6\,\text{s} \times 100\% = 0.6\,\text{s}$$

From equation (4.10), when the share of PV is 50%, the T_{MG} is calculated as follows

$$T_{MG} = T_{CG} \times s_{CG} = 0.6\,\text{s} \times 50\% = 0.3\,\text{s}$$

Hence the maximum allowable load step in the MG with $T_{CG} = 0.6\,\text{s}$ is the same as that with $T_{MG} = 0.3\,\text{s}$. The dynamic positive load step limit in the MG with a T_{MG} of $0.6\,\text{s}$ is generally greater than if T_{MG} is $0.3\,\text{s}$, because a lower system starting time constant results in faster frequency change which can lead to bigger frequency instability issues in case of any power disturbance.

The implementation of LSP and BB controller can improve the maximum allowable positive load step for all the cases that are shown in Figure 6.2. LSP and BB controller enhance the MG's control ability to limit its peak frequency under power deviation, thus the dynamic behavior can be improved and the maximum allowable positive load step can be brought closer to the steady state positive load change limit. The influence of LSP and BB controller on the maximum allowable positive load step decreases when there is more power generation of PV in the MG. In other words, the higher the share of PV is, the less effective LSP and BB controller are. This is because the designed control method is applied in the CG and only has impact on the active power of the CG. The dispatchable power of the CG is less if there is a higher share of PV in a MG of the same size.

Although LSP and BB controller improve the control ability of the MG, they do not influence the maximum allowable negative load step, no matter how big the system starting time constant is. The steady state load change limit is related to the operating points of the CG and the variation along the PV P-f characteristic curve as mentioned in chapter 5. If no stable point of the MG system can be reached after disconnection of a large load that causes an over-frequency above $51.5\,\text{Hz}$, the PV generation is disconnected instantly. The control system of the MG brings the frequency back to the acceptable range - between $47.5\,\text{Hz}$ and $50.05\,\text{Hz}$ - for at least $60\,\text{s}$. Then the PV generation starts to reconnect to the overall network. When the reconnection happens, due to the low load demand, no dispatchable capacity of the CG and the integrated PV generation, the frequency goes over $51.5\,\text{Hz}$ before the PV generation reaches its steady operating point along the P-f curve, which would trigger the disconnection of the PV generation again. The PV generation may then repeatedly try to reconnect to the grid as long as the frequency within the acceptable range for $60\,\text{s}$, which would lead to frequency oscillation. Therefore, the maximum allowable negative load step cannot be improved due to the possible repeated PV reconnection that can be caused by a large load decrease. Like the steady state load change limit, the dynamic limit of the negative load step depends on the capacity of the CG and the share of PV generation in the MG. In this case, the utilization of LSP and BB controller does not improve the maximum allowable negative

load step of the system. Other control schemes need to be considered. They will be discussed in detail in section 6.4.3.

For a load decrease, both CG and PV participate in power reduction. However, for a load increase, the PV generation feeds in at most 100% of its currently available active power at nominal frequency. If that is the case, its power infeed cannot increase further. Only the CG can react to the load increase in the MG. Hence the maximum allowable negative load step is generally bigger than the maximum allowable positive load step.

6.3   Optimization of Preset and Total time

According to the results presented in section 6.2, LSP and BB controller cannot enhance the dynamic operating limits of the simulated islanded MG in case of a load decrease. However, the maximum allowable positive load step can be increased, to some extent, by implementing LSP and BB controller with the same preset and total time under all tested shares of PV. Different choices of settings of preset and total time affect the behavior of LSP and BB controller in the MG and maximum allowable positive load step. Therefore, optimal settings of the preset time, in which LSP holds on the switch-on or -off signal, and total time, in which the BB controller controls the CG active power output, are analyzed in this section. The analysis focuses only on the maximum allowable positive load step and a discussion of maximum allowable negative load step will be given in section 6.4.3. The optimal preset and total time indicate the best settings of time parameters for LSP and BB controller, which result in the smallest dynamic frequency deviation following the criteria as described in section 5.4.3 if load changes in the MG.

6.3.1   Simulation Results

Two examples of the simulated islanded MG with 25% and 50% share of PV, respectively, are presented. Important parameters of the MG are listed out in Table 6.3.

Example: MG with 25% share of PV

In the first example, the MG has a 25% share of PV, meaning p_{n-CG} and p_{n-PV} being 0.75 p.u. and 0.25 p.u., respectively. As the starting time constant of the CG (T_{CG}) is 0.6 s, the overall MG system starting time constant (T_{MG}) is calculated following equation (4.10) as

$$T_{MG} = T_{CG} \times s_{CG} = 0.6\,\text{s} \times 75\% = 0.45\,\text{s}$$

Table 6.3: Parameters of exemplary islanded microgrid

Parameter	Description	Value
p_{L-in}	Initial load supplied by MG in per unit base	0.5 p.u.
p_{PVact}	Currently available active power of PV in per unit base	50% p_{n-PV}
p_{CGset}	Initial set point of active power of CG in per unit base	50% p_{n-CG}
$\left.\frac{dp}{dt}\right|_{max}$	CG's full rate of active power change	$\pm s_{CG}$ p.u./s
T_{CG}	CG's starting time constant	0.6 s
f_0	MG's initial frequency	50 Hz

According to Table 6.3, the 0.5 p.u. initial load is supplied by 50% of the CG's total capacity ($p_{CGset} = 0.375$ p.u.) and 100% of the currently available PV power ($p_{PVact} = 0.125$ p.u.). At $t = 0$, the load increase from 0.5 p.u. to 0.6 p.u. takes place as in the dynamic simulation presented in Figure 6.3. As can be seen, the frequency deviates after the load change. For investigating optimal preset and total time settings, dynamic simulations of the MG with implemented LSP and BB controller are carried out. For a range of preset and total time values, maximum and minimum frequency are recorded. The results are shown in Figure 6.4. The values of preset and total time are varied in 10 ms steps.

The two 3D diagrams in Figure 6.4 (a) show maximum and minimum frequency and Figure 6.4 (b) illustrates their top views. The blue areas in the diagrams are where frequency is within the tolerance. The darker the red is, the more severe the frequency instability issues would be. A high frequency may cause an over-frequency problem, which results in disconnection of PV as described in chapter 4, if both preset and total time of LSP and BB controller are too long. In this case, the CG generates active power before the load change. This causes frequency to raise over 51.5 Hz in advance. As shown in Figure 6.4, in the minimum frequency diagrams the critical area is larger than that in the maximum frequency diagrams. When both preset and total time are 0, meaning that LSP and BB controller are not active, the minimum frequency is close to 49 Hz, which is also presented in Figure 6.3. Along the black diagonal, preset time equals total time. Above, preset time is bigger than total time. This means that LSP delays the load step signal longer than the BB controller takes control actions. For the proposed control method, this would not be useful in real practices, but this combination of time settings
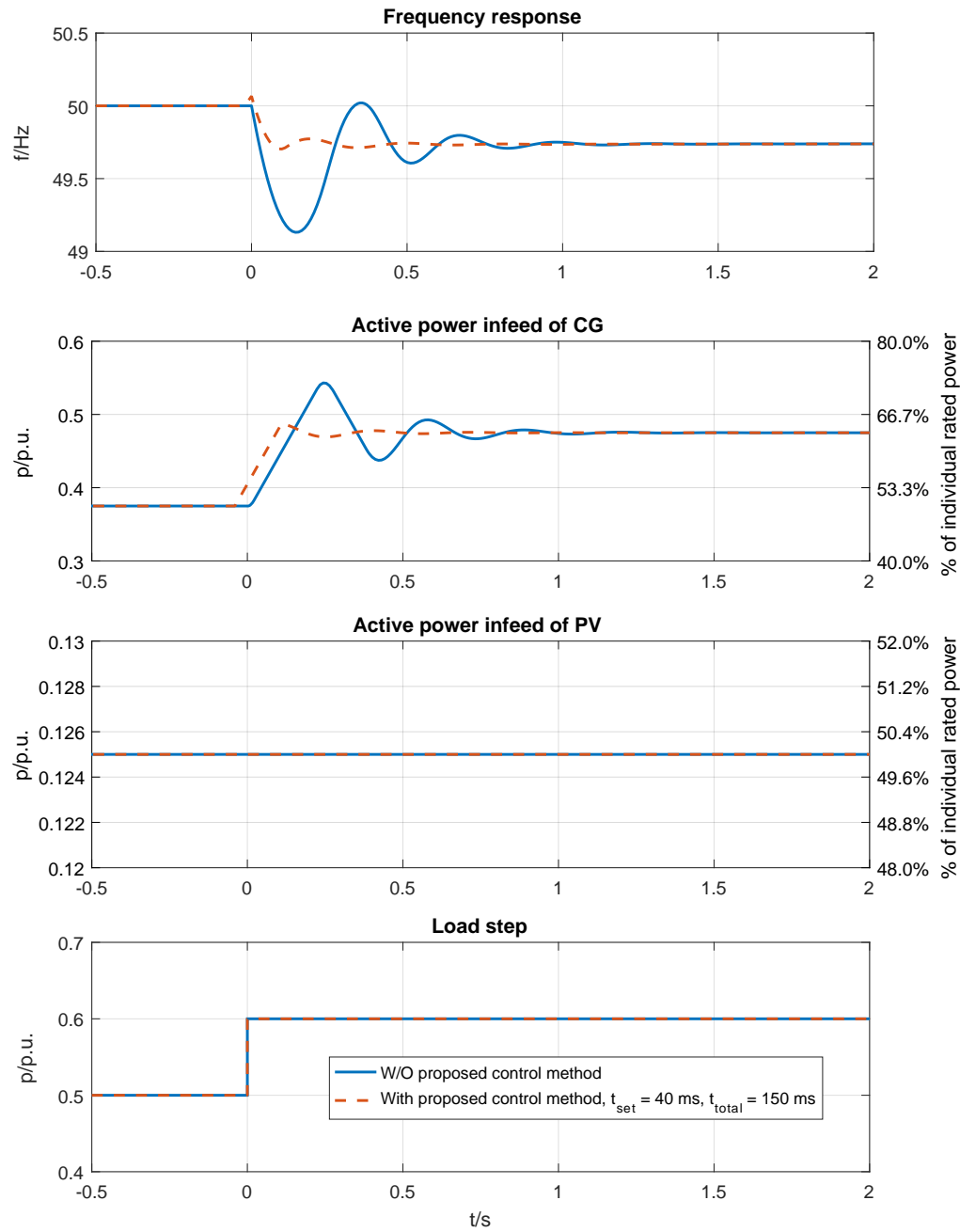
Figure 6.3: Dynamic simulations of the sample MG with 25% share of PV

(a) 3D view

(b) Top view
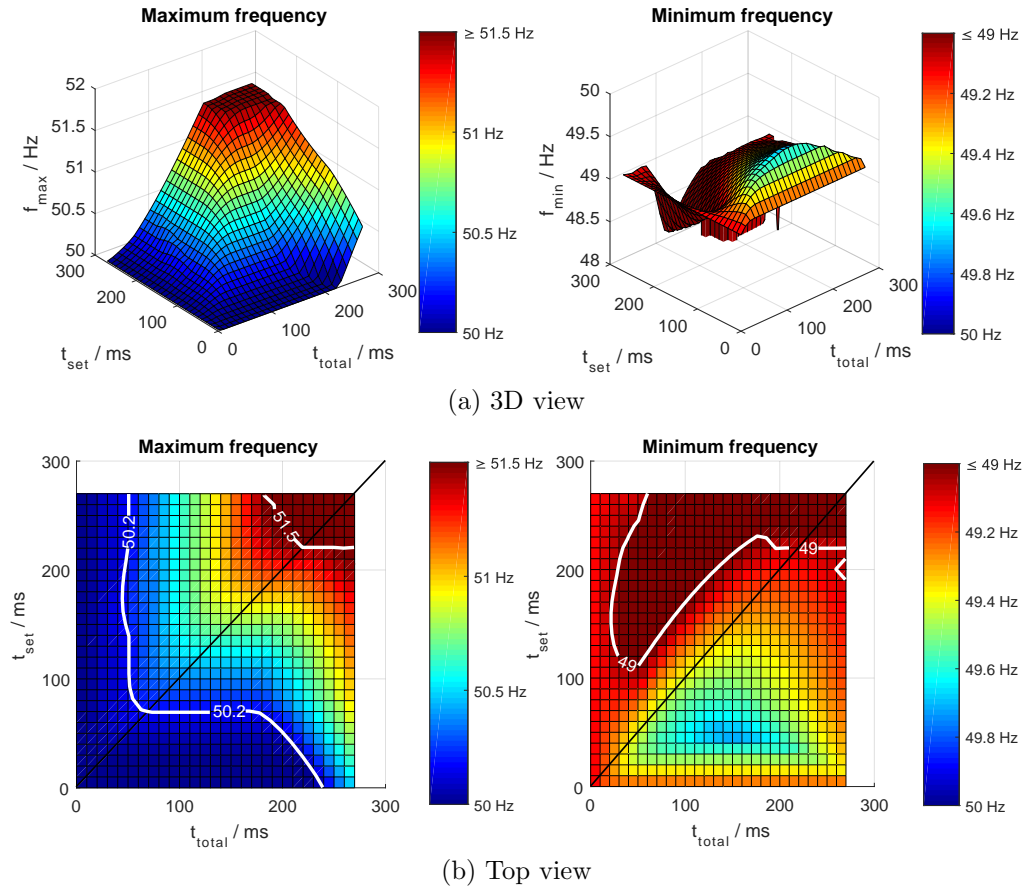
Figure 6.4: Maximum and minimum frequency in the islanded MG with
25% share of PV

is investigated for the sake of completeness. Hence the BB controller is turned off before
the load step is realized. Below the black diagonal, preset time is shorter than total
time. In these cases, the load step is released while the BB controller is still active. The
MG may collapse if either maximum frequency is above $51.5\,\mathrm{Hz}$ or minimum frequency
is below $49\,\mathrm{Hz}$ (dark red areas in Figure 6.4). For a better overview, those dark red areas
are eliminated as shown in Figure 6.5[17].

With implementation of the proposed control method in the MG, the dynamic positive
load step limit can be brought closer to the steady state positive load change limit.

---

[17]As can be seen, one area, where preset time is in a range from $100\,\mathrm{ms}$ to $270\,\mathrm{ms}$ and total
time is between $20\,\mathrm{ms}$ and $180\,\mathrm{ms}$, is deleted. This is because minimum frequency is below
$49\,\mathrm{Hz}$, even though maximum frequency of the MG is in the acceptable blue area.
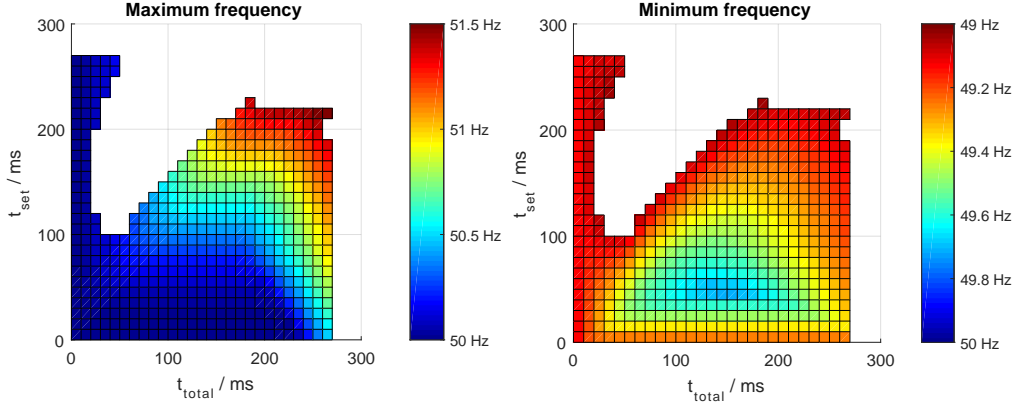
Figure 6.5: Top view of maximum and minimum frequency in the islanded MG with 25% share of PV (points with frequency above 51.5 Hz or below 49 Hz eliminated)

The dynamic operating limit is defined by the maximum allowable dynamic load step under optimal settings of preset and total time. To find optimal settings of preset and total time, the three optimization criteria described in section 5.4.3 are used. Following criterion 1, the smallest frequency deviation band (f_{band}) between the maximum and the minimum frequency that occurred in the MG during frequency response among all combinations of time parameters is searched. According to section 5.4.3, after eliminating points with frequency exceeding either the upper or the lower limit, the maximum frequency band is 2.5 Hz. A smaller value of f_{band} indicates a better dynamic behavior of the MG in case of a load change. The simulation results of the exemplary MG are presented in Figure 6.6 following criterion 1.

For the shown example, e.g. if the load in the MG with a 25% share of PV is increased by 0.1 p.u., the optimal settings of time parameters of the proposed control method are located in the dark blue area. Obviously, total time is longer than preset time for optimal settings, because otherwise the BB controller is turned off before load is switched on. According to evaluation by criterion 1 of the simulation results, the optimal preset time is 40 ms and the optimal total time is in the range of 140 ms to 150 ms. Dynamic behavior of the MG with the proposed control method having the optimal settings of time parameters is shown in Figure 6.3. The frequency band of 0.89 Hz in the MG solely with frequency control ($t_{set} = t_{total} = 0$) after the load increase, is taken as the reference value of f_{band} in order to check the control effect of the proposed control method. By applying the optimal preset and total time in the proposed control method, f_{band} is

approximately $0.36\,\text{Hz}$, which is $0.53\,\text{Hz}$ lower than the reference value $f_{band-ref}$ with only frequency control being implemented. Moreover, large load steps are possible.
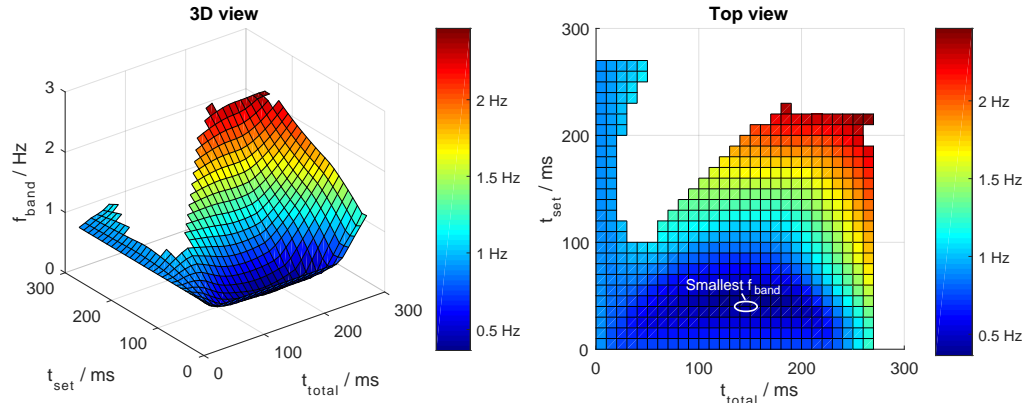
Figure 6.6: Frequency band following criterion 1 in the MG with 25% share of PV

According to the second criterion, the smallest frequency deviation area index is searched. The frequency deviation area index c_{area} is calculated by integrating the square of the difference between actual frequency and quasi-steady-state frequency in the time interval from $0\,\text{s}$ when the load change takes place to the end of the primary control action, which is around $2\,\text{s}$. The smaller this frequency deviation area index is, the better the dynamic behavior after load increase of the MG. The frequency deviation area index of the MG with different time settings is presented in Figure 6.7.
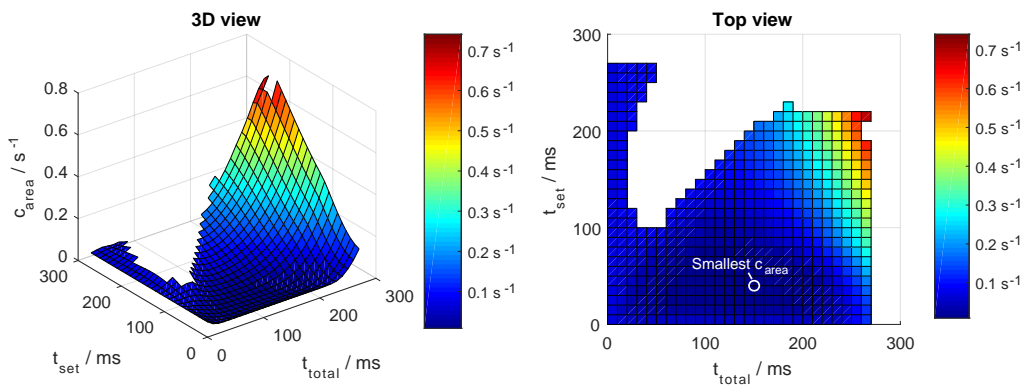
Figure 6.7: Frequency deviation area index following criterion 2 in the MG with 25% share of PV

For a load increase of 0.1 p.u. in the MG, $c_{area-ref}$ equals $0.0732\,\mathrm{s}^{-1}$ ($t_{set} = t_{total} = 0$). The optimal settings of preset and total time of LSP and BB controller are $40\,\mathrm{ms}$ and $150\,\mathrm{ms}$, respectively. The optimal c_{area} is approximately $0.0089\,\mathrm{s}^{-1}$, which is $0.0643\,\mathrm{s}^{-1}$ smaller than the reference value.

The third criterion combines criteria 1 and 2 by searching for the smallest sum index of frequency band and frequency deviation area index. Since the units of frequency band and frequency deviation area index are different, the sum of their relative values (c_{sum}) defines the optimal time parameters. The smaller sum index c_{sum} is, the less volatile the MG's frequency is.

All values of frequency band and frequency deviation area index under different settings of time parameters are compared to their reference points ($f_{band-ref}$ and $c_{area-ref}$) when both preset and total time are 0. Following criterion 3, the absolute values of f_{band} and c_{area}, which are presented in Figure 6.6 and Figure 6.7, are divided through the reference points. Both the relative values of $f_{band-ref}$ and $c_{area-ref}$ equal 1. For f_{band} and c_{area} being smaller than 1, LSP and BB controller can benefit the MG in its dynamic frequency response. For other cases, the proposed control method cannot improve frequency stability but rather undermine it. The reference point of the sum index of the relative values of f_{band} and c_{area} is 2.
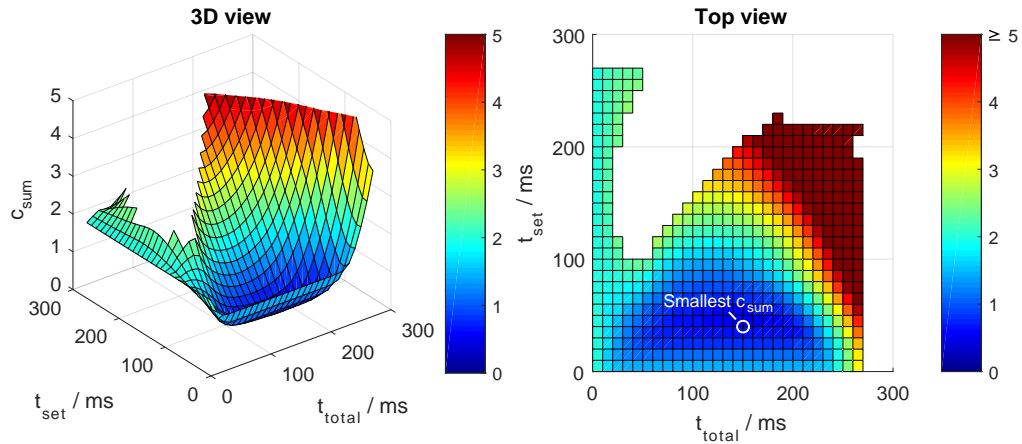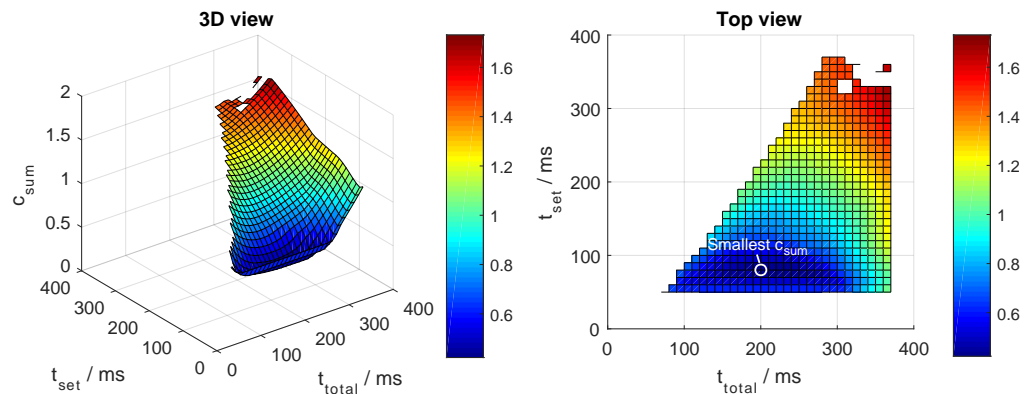

Figure 6.8: Sum index of relative values of frequency band and frequency deviation area index following criterion 3 in the sample MG

Figure 6.8 presents the sum index of relative values of frequency band and frequency deviation area index (c_{sum}) under different combinations of time parameters for LSP and BB controller in the MG. The optimum is located at where the time settings lead to the smallest value of the sum index. This is the case for preset time being $40\,\mathrm{ms}$ and

total time being 150 ms. The relative value of the optimal frequency band is 41% of the frequency band reference $f_{band-ref}$. The optimal frequency deviation area index is approximately 12% of the frequency deviation area index in the MG without LSP and BB controller. Therefore, the optimal sum index c_{sum} is equal to 0.53.

Example: MG with 50% share of PV

In the MG with 50% shares of installed capacity for the CG and PV, p_{n-CG} and p_{n-PV} are both 0.5 p.u. Relevant parameters of the exemplary MG are given in Table 6.3. The starting time constant of the CG (T_{CG}) is 0.6 s, so the overall MG system starting time constant (T_{MG}) is calculated according to equation (4.10) as

$$T_{MG} = T_{CG} \times s_{CG} = 0.6\,\text{s} \times 50\% = 0.3\,\text{s}$$

The load changes from 0.5 p.u. to 0.6 p.u. at $t = 0$. Dynamic simulations of the exemplary MG are shown in Figure 6.9. The MG with 50% share of PV faces a more severe frequency instability issue compared to that with 25% share of PV under the same amount of load increase. This is because the higher the share of PV is in the MG, the less power can be dispatched from the CG to compensate the increased load demand and the smaller the system starting time constant of the MG (T_{MG}) is. The islanded MG only has frequency control and no LSP and BB controller implemented for preset and total time being 0. Minimum frequency, in that case, is 48.18 Hz. According to chapter 4, this kind of load change, which causes a frequency drop below 49 Hz with only frequency control, is categorized as large load step. Without LSP and BB controller, the load change could not take place without load-shedding.

Maximum and minimum frequency depending on different combinations of preset and total time that are varied in steps of 10 ms are shown in Figure 6.10 (a). The corresponding top views are presented in Figure 6.10 (b).

The dark red areas, in which frequency is below 49 Hz or above 51.5 Hz, are deleted as for the previous example. Maximum frequency and minimum frequency after eliminating those dark red squares are shown in Figure 6.11. The minimum and maximum frequency deviation are close to their limits in the areas, where both preset and total time are above 300 ms. As those results where frequency slightly exceeds the set limits are not shown, while those where frequency is slightly within the limits are shown, the pattern in the upper right corner of Figure 6.11 appears.

The implementation of LSP and BB controller with the time parameter settings shown in Figure 6.11 allows the realization of 0.1 p.u. load increase without exceeding the frequency lower limit. To find the optimal settings of time parameters of LSP and BB controller, the same three criteria introduced in section 5.4.3 are applied.
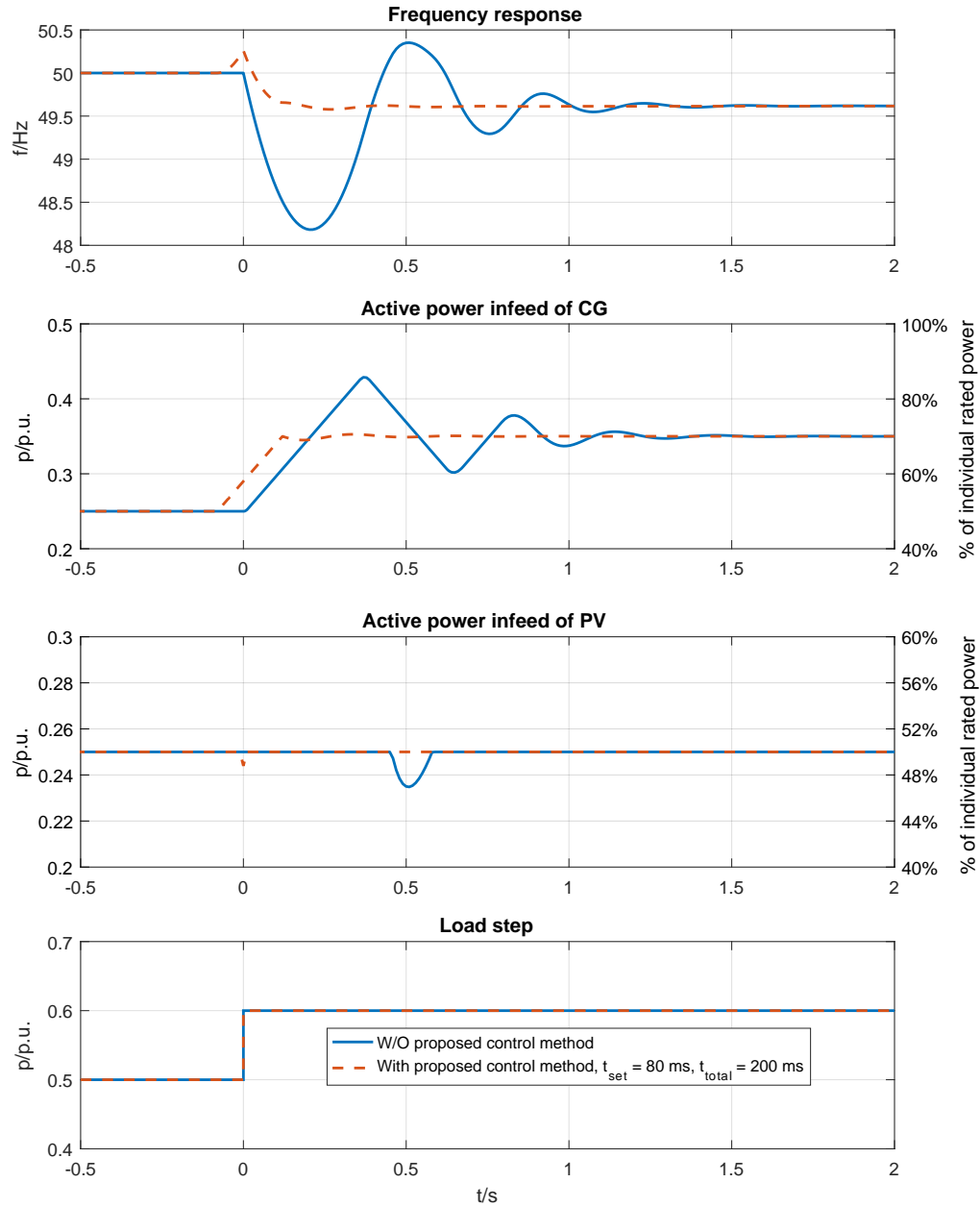
Figure 6.9: Dynamic simulations of the sample MG with 50% share of PV

(a) 3D view

(b) Top view
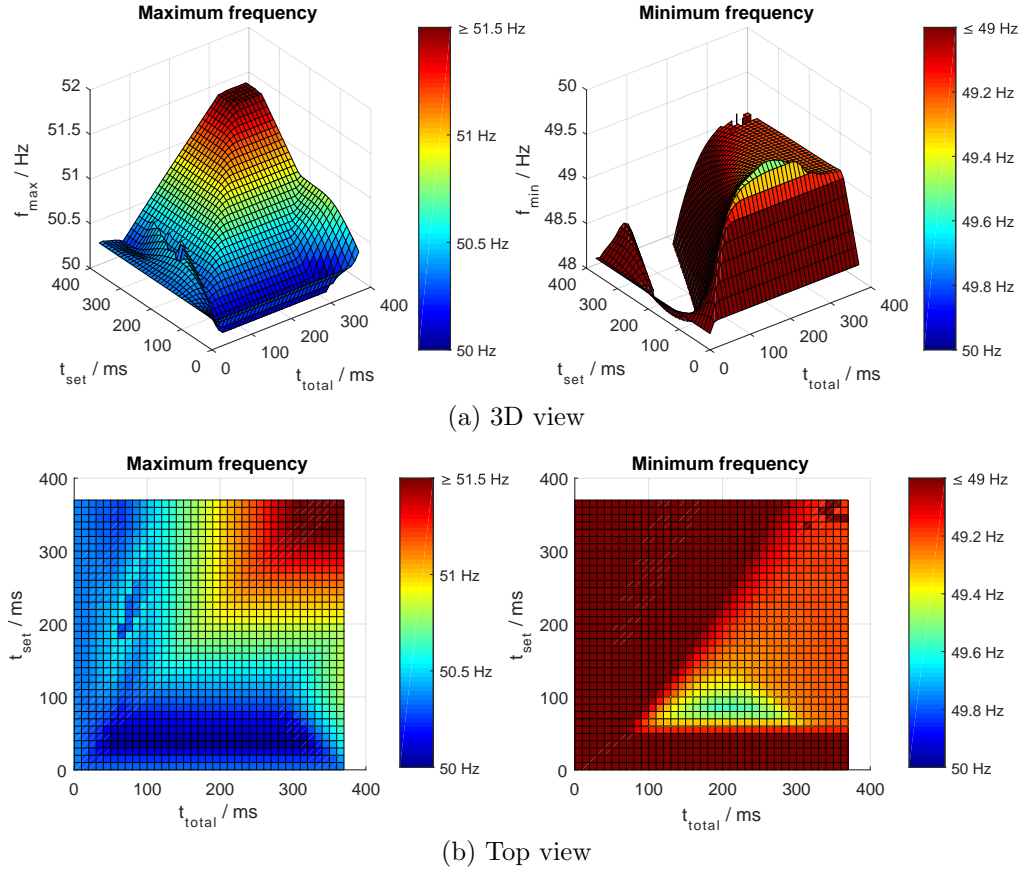
Figure 6.10: Maximum and minimum frequency in the islanded MG with 50% share of PV

The simulation results for the frequency band in the MG with different combinations of time parameters are presented in Figure 6.12. If load increases by 0.1 p.u. in the MG with a 50% share of PV, the frequency band is 2.19 Hz when preset and total time are 0. This is used as reference frequency band $f_{band-ref}$. Since minimum frequency at the reference point is below 49 Hz, this point is eliminated. The optimal settings of the two time parameters are located in the blue area. In this area, the total time of the BB controller is longer than the preset time of LSP. The optimal preset time is 80 ms and the optimal total time is 200 ms according to criterion 1. Under optimal settings of time parameters, the smallest frequency band is around 0.68 Hz, which is 1.51 Hz lower than $f_{band-ref}$.

Following criterion 2, the frequency deviation area index in the time interval from 0 s
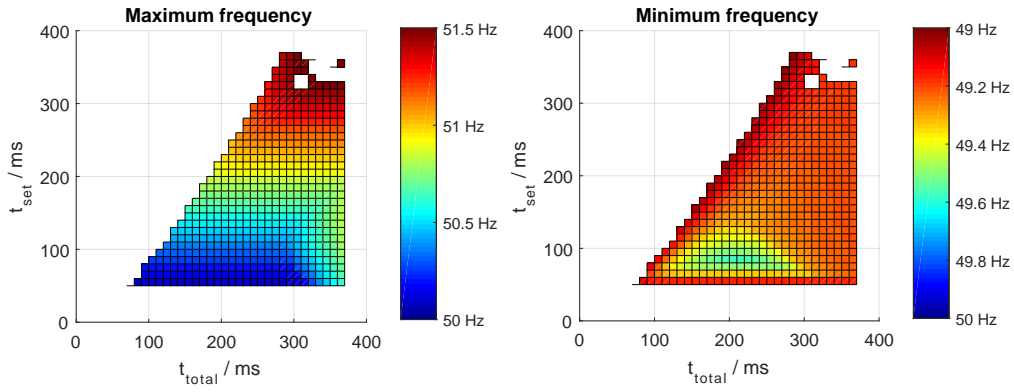
Figure 6.11: Top view of maximum and minimum frequency in the islanded MG with 50% share of PV (points with frequency above 51.5 Hz or below 49 Hz eliminated)
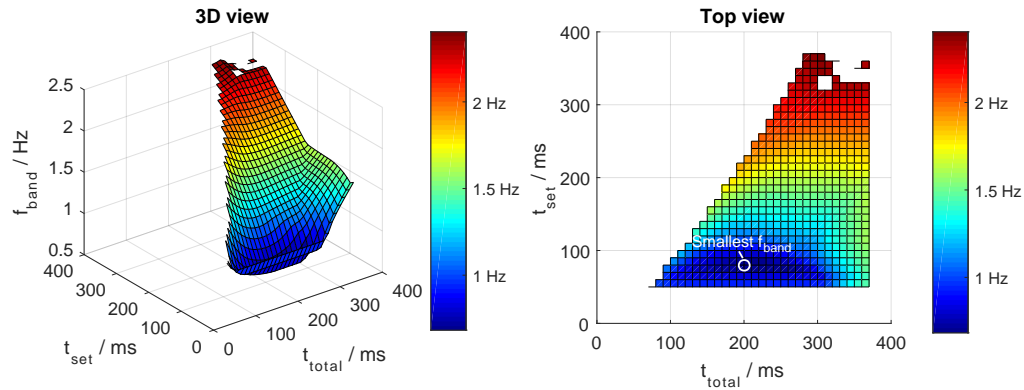
Figure 6.12: Frequency band following criterion 1 in the MG with 50% share of PV

when the load changes to the end of the primary control action, which is around $2\,\mathrm{s}$, is presented in Figure 6.13.
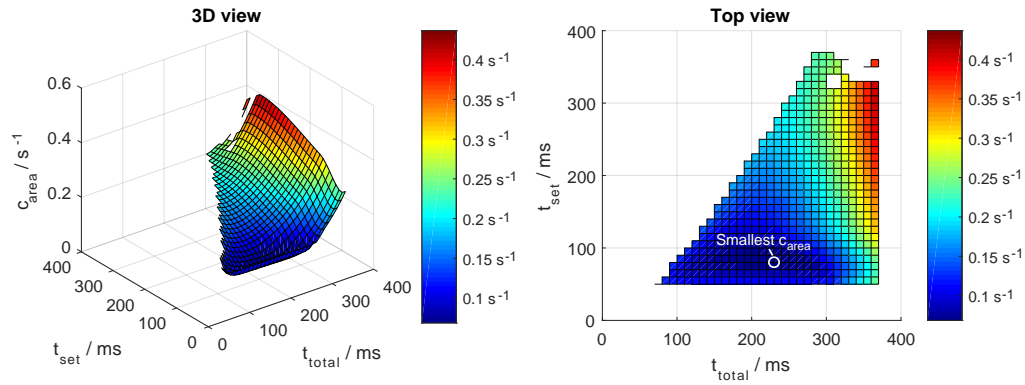
Figure 6.13: Frequency deviation area index following criterion 2 in the MG with 50% share of PV

According to the simulation results, when no LSP and BB controller are implemented, c_{area} is $0.6491\,\mathrm{s}^{-1}$. The optimal preset and total time of LSP and BB controller are $80\,\mathrm{ms}$ and $230\,\mathrm{ms}$ following criterion 2. The smallest frequency deviation area index is $0.0686\,\mathrm{s}^{-1}$, which is $0.5805\,\mathrm{s}^{-1}$ lower than the reference value.

Figure 6.14: Sum index of relative values of frequency band and frequency deviation area index following criterion 3 in the MG with 50% share of PV

Following criterion 3, c_{sum} is shown in Figure 6.14. The optimal c_{sum} is obtained when the preset time is $80\,\mathrm{ms}$ and the total time $200\,\mathrm{ms}$. The frequency band and frequency deviation area index of the MG only with frequency control after the load increase are

taken as references. The relative values of f_{band} and c_{area} are obtained by dividing through these reference points. For preset time being 80 ms and total time being 200 ms, the optimal frequency band f_{band} is approximately only 31% of its reference and the optimal frequency deviation area index c_{area} is approximately 11% of $c_{area-ref}$. The smallest sum index of relative values of f_{band} and c_{area} is about 0.42.

With increasing share of PV or load step size, the area of allowable preset and total time gets smaller. As an example, simulation results of the MG with 25% share of PV under a load increase of 0.25 p.u. are presented in Figure A2 and A3 in Appendix.

6.3.2   Sensitivity Analysis of Input Parameters

The simulation results of the islanded MG in section 6.3.1 show that the optimal preset and total time may differ in the islanded MG depending on the properties of the MG. These simulation results are obtained by changing two input parameters, share of PV and load step. There are other input parameters that influence the choice of optimal preset and total time. A common way to find out how the outcome of a model depends on changes of input parameters and which input parameters are the most sensitive to the outcome is to conduct sensitivity analysis [56]. The analytical method, in which one parameter is changed at one time while other parameters remain constant at their base values, is implemented. The MG with the parameters from Table 6.1 is used as a study case for sensitivity analysis. Based on the collected data, the sensitivity of the optimal time parameters to input parameters is presented, analyzed and compared in this section.

In Table 6.4, the base values, ranges of variation and increments of the parameters that are examined in the sensitivity analysis are stated. Figure 6.15 illustrates how the optimal time parameters resulting from criterion 3, as described in section 5.4.3, change, while the input parameters shown in Table 6.4 are varied stepwise in the given range. Increment shows the step size. According to the dynamic simulation results shown in Figure 6.1, the exemplary islanded MG without LSP and BB controller encounters a frequency drop below 49 Hz after a 0.15 p.u. load increase under the parameters' base values given in Table 6.4. As presented in Figure 6.15, to achieve optimal f_{band} and c_{sum} in the MG following criteria 1 and 3, the preset and total time of the proposed control method are 80 ms and 200 ms, respectively. For an optimal c_{area} according to criterion 2, the preset and total time are 70 ms and 230 ms.

The choice of optimal time parameters is apparently independent from three input parameters, namely initial load status, total size of the MG and amount of active power of PV being available. As discussed in chapter 5, the dynamic operating limits indicate the maximum dynamically allowable positive and negative load steps that can be handled

Table 6.4: Input parameters used in sensitivity analysis of time parameters

Parameter	Description	Range	Base value	Increment	Unit
Δp_L	Load step	0.075 - 0.225	0.15	0.015	p.u.
$\left.\frac{dp}{dt}\right\|_{max}$	Full rate of CG's active power change	0.375 - 1.125	0.75	0.075	p.u./s
s_{PV}	Share of PV	12.5% - 37.5%	25%	2.5%	-
p_{L-in}	Initial load supplied by MG	0.25 - 0.75	0.5	0.05	p.u.
P_{n-L}	Total size of MG	20 - 60	40	4	MW
T_{CG}	Starting time constant of CG	0.3 - 0.9	0.6	0.06	s
p_{PVact}	Currently available active power of PV	0.0625 - 0.1875	0.125	0.0125	p.u.

by the islanded MG without violation of the frequency limits. According to equation (5.20), frequency disturbances are caused by imbalances between power generation and demand. In the simulated MG, which is assumed to have power balance initially, initial load status is not a reason for frequency deviation, but load steps are, as will be discussed later. The initial load status is one factor determining the steady state load change limit of the MG, which restricts the dynamic operating limits. However, it does not influence the MG's dynamic frequency behavior in case of the same load steps from different initial load statuses as long as the load steps are within the defined steady state load change limits. Therefore, for all parameters shown in Table 6.4, the optimal settings of time parameters are independent from the MG's initial load status. Total size of the MG is defined by the maximum load demand that can be supplied by the MG. It is chosen as the base value of active power. Since all the quantities, e.g. frequency and active power, in the MG are normalized to per unit base, changing the total size of the MG does not affect the relation between any of them as well as the system dynamic behavior. The available amount of active power of PV is a percentage of the PV rated power that is currently available to be fed into the MG. It is assumed to be constant

in the simulated MG. A different available PV active power results in the power im-
balance between generation and load demand being compensated by the CG as can be
seen in Figure A4 in Appendix. Since the PV reacts on frequency deviation following
the P-f characteristic curve defined by the VDE-AR-N 4105 standard as described in
chapter 4, time periods of frequency exceeding $50.2\,\text{Hz}$ during frequency response on the
load change have a different impact on frequency behavior for other amounts of available
PV active power. However, as these time periods are short in the tested cases, this effect
can be neglected. Therefore, the available active power of PV has basically no influence
on the system dynamic behavior as well as the optimal settings of preset and total time,
at least for the given cases.

However, the other four parameters listed in Table 6.4 have an influence on the optimal
settings of the time parameters. For example, the optimal preset and total time should
be set to be higher than the base value in case of a load step increase, and vice versa.
This is because a higher load step requires a larger power increase from the CG in the
MG, which results in a longer time of power change. If the CG has a bigger full rate
of power change ($\left.\frac{dp}{dt}\right|_{max}$), it needs a shorter time to reach the expected load demand.
Thus, both optimal preset and total time are shorter while full rate of CG's power change
increases. In Figure 6.15, varying share of PV also changes the parameter $\left.\frac{dp}{dt}\right|_{max}$, since
full rate of power change of the CG is assumed to be $\pm100\%$ of its rated power per second
as described in section 4.2.4. For a fixed MG total size, a higher share of PV means a
smaller rated power of CG. In this case, $\left.\frac{dp}{dt}\right|_{max}$ in the used p.u. base becomes smaller,
while the absolute gradient remains the same. This leads to the CG needing a longer
time to increase its power generation to match the same amount of load change. If the
MG has a higher share of PV, the optimal time parameters are longer in comparison to
that having a lower share of PV. However, if $\left.\frac{dp}{dt}\right|_{max}$ is fixed and independent from share
of PV, the time that the CG needs to meet a certain change in load demand is the same
regardless of share of PV. This means the optimal settings of preset and total time are
independent from share of PV if full rate of power change of the CG is kept constant.
To keep $\left.\frac{dp}{dt}\right|_{max}$ constant, share of PV and percentage of the rated power change of CG
per second have to be adapted accordingly in the MG with a fixed total size.

The bigger the starting time constant of the CG (T_{CG}), which slows down the frequency
change of the MG in case of a power deviation, is, the smaller the optimal preset time.
However, the optimal total time does not vary strongly while the starting time constant
varies on either side of the base values. Table 6.5 presents the best functional approxi-
mation for each parameter in the given range. The three input parameters - load step,
share of PV and system starting time constant of the CG - show a near linear relation
to both preset and total time. An exponential behavior is observed for the full rate of
active power change. The goodness of the functional approximation is described by R^2.
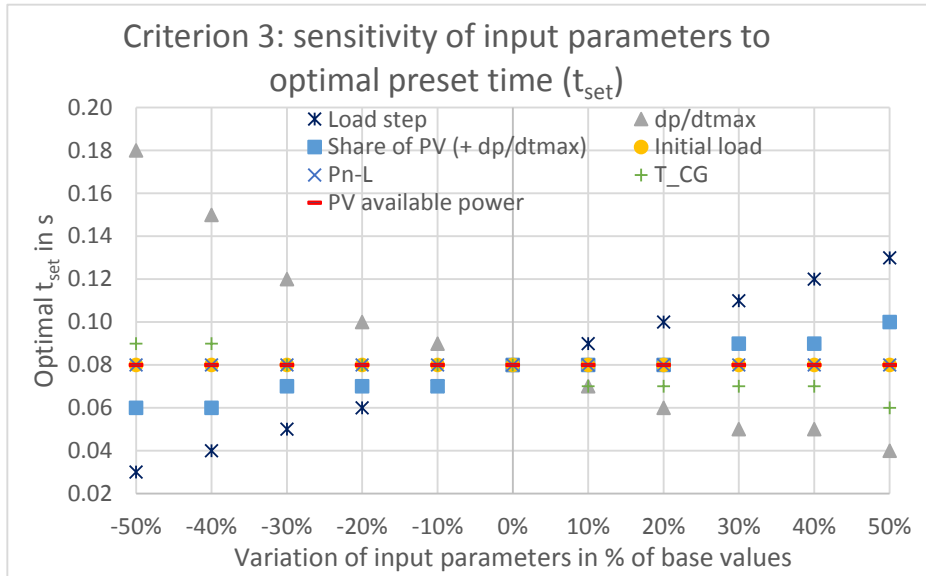
(a) Optimal preset time
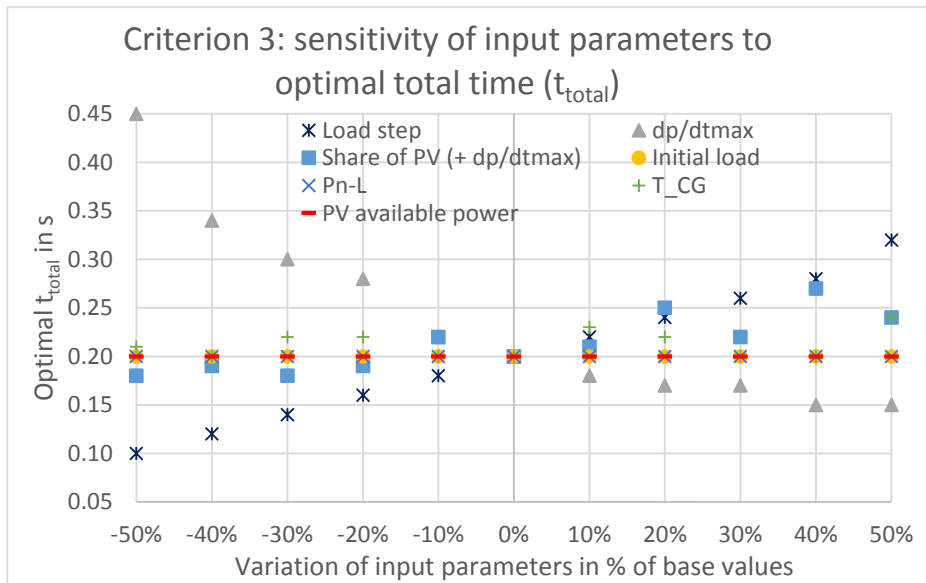
(b) Optimal total time

Figure 6.15: Sensitivity of input parameters to optimal outcomes [18]

R^2 being closer to 1 means that the approximation fits the data better. Since the values

---

[18]When the initial load is increased by 50%, the initial set point of the CG is increased by 66.7% from 0.375 p.u. to 0.625 p.u. Due to the system dynamics of the simulated MG, there is no stable point that can be reached after a load increase of 0.15 p.u. So this point is left out.

of preset and total time are varied in steps of $10\,\text{ms}$, R^2 may be artificially worsened and several R^2 appear to be exactly 1. Furthermore, there are small fluctuations that are caused by the nature of criterion 3. They lead to a low R^2 value, especially for weak dependencies, e.g. in case of optimal total time regarding share of PV and T_{CG}. Also, T_{CG} has a very small impact on t_{total}, such that a linear dependency cannot be shown faultlessly.

Table 6.5: Best functional approximation for each input parameter

Parameter	Best approximation	R^2 for t_{set}	R^2 for t_{total}
Δp_L	Linear, positive slope	1	0.99
$\left.\frac{dp}{dt}\right|_{max}$	Exponential decay	0.99	0.93
s_{PV}	Linear, positive slope	0.94	0.74
T_{CG}	Linear, negative slope	0.89	0.06
p_{L-in}	Constant	1	1
P_{n-L}	Constant	1	1
p_{PVact}	Constant	1	1

The four input parameters that exhibited a detectable influence in Table 6.5 have different degrees of sensitivity to the optimal preset and total time. A comparison of them is shown in Figure 6.16. The maximum change of the input parameters is $\pm\,50\%$. For a decrease from the base value, the full rate of power change of the CG has the biggest impact on the optimal preset and total time; for an increase, the size of load step is most sensitive. Table 6.6 gives an overview of the overall sensitivity of the four parameters presented in Figure 6.16. Additionally, the influence of the input parameters on the optimal settings of preset and total time is also shown in Figure 6.17.

The sensitivity analysis shows similar results for criteria 1 and 2 as for criterion 3. The data regarding criteria 1 and 2 is presented by Figures A5, A6, A7 and A8 in Appendix. The four input parameters listed in Table 6.6 are relevant regarding optimal settings of time parameters. If a MG system is set up including LSP and BB controller under the given parameters in Table 6.4, the preset and total time should be adapted to the change of these parameters. The other three parameters, namely p_{L-in}, P_{n-L} and p_{PVact}, do not need to be considered. A further analysis of the influence of preset and total time on the frequency stability in the MG will be discussed in section 6.3.4.
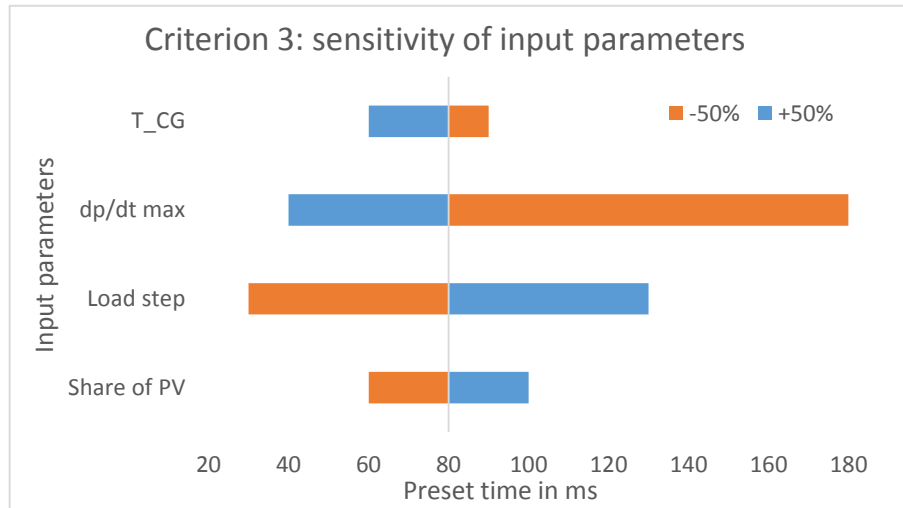
(a) Optimal preset time
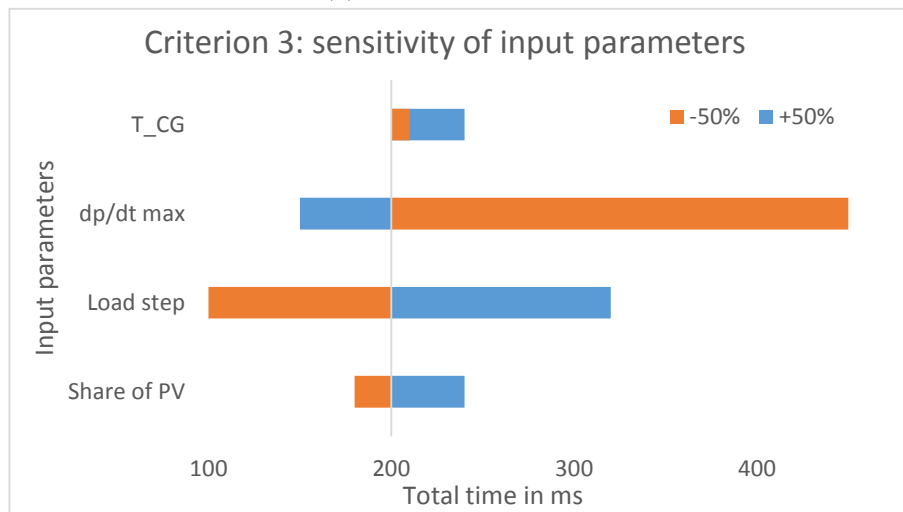
(b) Optimal total time

Figure 6.16: A comparison of sensitivity of input parameters to optimal outcomes

Table 6.6: Sensitivity of four input parameters

Sensitivity ranking	Parameter	Time difference between two extremes (t_{set})	Time difference between two extremes (t_{total})
1	$\left.\frac{dp}{dt}\right\|_{max}$	140 ms	300 ms
2	Δp_L	100 ms	220 ms
3	s_{PV}	40 ms	60 ms
4	T_{CG}	30 ms	40 ms
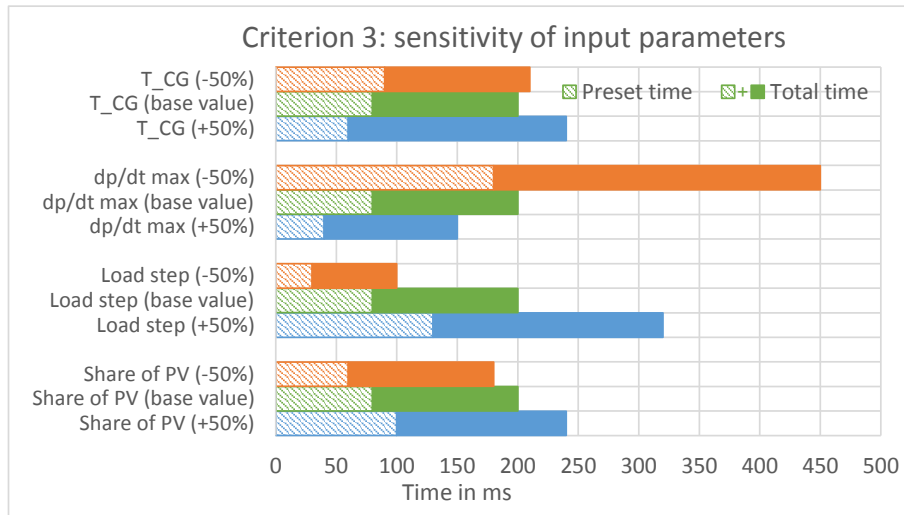
Figure 6.17: Influence of input parameters on optimal settings of preset and total time

6.3.3   Analysis of Optimal Time Parameters

As discussed in section 6.3.2, optimal preset and total time are influenced by share of PV, load step, starting time constant and full rate of power change of CG. For one CG, starting time constant and full rate of power change are constant, therefore, they are not in the focus of this investigation. The impacts of share of PV and load step are further analyzed while other input parameters are fixed in this section. The MG with the parameters from Table 6.3 is used as a study case. The full rate of power change of the CG is assumed to be 100% of its rated power per second and its starting time

constant $0.6\,\mathrm{s}$. The initial load to be supplied is $0.5\,\mathrm{p.u.}$ at $50\,\mathrm{Hz}$ and the available active
power of the PV is 50% of its rated power.

To test how the share of PV influences the optimal settings of the preset and total time
of LSP and BB controller in the islanded MG, the load increase is assumed to be $0.1\,\mathrm{p.u.}$
Figure 6.18 presents the relation between share of PV and optimal preset time. The
blue, green and red curves represent the optimal preset time determined by criteria 1, 2
and 3, respectively. Since criterion 3 is a combination of criterion 1 and 2, its results are
expected to always lay within the range of results of criterion 1 and 2. As can be seen,
for all three criteria described in section 5.4.3, the optimal setting of preset time should
be larger with an increase in share of PV for the same size of load step.
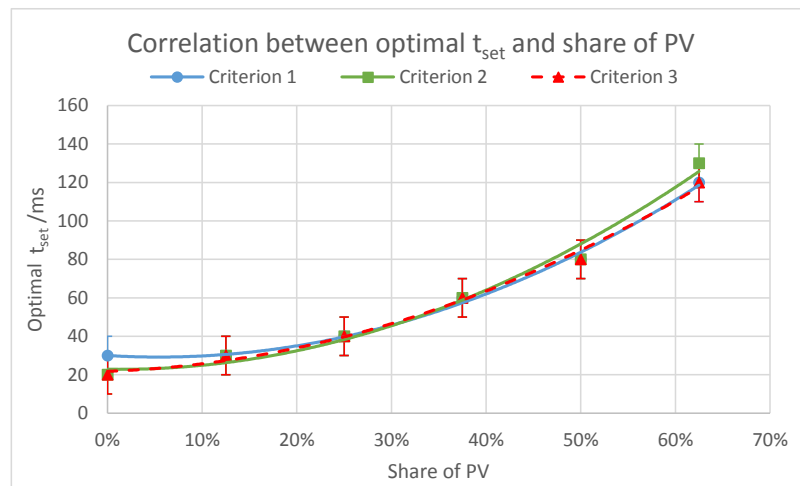
Figure 6.18: Correlation between preset time and share of PV

Figure 6.19 shows the correlation between optimal total time and share of PV as well as
between adapting time and share of PV. As discussed in section 5.4, the adapting time of
the CG refers to the time that it needs to change its mechanical power at full rate until
it matches the amount of power that the increased or decreased load demand requires.
It can be calculated following equation (5.30). In the exemplary MG, the PV generator
feeds 100% of its actual active power into the MG when frequency is $50\,\mathrm{Hz}$, therefore,
the load increase can be compensated only by the CG, which means $\Delta p_L = \Delta p_{CG}$. All
three criteria show that optimal total time is close to the adapting time of the CG.

Both preset and total time have a non-linear relation to the share of PV in the MG
as shown in Figures 6.18 and 6.19. Based on equations (5.30), (4.13) and (4.7), the
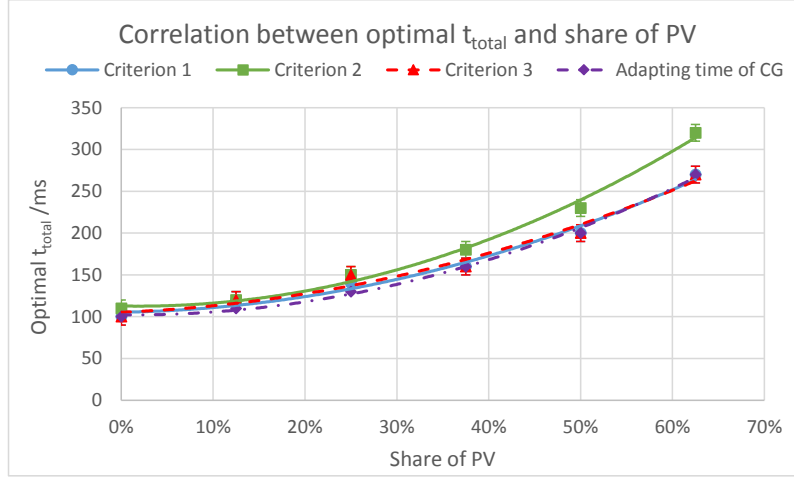
Figure 6.19: Correlation between total time and share of PV

adapting time of the CG (t_{adp}) in case of load increase Δp_L under the assumption of $\left.\dfrac{dp}{dt}\right|_{max} = \dfrac{p_{n-CG}}{1\,\mathrm{s}}$ results in

$$t_{adp} = \frac{\Delta p_{CG}}{\left.\dfrac{dp}{dt}\right|_{max}} = \frac{\Delta p_L \times 1\,\mathrm{s}}{s_{CG}} = \frac{\Delta p_L \times 1\,\mathrm{s}}{1 - s_{PV}} \qquad (6.1)$$

Therefore, t_{adp} shows an inverse relation to $1 - s_{PV}$ and a linear relation to the load step Δp_L. As optimal total time is close to the adapting time of the CG as shown in Figure 6.19, t_{adp} and optimal total time have a similar relation to share of PV in case of a load increase of Δp_L, as can be seen in Figure 6.19. Equation (6.1) is also valid for the optimal preset time to some extend, however, the optimal amount of active power generated by the CG during the preset time interval regarding expected load change Δp_L cannot be pre-determined with the proposed control method. Since the load step is kept constant while the share of PV varies in the tested cases, the preemptively generated active power of CG is expected to be constant as well. Hence the relation between optimal preset time and $1 - s_{PV}$ is also expected to be an inverse function. This can be seen in Figure 6.18.

For analyzing the relation between preset time and load step as well as between total time and load step, the share of PV is kept fixed, e.g. at 25% and 50%. The results are presented in Figures 6.20 and 6.21, respectively.

(a) 25% share of PV
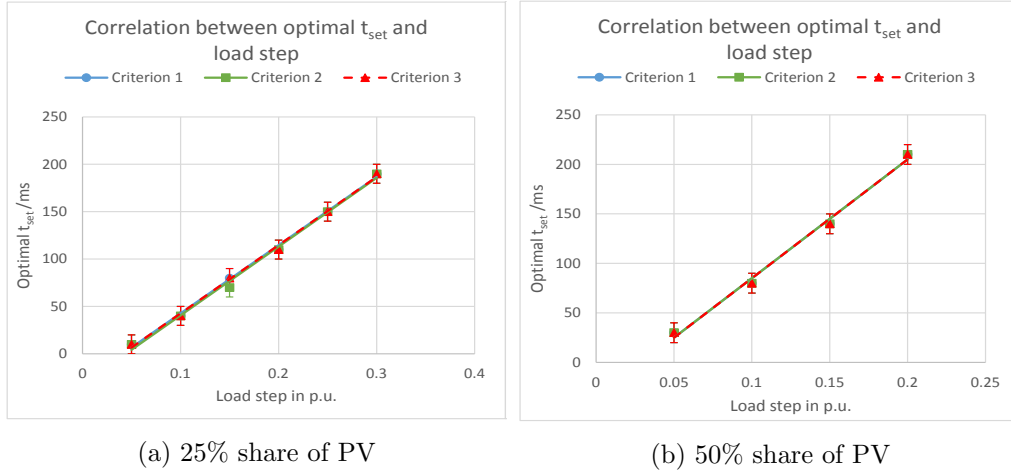
(b) 50% share of PV

Figure 6.20: Correlation between preset time and load step

(a) 25% share of PV
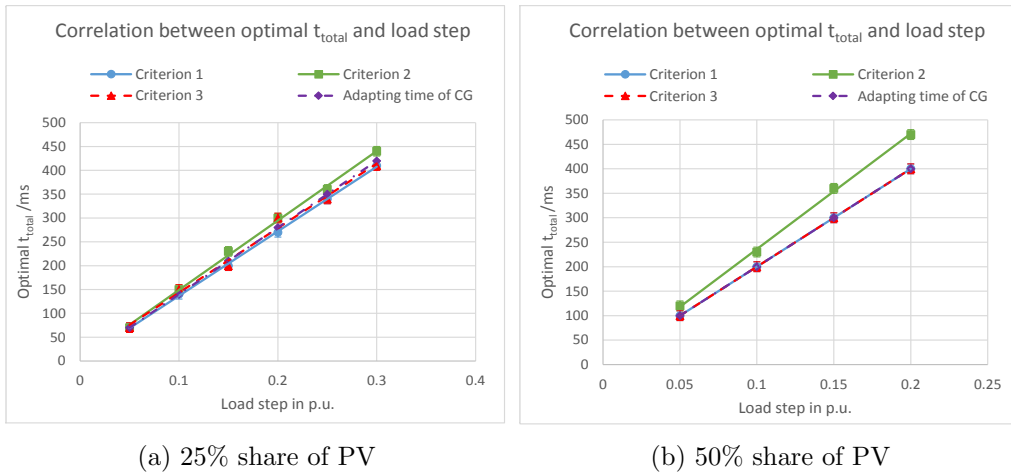
(b) 50% share of PV

Figure 6.21: Correlation between total time and load step

In the islanded MG with both 25% and 50% share of PV, optimal preset and total time depend almost linearly on the load step. A larger load step requires higher preset and total time in both MGs to achieve a better dynamic behavior, as more active power is required from the CG. The optimal total time is again shown to be close to the adapting time of the CG to reach the expected load demand change, independent from share of PV in the MG.

According to the simulation results, optimal total time of the proposed control method is estimated to be the same as the adapting time of the CG (t_{adp}) to match its active power to the expected load change. This is because it is practical for the BB controller to command the CG to increase its active power up to the amount that is required by the load demand. The CG generating too much or too little active power according to the BB control signal may result in the need of a further change of power in the MG due to power imbalance.

Unlike total time, mathematical prediction of optimal preset time was found difficult to be made. Optimal preset time is only determined by simulations. Since LSP and BB controller are implemented in the CG, they can only influence the active power generation or reduction of the CG. A further analysis between optimal preset time and loading status of the CG is conducted. As discussed in section 6.3.2, the optimal settings of preset and total time are independent from the initial load status. This is also valid for the initial loading status of the CG under the assumption of linear behavior of the CG as can be seen in Figure A9 in Appendix. Therefore, the relation between optimal preset time defined by the optimization criterion 3 and expected change of CG loading[19] is presented in Figure 6.22. Each optimal preset time is obtained while total time is set to be at its optimum.

As can be seen, optimal preset time shows a nearly linear dependency on the expected change of CG loading for all test cases. However, if the expected change of CG loading is smaller than 5%, optimal preset time is 0. For load steps that require less than 5% change of CG loading, the proposed control method does not need to be implemented in the MG, as the frequency deviation that is caused is small. These load steps can be carried out only under frequency control without leading to frequency instability. However, LSP and BB controller with preset time being 0 and total time being at its optimal value can improve frequency dynamic behavior. In this case, the BB control makes the CG change its active power at a faster rate once the load changes in comparison to the CG only being regulated by frequency control. Therefore, system frequency response is enhanced as will be discussed in section 6.3.4. If preset time is not equal to 0 while total time is at

---

[19]This refers to the difference between CG loading after a load step occurs and its initial loading status.

optimum, the proposed method changes active power of the CG before the load change, and thus, increases system frequency by the end of the preset time interval. As for small changes, the frequency maximum is the peak when positive load steps occurs. Its size increases for growing t_{set} and it is expected that a higher peak at this moment results in a lower frequency nadir in a given setup. Therefore, frequency dynamic response in the MG may be worse than if preset time is 0, while total time is at its optimum. This means that the control effect of LSP and BB controller is worsened for non-zero preset time. Hence optimal preset time is expected to be 0 if load steps cause small change of CG loading.
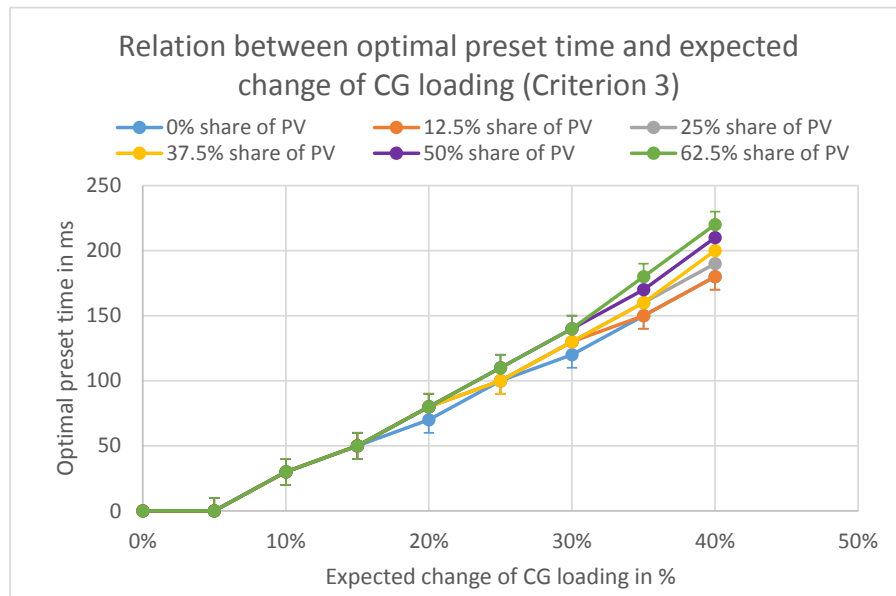
Figure 6.22: The relation between optimal preset time and expected change of CG loading in case of a load change

As shown in Figure 6.22, if load steps require more than 20% change of CG loading, a higher share of PV results in a longer optimal preset time for the same expected change of CG loading. As discussed in section 5.4.2, preset time being longer than 70 ms leads to a frequency increase over 50.2 Hz in the MG regardless of share of PV if the CG has the dynamic properties as described. Optimal preset time is approximately 70 ms when the expected change of CG loading is 20%, see Figure 6.22. In case of the preset time being higher than 70 ms, the PV reduces its active power infeed following the frequency change by the end of the preset time interval according to the VDE-AR-N 4105 standard under the assumption of the PV generation reacting to frequency deviations instantly.

This requires the CG to further increase its active power before the load step takes place. Therefore, if the expected change of CG loading is higher than 20%, it takes longer for the CG to meet the load demand in the MG with a higher share of PV, meaning a longer optimal preset time. This effect gets bigger if the expected change of CG loading increases. For larger load steps, change of CG loading is required to be larger as well. This leads to a higher frequency increase by the end of the optimal preset time interval. Corresponding to larger frequency increase, the PV reduces its active power infeed more strongly. Hence the influence of share of PV on optimal preset time increases when the expected change of CG loading is higher.

Figure A10 in Appendix shows a similar relation between optimal settings of preset time determined by criteria 1 and 2 and expected change of CG loading after a load increase.

6.3.4   Influence of Time Parameters

It is important to examine the effect of time parameters being set to be longer or shorter than their optima on frequency deviation of the islanded MG. Thus, a sensitivity analysis is conducted. In order to observe the influence of preset and total time on frequency deviation, all parameters of the exemplary MG are assumed to remain constant at their respective base values in Table 6.4, except for preset and total time. For the investigation, optimal preset and total time of LSP and BB controller in the MG with parameters at their base values are determined by criteria 1 and 3. This results in the preset time being equal to 80 ms and the total time being 200 ms. The base values, ranges of variation and increments of the tested time parameters in the sensitivity analysis are given in Table 6.7.

Table 6.7: Time parameter values in sensitivity analysis

Parameter	Description	Range	Start value	Increment	Unit
t_{set}	Preset time	0 - 210	80	10	ms
t_{total}	Total time	0 - 380	200	20	ms

The influence of the preset time of the proposed method on the frequency deviation is presented in Figure 6.23. It is analyzed by changing the optimal preset time with an increment of 10 ms, while the other parameters including the total time are fixed at their base values. Following criterion 1, the frequency deviation band between the maximum and minimum frequency during the dynamic frequency response f_{band} is approximately 0.69 Hz, when the preset time is set to be 80 ms and the total time 200 ms. In the

same MG without LSP and BB controller, meaning both preset and total time being 0, the frequency deviation band $f_{band-ref}$ is around 2.23 Hz. In this case, f_{band} is approximately 30.9% of $f_{band-ref}$ when preset and total time are at their optimal values. This percentage is used as the comparison value for criterion 1 as shown in Figure 6.23. Changing preset time results in a different f_{band}, which is then compared with the reference $f_{band-ref}$. The same procedure is carried out for criteria 2 and 3 to obtain $c_{area}/c_{area-ref}$ and $c_{sum}/c_{sum-ref}$. The optimal preset time under the three introduced optimization criteria is marked by purple circles in Figure 6.23.
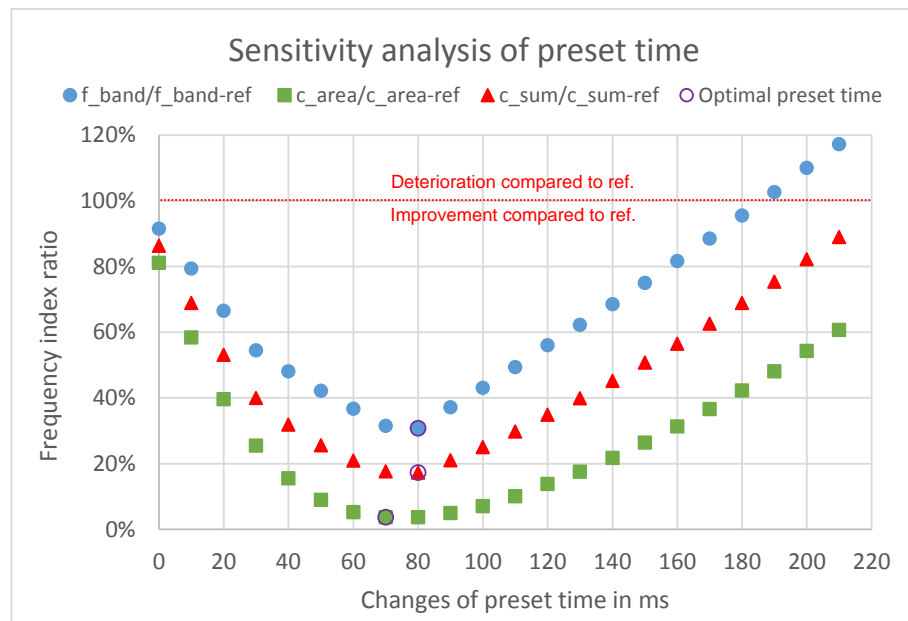
Figure 6.23: Sensitivity of preset time to optimized outcomes

According to the results, frequency deviation obviously becomes worse when preset time is changed into either direction from its base value. Furthermore, frequency deviation is more sensitive to a change of preset time towards smaller values than towards longer ones. If the frequency index ratio is below 100%, the three variables f_{band}, c_{area} and c_{sum} are smaller than their reference values that occur in the MG without LSP and BB controller. If so, LSP and BB controller have a positive effect on the frequency deviation caused by power imbalance in the islanded MG, although preset time is not at its optimal value. In addition, even if preset time is 0, meaning no pre-announcement before a load change and only the CG changing the active power at its full rate, the frequency performance of the MG can be enhanced. Only when the preset time becomes

higher than 190 ms, which is very close to the optimal total time, the frequency deviation band (f_{band}) defined by criterion 1 becomes worse than if no LSP and BB controller are applied.
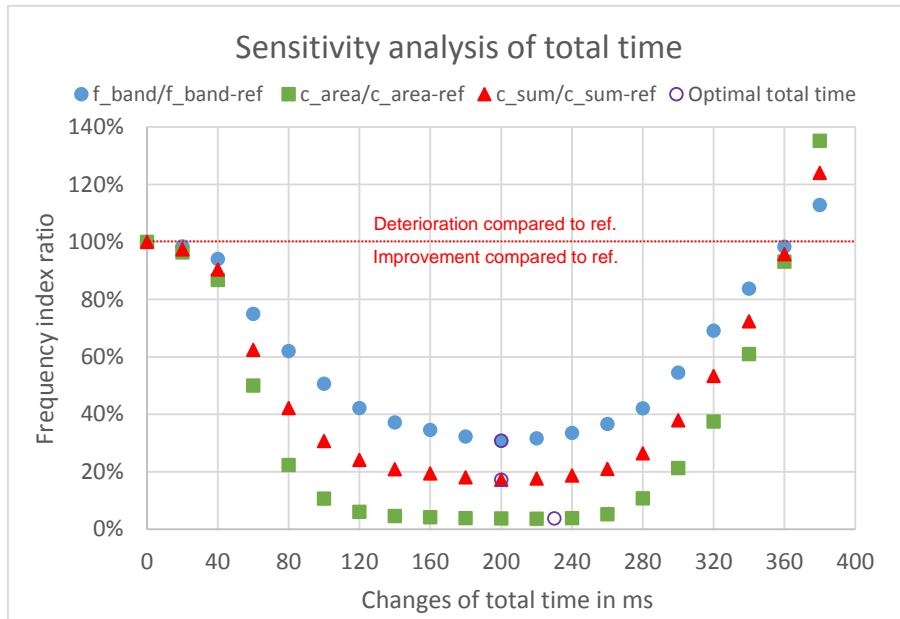
Figure 6.24: Sensitivity of total time to optimized outcomes

Figure 6.24 shows the influence of the total time of the proposed method. In the analysis, all parameters except for total time remain constant at their base values. The base value of the optimal total time is given as 200 ms following criteria 1 and 3 and the increment of the total time is 20 ms. The optimal total time defined by the three criteria is presented by purple circles in the diagram. The same calculation applied in the sensitivity analysis of the preset time is performed and the three frequency index ratios, namely $f_{band}/f_{band-ref}$, $c_{area}/c_{area-ref}$ and $c_{sum}/c_{sum-ref}$, are obtained for different settings of total time. As shown in Figure 6.24, a higher or lower total time worsens the frequency behavior in comparison to that of the islanded MG with optimal total time. However, the dynamic frequency behavior is improved by implementation of LSP and BB controller with a total time near its optimal setting. The total time at 0 ms and 360 ms for the test case are the limits, within which LSP and BB controller can benefit the dynamic behavior of the MG.

The three optimization criteria determine how long preset and total time should be so that the system dynamic behavior is improved. If one of the three frequency index ra-

tios exceeds 100%, the respective setting of preset and total time should not permitted, because the situation is deteriorated. Comparing the two time parameters of the proposed control method, the frequency deviation is less sensitive to the total time near its optimal value than the preset time. In addition, the total time can variate in a wider range, within which the control effect of LSP and BB controller is barely compromised, than the preset time.

6.4   Discussion

6.4.1   Effects of LSP and BB Controller on Dynamic Limits

A comparison of dynamic operating limits of the simulated islanded MGs having different shares of PV is presented in this section. Table 6.8 lists out the related parameters of the MG.

Table 6.8: Parameters of exemplary islanded microgrid

Parameter	Description	Value
P_{n-L}	Maximum load demand in the MG, which is the base value of active power	$40\,\text{MW}$
p_{L-in}	Initial load supplied by MG in per unit base	$0.5\,\text{p.u.}$
p_{PVact}	PV's current available active power in per unit base	$50\%\ p_{n-PV}$
p_{CGset}	Initial set point of active power of CG in per unit base	$50\%\ p_{n-CG}$
$f_{0_{p.u.}}$	MG's initial frequency in per unit base	$1\,\text{p.u.}$

The dynamic limits of the simulated islanded MG with shares of PV of 25% and 50% are shown in Figure 6.25. As can be seen, both the steady state and dynamic limits in the islanded MG with 25% share of PV are higher than the one with 50% share of PV. This is because less dispatchable active power is available to supply load demand if more PV is integrated. The maximum dynamically allowable negative load step limits are greater than the maximum positive load step limits. This is because both CG and PV participate in stabilizing frequency during frequency rise in case of load reduction whereas only the CG is able to increase its power if frequency drops due to more load to be supplied.

(a) 25% share of PV
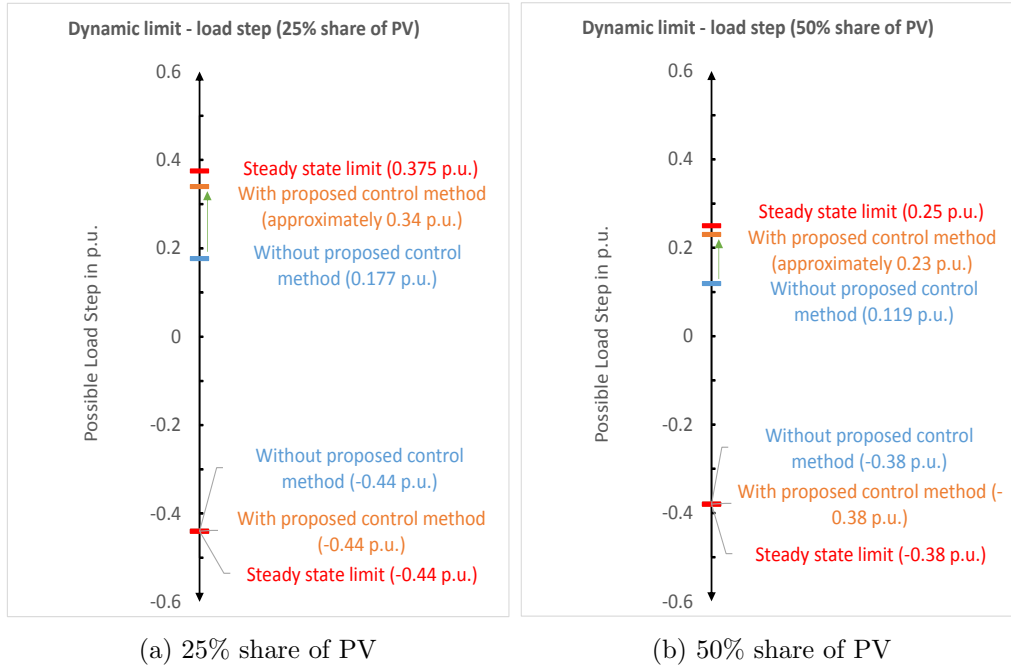
(b) 50% share of PV

Figure 6.25: Dynamic limit improvement by implementing LSP and the
BB controller

If only frequency control is applied in the islanded MG, the allowed maximum positive load step is 0.177 p.u. in the MG with 25% share of PV while the allowed maximum positive load step is 0.119 p.u. in that with 50% share of PV. If LSP and BB controller with optimal preset and total time settings are included in the system, the maximum allowable positive load steps of both MGs are 0.34 p.u. and 0.23 p.u. respectively. In comparison to the MG only with frequency control, the maximum allowable load steps can be brought closer to the steady state limits of the MGs with both 25% and 50% share of PV by implementing the proposed control method. The improvement of the dynamic positive load step limit with LSP and BB controller is larger in the MG with 25% share of PV than with 50% share of PV. Since LSP and BB controller only have an influence on the active power output of the CG, their control effect is stronger and more active power can be dispatched if the MG has a higher share of CG and a lower share of PV.

In the exemplary MG model, the frequency does not exceed 52 Hz, independent from the size of the negative load step. This would probably not trigger over-frequency protection (OFP) action of the CG. However, the situation for a positive load step is different. A

large load increase in this test MG can cause under-frequency protection (UFP) action of the CG at 47.5 Hz.

The reason for the MG not to be stable in case of a large load decrease, although no OFP is triggered, is repeated PV reconnection if the MG's load demand is small. This has been briefly described in section 6.2 for LSP and BB controller having fixed time parameters and the PV reconnection issues will be further discussed in section 6.4.3. Therefore, the dynamic negative load step limits are equal to the steady state negative load change limits. Implementing LSP and BB controller with optimal time parameters can reduce the peak frequency and improve the dynamic behavior at inertia response, but it does not allow dynamic operating limits to exceed steady state limits. Hence the dynamic negative load step limits of the MGs with 25% and 50% share of PV are the same as their respective steady state limits as shown in Figure 6.25. However, in case of a higher initial load, or a lower share of CG, or no immediate reaction to the frequency change from the PV [57], frequency increase may still exceed 52 Hz and trigger the over-frequency protection of the CG. In such a case, the dynamic limits of load decrease can, thus, be different from steady state limit.

6.4.2   Impact of Time Delay

As stated in section 4.3.2, if frequency is above a certain value, according to the VDE-AR-N 4105 standard, PV changes its active power to support stabilizing the system frequency. This behavior is specified as limited frequency sensitive mode at over-frequency (LFSM-O) in the ENTSO-E network code on requirements for grid connection of generators (NC RfG) as well. According to Article 13(2)(e) of the NC RfG, during LFSM-O operation, power generating modules shall be capable of activating a power frequency response with an initial delay that is shorter than 2 s [58]. These 2 s are considered to be the maximum allowable time duration that generators need to react and control their active power output accordingly, without informing related network operators.

In control systems of electrical networks, time delay can degrade system performance and even cause system instability [34, p. 89-91]. As described in chapter 3, under implementation of LSP and BB controller, the CG changes its power generation in advance. In case of pre-generated power from the CG, system frequency increases. The PV reduces its active power infeed to enhance system frequency stability if frequency raises above 50.2 Hz. In conventional power systems with large inertia, the initial delay of 2 s for the PV to activate its power frequency response in LFSM-O is not expected to have a strong impact on system frequency stability. However, it can cause frequency instability issues in islanded MGs, especially if long preset and total time are necessary for them to carry out large load steps. As frequency changes fast in case of a power imbalance due

to low inertia, frequency limits are more likely to be violated during the preset time period because of the delayed power reduction of the PV. Therefore, a shorter maximum time delay for the PV to regulate its active power in response to frequency increase in LFSM-O is beneficial to have a tolerable system dynamic behavior in islanded MG under the implementation of the proposed control method. According to section 5.4.2, the maximum allowable preset time to make frequency reach its upper limit during the CG pre-generating period is 191 ms for the test MG, without considering the frequency-dependent PV power reduction. As this is equivalent to an infinite LFSM-O time delay for the PV, a shorter time delay may allow a longer preset time setting as shown in Figure 6.20. In such a case, load step limits are extended. Therefore, the investigations in this thesis can be used as a definition of the following extreme cases:

- no time delay: perfect frequency measurement and LFSM-O implementation;

- very long time delay: current state of the art of frequency measurement.

There are two kinds of delay considered in this thesis, namely measurement and communication delay. As described in [57], frequency measurement in 50 Hz systems can be updated at a rate between 10 and 50 frames per second with available phasor measurement unit devices. In case of a rate of 10 frames per second, the measurement is updated every 100 ms. This means that control systems keep previously measured frequency until a new measurement is reported. Communication infrastructure plays a key role for operation and control of electrical power systems. Communication delay refers to the duration of the transmission of measured signals to the control center. For large power systems, communication delay cannot be avoided due to long distances between their elements. This delay is usually in the range of 0.1 s to 1 s [34, p. 89-91]. In islanded MGs, as distances are shorter, the communication delay of measurements tends to be smaller. However, overhead may cause a constant "offset" communication delay which may be significant depending on the used technology. As communication between microgrid central controller (MGCC) and local controllers (LCs) is necessary for the proposed control method, the impact of communication delay cannot be neglected.
In this section, the impact of time delay, involving both measurement and communication delay, as one potentially severe problem in the operation of LSP and BB controller is analyzed. For the investigation, the measurement of the actual MG's frequency is assumed to be reported to the PV generator with different settings of time delay[20]. The defining parameters of the simulated MG are listed out in Table 6.9.

---

[20]This time delay is realized by adding one first-order lag block between the actual system frequency signal and the look-up table for PV's frequency-dependent active power characteristic curve in the PV model in Simulink as shown in Figure 4.13.

Table 6.9: Settings of exemplary islanded microgrid in per unit base

Parameter	Description	Value
s_{CG}	Share of CG	50%
s_{PV}	Share of PV	50%
p_{n-CG}	Rated active power of CG	0.5 p.u.
p_{n-PV}	Rated active power of PV	0.5 p.u.
p_{L-in}	Initial load supplied by MG	0.5 p.u.
p_{PVact}	PV's currently available active power	0.25 p.u.
p_{CGset}	Initial set point of active power of CG	0.25 p.u.
Δp_L	Expected load change in MG	0.15 p.u.
f_0	MG's initial frequency	50 Hz
T_{CG}	CG's starting time constant	0.6 s

According to Table 6.9, the test MG with 50% share of PV is supposed to supply 0.5 p.u. load initially at nominal frequency. At $t = 0$, a load step increase of 0.15 p.u. is expected. In this case, the nadir of the frequency deviation can be approximated based on equations (4.13), (4.10), (5.30) and (5.31) as

$$
\begin{aligned}
f_{p.u.}(t = t_{adp}) &\approx -\frac{\Delta p_L^2}{T_{MG} \times \left.\dfrac{dp}{dt}\right|_{max}} + 1 \\
&= -\frac{(0.15\,\text{p.u.})^2}{0.6\,\text{s} \times 50\% \times 0.5\,\text{p.u.}/\text{s}} + 1 \\
&= 0.85\,\text{p.u.}
\end{aligned}
$$

The approximation indicates that frequency drop caused by a 0.15 p.u. load increase in the MG without the proposed control method is far below the lower limit 0.95 p.u. (47.5 Hz). Without LSP and BB controller, the load step increase cannot be carried out in the MG with the parameters given in Table 6.9. A simulation of this event shows the same result. Therefore, LSP and BB controller should be applied additionally to improve MG's frequency stability. Following optimization criteria 1 and 3 as mentioned in section 5.4.3, the optimal preset and total time are 140 ms and 300 ms, respectively. To investigate the impact of delay, dynamic simulation results of the exemplary MG,

in case of instant PV reaction on frequency changes, reaction with 100 ms delay or no reaction at all, are presented in Figure 6.26.

As can be seen, the system's dynamic behavior of the islanded MG under three different settings of time delay does not show significant differences. Because of preset time being 140 ms, the preemptively increased active power of the CG causes frequency to exceed 50.2 Hz. If PV reacts immediately on frequency changes, PV decreases the active power by approximately 8% of its rated power at most. For the case of PV not reacting on frequency deviations, there is no active power reduction of PV in the MG. If there is a 100 ms delay in updating frequency measurement, the power reduction of PV is also delayed for 100 ms and the highest decrease is 3% of the rated power. Since the active power of PV is decreased most in the MG without measurement and communication delay, its frequency at the end of the preset time interval is lowest. At $t = 0$, the load step is carried out. The rate of change of frequency (ROCOF) stays negative until power generation equals load demand. This means that frequency continues dropping till the end of the total time interval, if total time is optimized, and therefore, runs out when power balance is reached. For the MG without delay, PV reduces its active power as a reaction on frequency exceeding 50.2 Hz, and thereby, limits the frequency peak at the end of the preset time interval (blue solid curve). The peak value of frequency is, thus, lower in comparison to the other two cases with time delay as can be seen in Figure 6.26. The effect of instant active power reduction of the PV generation is responsible for the slightly smaller MG frequency after the load step is carried out. Therefore, when the BB control signal ends, the MG's frequency is nearly at the value defined by the settings of the CG's droop control. If there is a time delay in updating frequency measurement to the PV, frequency at the end of the total time interval is higher than it should be corresponding to the amount of active power generation of the CG following its droop settings. Hence, after activation of BB control, there are further frequency deviations caused by droop control as shown by yellow dashed and red dotted lines. The longer the measurement and communication delay are, the bigger the frequency deviations after the total time interval are. However, this does not lead to a frequency instability in the MG under the given parameters, because the frequency deviations are small in comparison to those caused by the load step.

According to the simulation results of the test cases, the improvement of the dynamic behavior of the MG with time delay on frequency measurement and communication by implementation of the proposed control method is similar to that of the MG without delay. The optimal settings of preset and total time determined by criteria 1 and 3 if PV reacts instantly are also valid for the cases if frequency measurements are updated to PV with time delays. As discussed in section 5.4.2, system frequency at the end of the preset time interval is approximated without considering frequency-dependent active
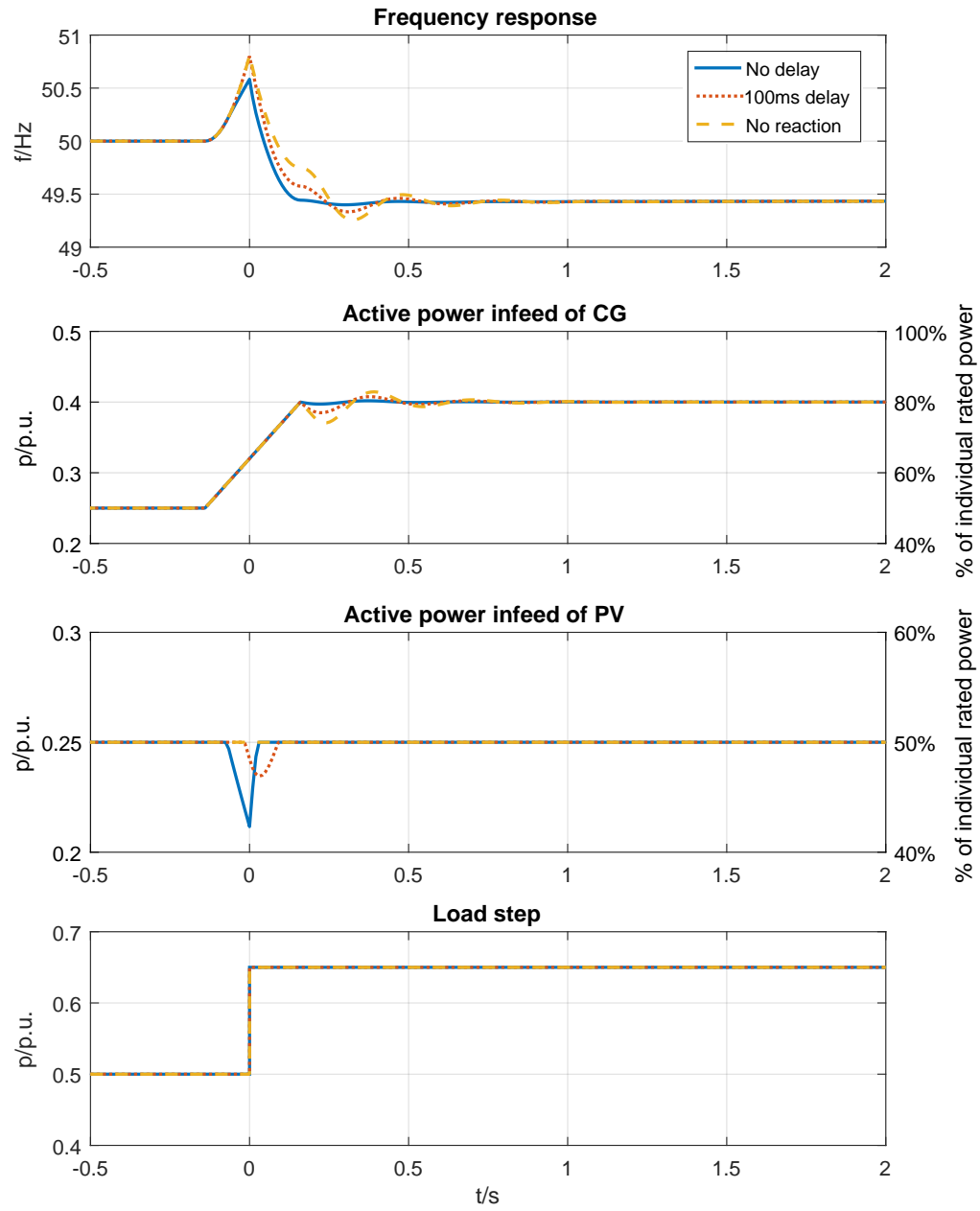
Figure 6.26: Dynamic simulation results of the test islanded microgrid
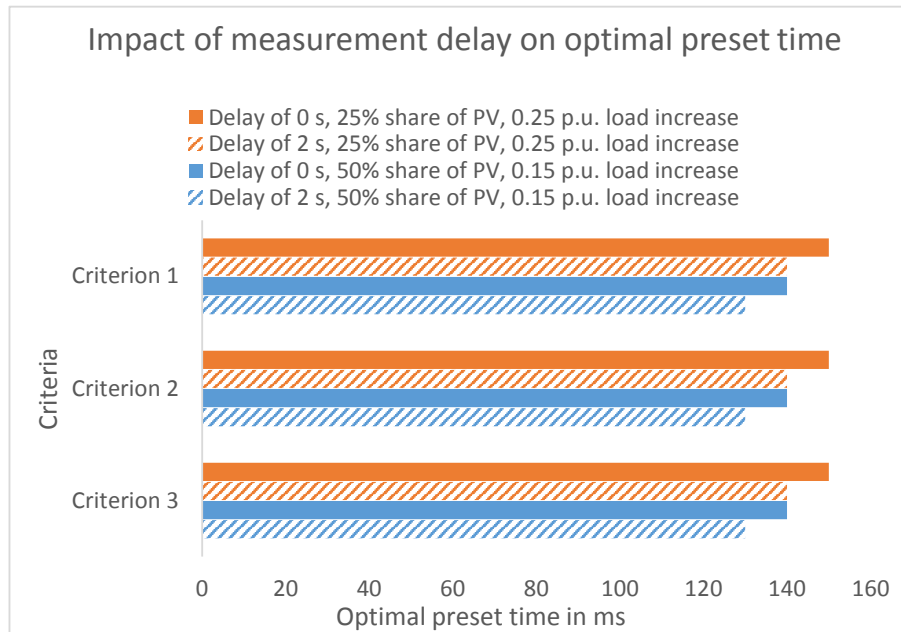
(a) Preset time
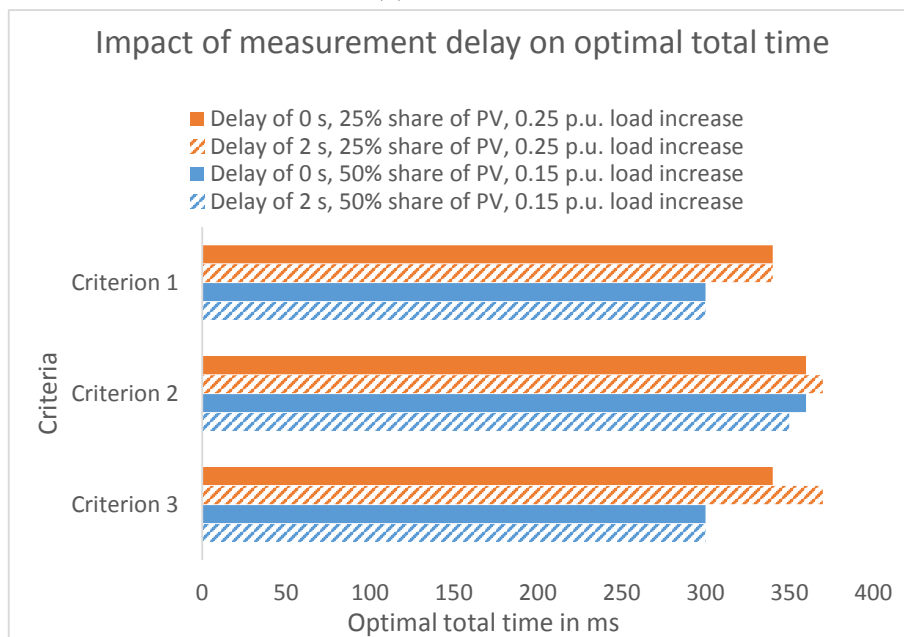
(b) Total time

Figure 6.27: Impact of measurement delay

power reduction of PV, as shown by the yellow dashed line in Figure 6.26. Therefore, regardless of share of PV in the islanded MG with measurement and communication delay, preset time of the proposed control method should be set to be strictly smaller than or equal to the values that are determined by frequency limits presented in Figure 5.12. Figure 6.27 shows the optimal settings of preset and total time determined by the three criteria described in section 5.4.3 under different time delays.

As for the test cases, there is only a $\pm$ 10 ms difference for both preset and total time between the MG with no delay and a large time delay. There is nearly no influence of frequency measurement delay on the optimal settings of time parameters for LSP and BB controller. Therefore, the optimal preset and total time applied in the MG without measurement and communication delay are the optimum for the MG if there is small time delay as well. However, if share of PV or load step is large enough, a preset time being bigger than its allowable value, e.g. 191 ms for load increase or 154 ms for load decrease as described in section 5.4.2, can be required. In such a case, disconnection of PV generation or load shedding will be triggered. Those dynamically allowable load steps needing a preset time above the limits in the MG without measurement and communication delay may not be able to be realized in that with delay.

The impact of time delay on the optimal settings of preset and total time is presented more in detail by Figure A11 in Appendix.

6.4.3   PV Reconnection Issues

This reconnection issue caused by the PV generation has been discussed and solution is given in [22]. As stated above, by implementing LSP and the BB controller, the maximum sudden load increase which can be handled by the system can be improved to some extent. However, they cannot improve the response to a load decrease because of an issue of repeated PV reconnection which is presented in Figure 6.28.

As it can be seen, LSP and the BB controller can reduce the transient peak frequency by decreasing the CG active power before the load release. The PV generator still cannot find a steady point along the P-f curve according to the VDE-AR-N 4105 even though the CG would cut its power output and go to idle mode. This is because the islanded MG has a high share of PV, low controllable capacity of the CG and low load demand. The PV generator disconnects from the rest of the grid once frequency exceeds 51.5 Hz. When the system frequency has returned to the range between 47.5 Hz and 50.05 Hz for more than 60 s, PV starts to reconnect to the grid. However, before its infeed power reaches the lowest active power steady point of the P-f curve, the PV generator disconnects again because of over-frequency. It tries to connect to the grid repeatedly after disconnections, when the system frequency is back to the reconnection range. Hence the frequency is
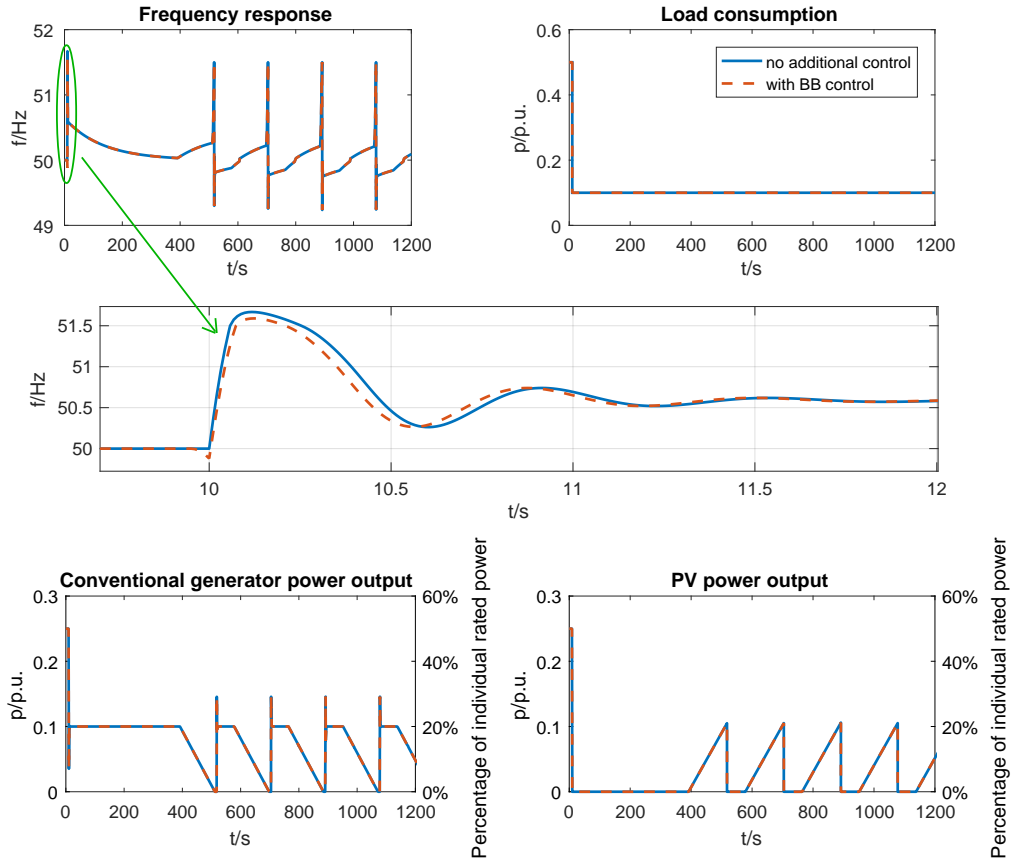
Figure 6.28: Dynamic simulation results of islanded MG without adapted
reconnection schemes

not stabilized. The dynamic negative load step limit is closely related to the system
steady state load change limit. Other control methods are required in case of a large
load loss in MGs.

Scenario 1: After the PV generator disconnects from the rest of the MG because of over-
frequency, it will reconnect to the grid when the reconnection conditions are fulfilled.
If the reconnection is not successful, it will be repeated after 60 s. The reconnection of
the PV generator will be stopped after twice trying to reconnect and failing to reach a
steady state. The PV generator can then only reconnect again when there is sufficient
load in the MG again.

Scenario 2: The MGCC checks the available CG capacity and load demand regularly.
If the controllable CG capacity or load is smaller than the lowest active power steady

point on the P-f curve from VDE-AR-N 4105, which is 48% of the PV actual possible active power, PV should not reconnect after a disconnection. Otherwise, PV is allowed reconnect to the MG.

Scenario 3: Instead of the characteristic curve which is provided by the VDE-AR-N 4105 standard, a new PV characteristic curve between 50.2 Hz and 51.5 Hz is proposed to be a linear function for islanded MG operation. The modified characteristic curve is presented in Figure 6.29.
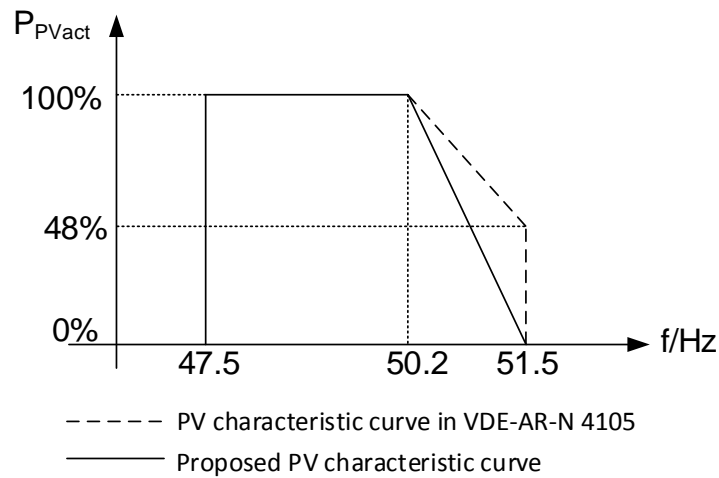
Figure 6.29: Proposed PV characteristic curve in islanded MG operation

Scenario 4: The MGCC gathers information of the available CG capacity and load demand, and gives a command to the PV generator to only feed in a certain percentage of the available PV active power to the grid. This percentage is the ratio of load to the lowest active power steady point of the P-f curve. The amount of power supplied by the PV generator should cover the load demand and ensure the grid stability.

To improve the system stability, four additional control scenarios for the reconnection process are implemented in the islanded MG with LSP and the BB controller. The simulation results are shown in Figure 6.30.

As shown in the graph, all 4 different control scenarios can prevent the frequency oscillation from the repeated PV reconnection shown in Figure 6.28. The possible steady state operating points of the MG can be extended by applying these control scenarios, so that the maximum negative load step that the system can support can be increased from the previous limit 0.38 p.u. to 0.5 p.u. Both scenario 1 and 2 block the PV generator to reconnect to the grid, scenario 1 after two unsuccessful events, and scenario 2 right away. Hence, the CG supplies the load alone after PV disconnection. Scenario
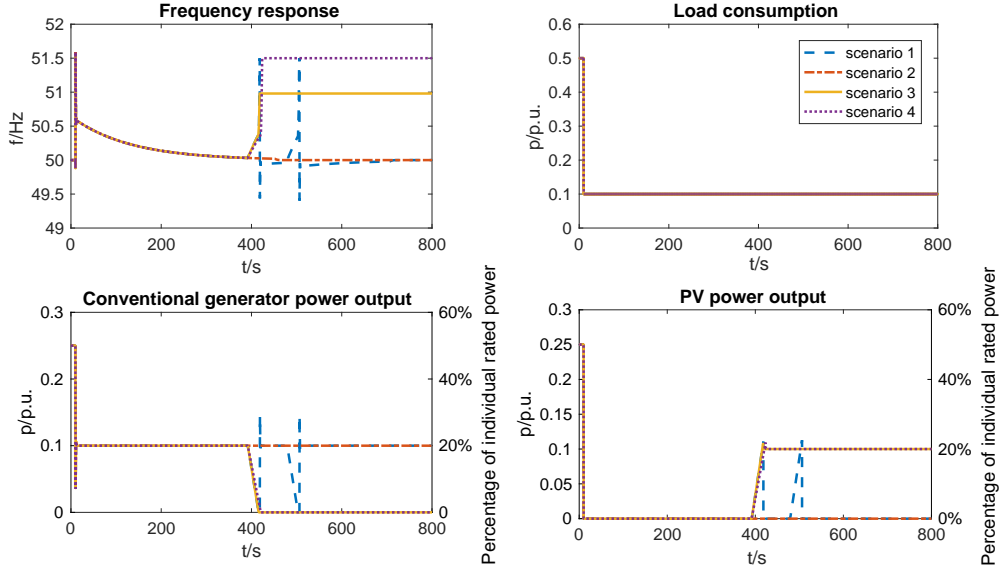
Figure 6.30: Frequency response under four different reconnection control scenarios

3 changes the sharp switching off action of the PV generator at 51.5 Hz to a smooth linear curve. It offers the possibility to the PV generator to always find a steady point for its active power infeed along the modified P-f characteristic curve. Therefore, the PV generator provides power to the load when the load decreases. Scenario 4 requires a certain percentage of PV power to feed into the MG depending on the available CG capacity or load demand. This solves the PV repeated reconnection problem, however, the MG frequency is always close to the upper limit when the load demand is lower than the lowest active power steady point on the PV P-f curve.

A comparison of the islanded MG with different control scenarios is presented in table 6.10. According to the table, all four scenarios can increase the possible system steady state operating points, and hence extend the negative load step limit. Scenario 3 and 4 ensure that the PV generator is supplying power after the load decrease, which makes maximum use of renewable energy sources, while scenario 1 and 2 utilize the CG power. Scenario 1 and 3 do not require additional communication, while in scenario 2 and 4, the MGCC collects data regularly from metering devices and sends out control signals to local units. Thus, communication is needed for scenario 2 and 4.

Table 6.10: Comparison of the islanded MG with different control scenarios

Islanded MG with 50% share of PV	Dynamic negative load step limit	Power source in stable condition after load decrease	Communication requirements
Original system (W&WO BB controller)	-0.38 p.u.	PV	Communication for the coordination of MGCC
Scenario 1	-0.5 p.u.	CG	No additional communication needed
Scenario 2	-0.5 p.u.	CG	Communication for MGCC to collect data from metering devices and send control signal
Scenario 3	-0.5 p.u.	PV	No additional communication needed
Scenario 4	-0.5 p.u.	PV	Communication for MGCC to collect data from metering devices and send control signal

Chapter 7

Conclusion and Outlook

7.1 Conclusion

This thesis introduces a novel control method - load step pre-announcement (LSP) and bang-bang (BB) controller - to improve frequency dynamic behavior in islanded microgrids (MGs). The proposed control method can be applied in either centralized or decentralized control architectures depending on the MG's control system structure. As an example, an islanded MG, consisting of a conventional generator (CG), a photovoltaic (PV) generator and a lumped load, is simulated in the Matlab Simulink environment. The CG is regulated by frequency control, including primary and secondary control. The PV generator is operated following a typical P-f characteristic curve as given in the VDE-AR-N 4105 standard. LSP and BB controller are implemented in coordination with frequency control to regulate the CG in the islanded MG. As the main focus, both steady state and dynamic operating limits of the MG under initial conditions of nominal frequency are analyzed. In this section, the important findings of this work are summarized. The main research questions raised in chapter 1 are answered

- Research question: Can the proposed control method benefit frequency stability of islanded MGs? How?

In this thesis, the steady state limit of the MG represents the maximum possible positive and negative load change that can be realized from the initial load. It is influenced by the properties of the MG, such as the initial state of the MG system, the CG operating points and the PV P-f characteristic curve. Unlike the steady state limit that neglects dynamic frequency disturbances caused by the power mismatch, the dynamic operating limit of the MG represents the maximum allowable positive and negative load step that

can be dealt with by the islanded MG taking dynamic frequency deviations into account. Beyond the dynamic operating limit, frequency instability problems can be caused by the inability of the MG to reach a theoretically stable operating point due to system dynamic limitations. The MG's dynamic operating limit is restricted to a baseline defined by the steady state limit.

According to the dynamic simulation results, LSP and BB controller can improve frequency stability of the islanded MG significantly. Preset and total time are the two parameters that define the operation of LSP and BB controller. Different settings of them influence the control effect of the proposed method. Optimal preset and total time result in MG's frequency being least volatile in case of a load change.

In the study case, larger positive load steps can be realized if the proposed control method even with fixed preset and total time is implemented. The improvement of the maximum positive load step depends on the share of PV. Generally, smaller load changes are allowed in systems with a higher share of PV because of less dispatchable generation. This is because only the CG can react to compensate the power imbalance in case of a load increase, whereas both the CG and PV reduce their power when load drops. Thus, the maximum allowable negative load step is greater than the maximum allowable positive load step. Under the assumption that the PV generator reacts to frequency deviations instantly, implementing LSP and BB controller does not have any impact on a large negative load step. The maximum allowable negative load step is mainly governed by the capacity of the CG and the share of PV.

- Research question: How can the time parameters be optimized to obtain the best performance of the proposed scheme? Which parameters have an influence on the choice of preset and total time of LSP and BB controller?

Preset and total time are optimized in this work following three criteria, which determine the smallest frequency deviation band, frequency deviation area index and sum index that combines both. For criterion 1, the frequency deviation band is the difference between maximum and minimum frequency that occurs during the dynamic frequency response. This criterion indicates the limit width of the frequency deviation. If it exceeds a certain value, e.g. $2.5\,\mathrm{Hz}$ in this thesis, the setting of preset and total time is not allowed. Regarding criterion 2, the integral of the square of the frequency difference between final frequency at quasi-steady state after primary control and actual frequency in the time interval from when the load change happens until the end of primary control is calculated. Therefore, frequency deviation has a second-order influence and regulating time a first-order influence on the frequency deviation area index c_{area}. In criterion 3, a sum index, which combines criteria 1 and 2, is calculated. This criterion is highly sensitive to frequency deviation and slightly sensitive to the regulating time, however,

regarding regulating time not as much as criterion 2. Criterion 3 is applied as the indicator to find the optimal preset and total time. Meanwhile, criterion 1 minimizes and limits the absolute frequency deviation and criterion 2 minimizes frequency deviation area. Any setting of time parameters leading to a worse system dynamic frequency behavior in comparison to that of the MG without implementation of LSP and BB controller is not permitted in the proposed scheme.

The choices of preset and total time are influenced by four parameters, namely size of load step, full rate of CG's active power change, share of PV, and CG starting time constant. Optimal total time is found to be as long as the adapting time of the CG to change its active power output to match the expected load change. Unlike total time, it is rather unfeasible to get a reliable mathematical prediction for the optimization of preset time. It nearly has a linear relation to the expected change of CG loading. According to the optimization results, in order to have an optimal MG's dynamic behavior in case of a load change, optimal preset time should be set to be shorter than optimal total time in general. Otherwise, the CG stops adjusting its active power before the load step takes place.

- Research question: How is the performance of LSP and BB controller if the time parameters are not at their optimal values? What if preset and total time are at their optimal values?

Frequency deviation obviously becomes worse when preset or total time is changed into either direction from its optimal value. However, according to the sensitivity analysis of the test case described in section 6.3.4, implementing LSP and BB controller still has a positive effect on the MG's frequency dynamic behavior if preset time varies between $0\,\text{ms}$ and $180\,\text{ms}$ while total time is set to its optimum. Regarding the total time, any values between $0\,\text{ms}$ and $360\,\text{ms}$ enhances frequency stability while preset time is at its optimal value. Therefore, even if preset or total time is not at the optimal value, the proposed control method shows a high tolerance to still benefit the dynamic behavior of the MG for the test case.

Steady state and dynamic operating limit of sample MGs with 25% and 50% share of PV are compared. The steady state limit of the MG with lower share of PV is larger than that with higher share of PV, because more PV generation being integrated into the MG with a fixed total size decreases the dispatchable active power. By applying LSP and BB controller with optimal preset and total time, MG's dynamic operating limit can be maximized. However, optimal time parameters do not increase maximum allowable negative load step, as dynamic operating limit is already as large as the steady state limit in the test case.

- Research question: Would the control effect of LSP and BB controller be worsened if MGs are not operated under ideal conditions, e.g. system has measurement and communication delay?

Since choices of preset and total time define the control effect of the proposed method, it is necessary to investigate what influence time delay of frequency measurement and communication has. A sensitivity analysis of time delay in updating frequency to the PV generator is carried out. According to the results of the study case, there is only a small influence of frequency measurement and communication delay changing the optimal settings of the time parameters for LSP and BB controller only slightly. If share of PV or load step is large enough, a preset time being bigger than its allowable value as given in section 5.4.2 can be required. In such a case, disconnection of PV generation or load shedding will be triggered in the MG with frequency measurement and communication time delay. Those dynamically allowable load steps needing a preset time above the defined limit may not be able to be realized in the MG with delay.

- Research question: How can the dynamic negative load step limit be increased?

To improve the maximum allowable negative load step, four control scenarios for PV reconnection in islanded MGs are presented and compared. According to the comparison of the results as shown in Table 6.10, all four control scenarios are able to extend the possible steady state operating points to be handled by the system, and therefore, increase the negative load step limit. Scenario 3 can be implemented by simply modifying the P-f characteristic curve, hence no additional communication is required. Furthermore, in this scenario, the load demand is supplied by the PV generator after a large load loss instead of the CG.

In conclusion, frequency changes fast when there is a mismatch between power generation and demand in islanded MGs because of their commonly low inertia. LSP and BB controller can support frequency control and improve system dynamic behavior in case of load change in the MG. For a possible implementation, load changes are classified into three categories, namely normal, large and critical load steps. Frequency disturbances caused by normal load steps can be handled by frequency control directly, thus, the proposed control method is not required. Critical load steps refer to the load changes which exceed the system steady state operating limits. Therefore, no matter which kind of control scheme is applied, the load step cannot be realized to reach a stable state. Large load steps can cause severe frequency disturbances, meaning the frequency nadir being below or above critical limits, e.g. below 49 Hz or above 51.5 Hz in this thesis, in the MG. In these cases, the system frequency would not be stable without emergency control, like activating load shedding or cutting off the PV generation. By implementing

the proposed control method to limit peak frequency, large load steps can be conducted though. LSP and BB controller are considered to improve system dynamic behavior in case of large load steps occurring in the islanded MG. They are simple to be designed, implemented and operated. It is the best solution to combine LSP and BB controller and scenario 3 to improve frequency stability and avoid repeated PV reconnection in islanded MGs. With the combination of the proposed control method and scenario 3, bigger load steps, both positive and negative, can be realized without causing frequency instability issues.

7.2   Outlook

As discussed in chapter 6, optimizing preset and total time can maximize the control effect of LSP and BB controller. There is only a reasonable mathematical prediction for optimal total time but none for optimal preset time. Therefore, optimal total time can be directly calculated and applied in any MG setup. In the current situation, optimal settings of preset time have to be obtained via simulations for every particular case. Hence further investigation on an approximation for optimal preset time is highly beneficial to the application of this proposed control method.

In this thesis, load change are simulated by step signals. Investigating the impact of the proposed method on other kinds of load changes, e.g. ramp signals, may also be of interest. In case of a load ramp signal, a comparison between full rate of CG's active power change and slope of load ramp signal may show an optimal switch-on and -off rate of load signals as well as different optimization of preset and total time for the proposed control method.

Maximum allowable positive load step limits are the main concern in this thesis. Because of the setup of the study cases, maximum allowable negative load step limits are the same as steady state limits. In case of different negative steady state and dynamic operating limits, the influence of settings of time parameters on the control effect of LSP and BB controller under load decrease may still be investigated. A comparison between optimal settings of time parameters for the same positive and negative load steps in the MG may help defining optimal preset time.

All study cases in this thesis are investigated assuming the initial frequency being at its nominal value. However, realistically this often is not the case. An analysis of LSP and BB controller implemented under initial conditions of non-nominal frequency is necessary for a further application-related understanding of this control method.

In addition, since MGs can be operated both in grid-parallel and islanded mode, LSP and BB controller should be further studied in both modes as well as during the transient

period from one to another.

In this thesis, the analysis of the proposed control method is only based on simulation results. A test of LSP and BB controller in a laboratory-based MG may give a deeper insight to the implementation and real performance of this method.

Appendix
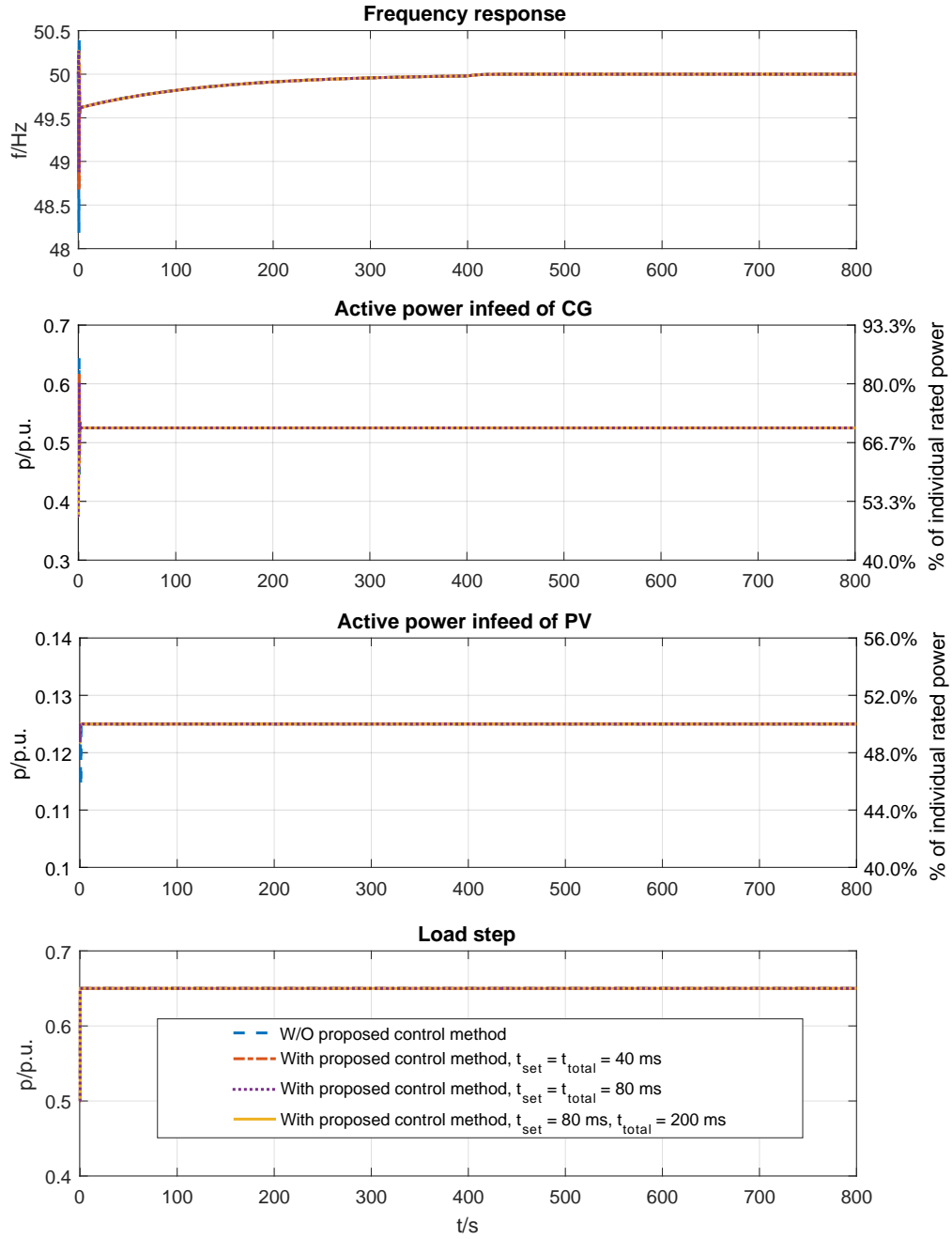
Figure A1: Dynamic simulations of islanded microgrid under different control methods
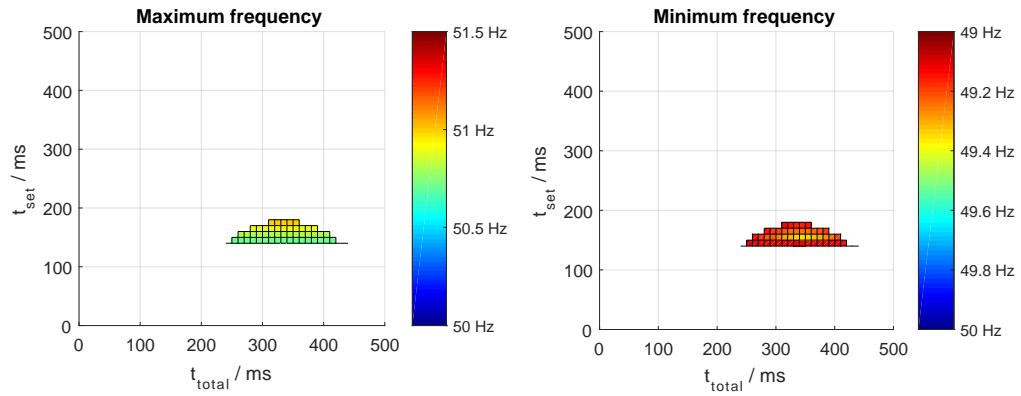
Figure A2: Top view of maximum and minimum frequency in the islanded MG with 25% share of PV under a load increase of 0.25 p.u. (points with frequency above 51.5 Hz or below 49 Hz eliminated)
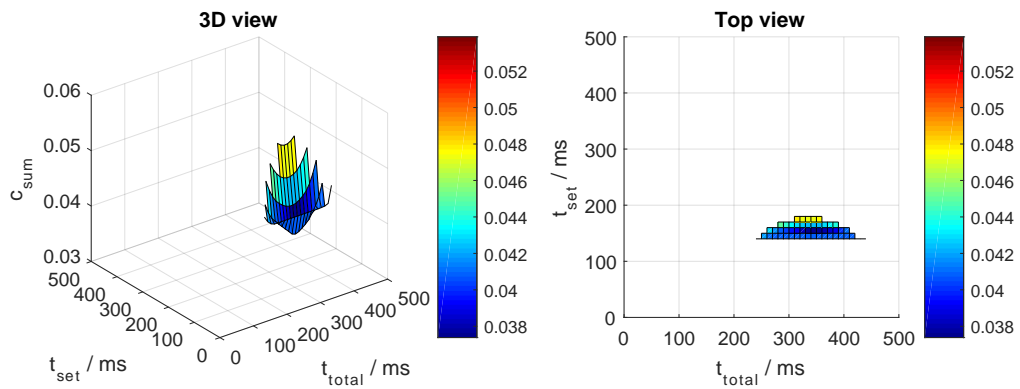
Figure A3: Sum of relative values of frequency band and frequency deviation area following criterion 3 in the MG with 25% share of PV under a load increase of 0.25 p.u.
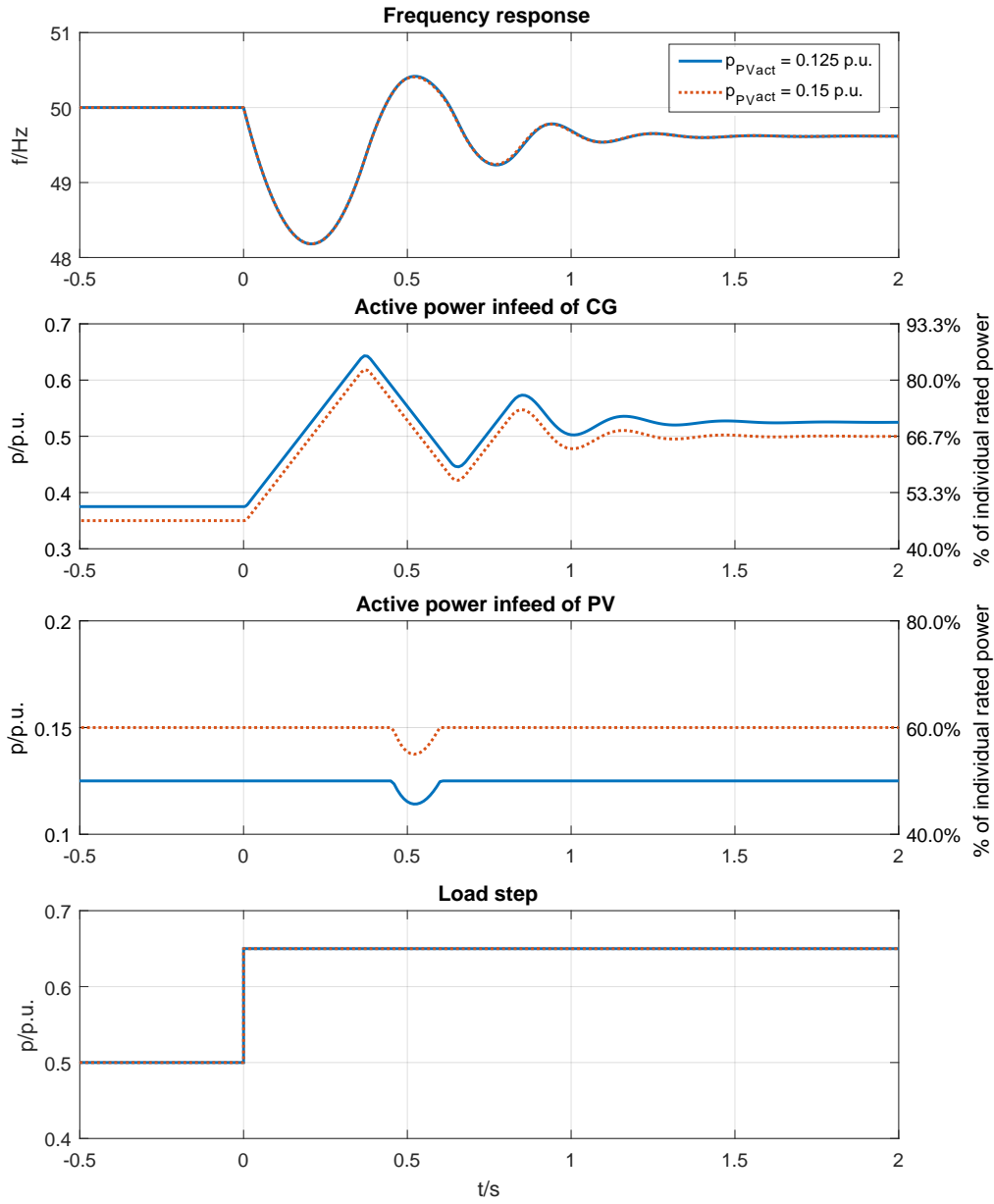
Figure A4: Dynamic simulations of islanded microgrid with 25% share of PV under different PV available active power
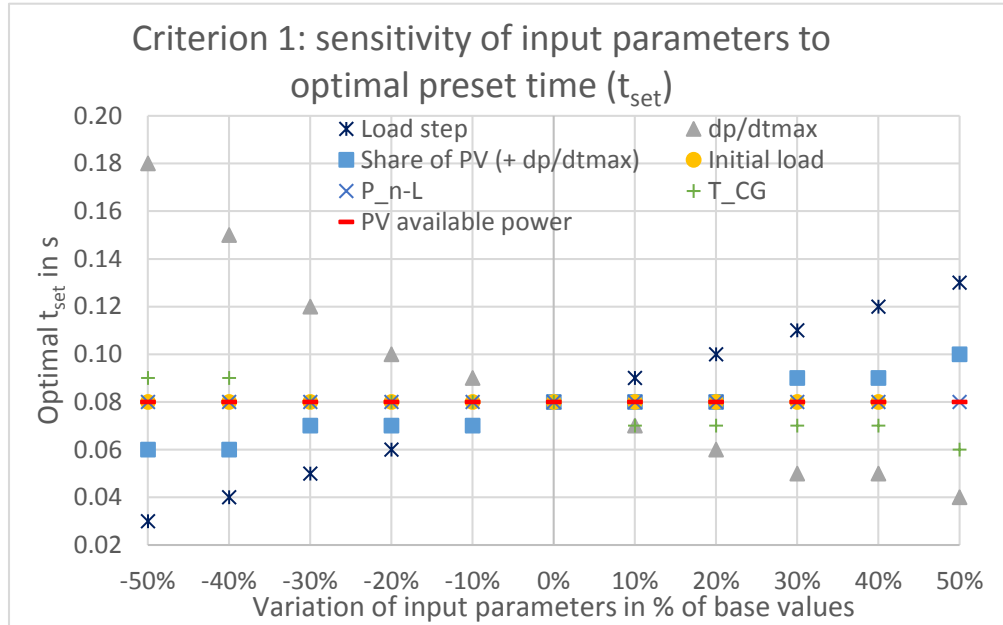
(a) Optimal preset time
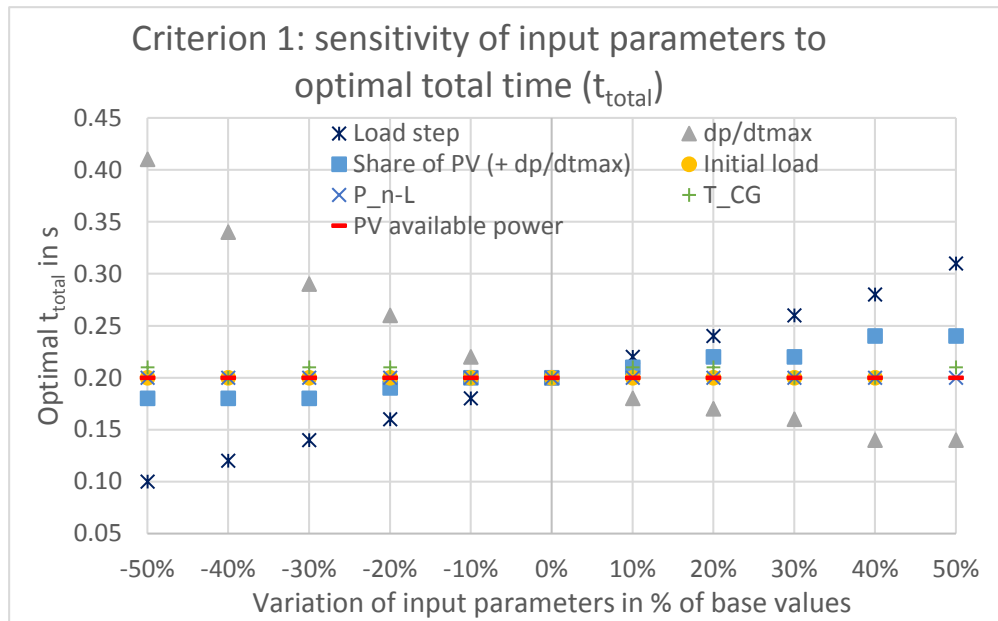
(b) Optimal total time

Figure A5: Sensitivity of input parameters to optimal outcomes (criterion 1)
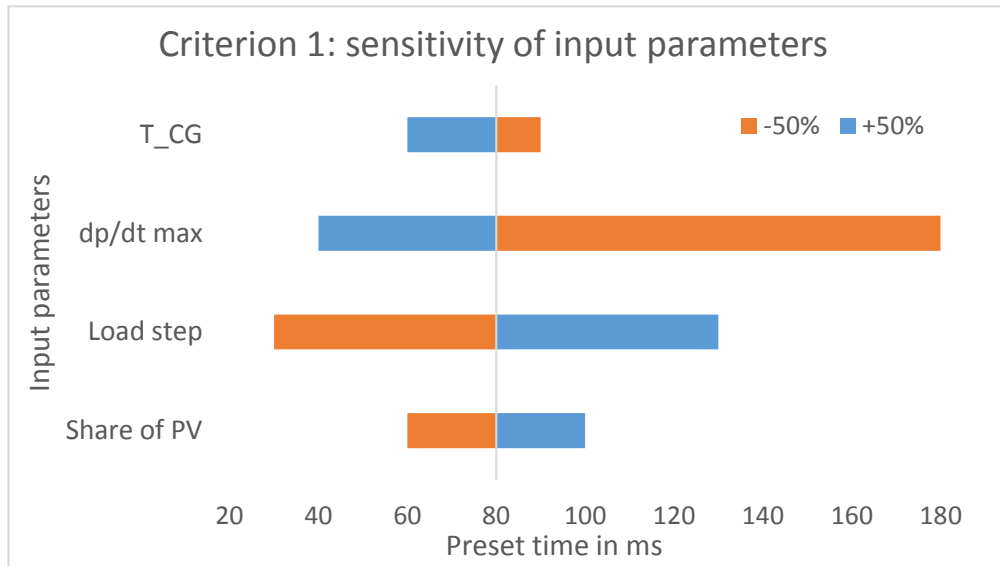
(a) Optimal preset time
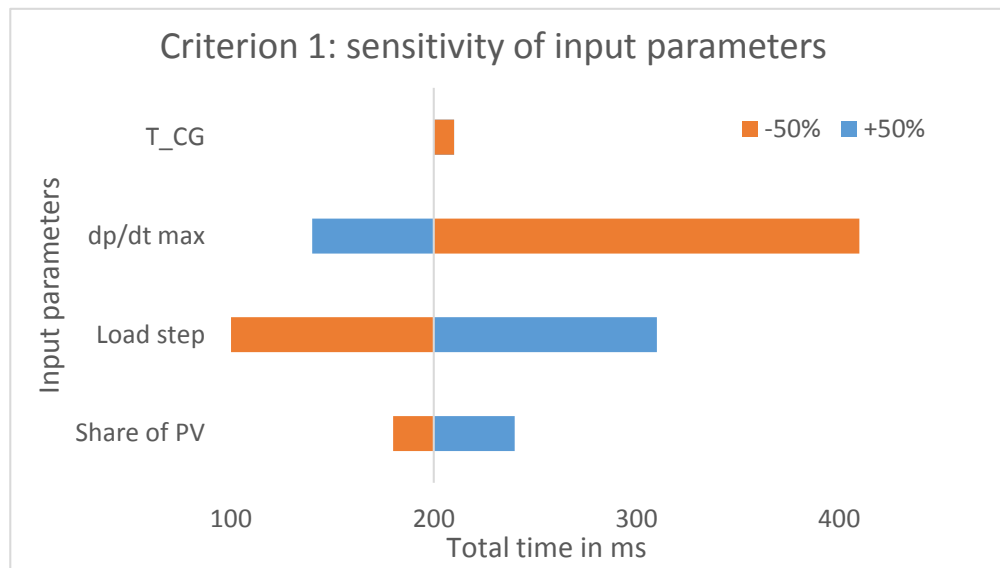
(b) Optimal total time

Figure A6: A comparison of sensitivity of input parameters to optimal outcomes (criterion 1)
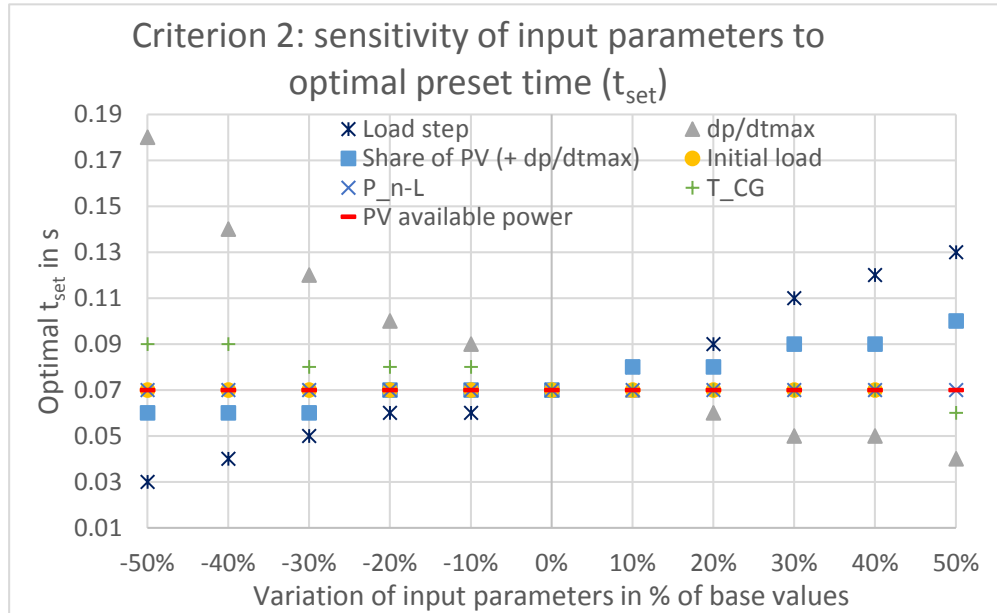
(a) Optimal preset time
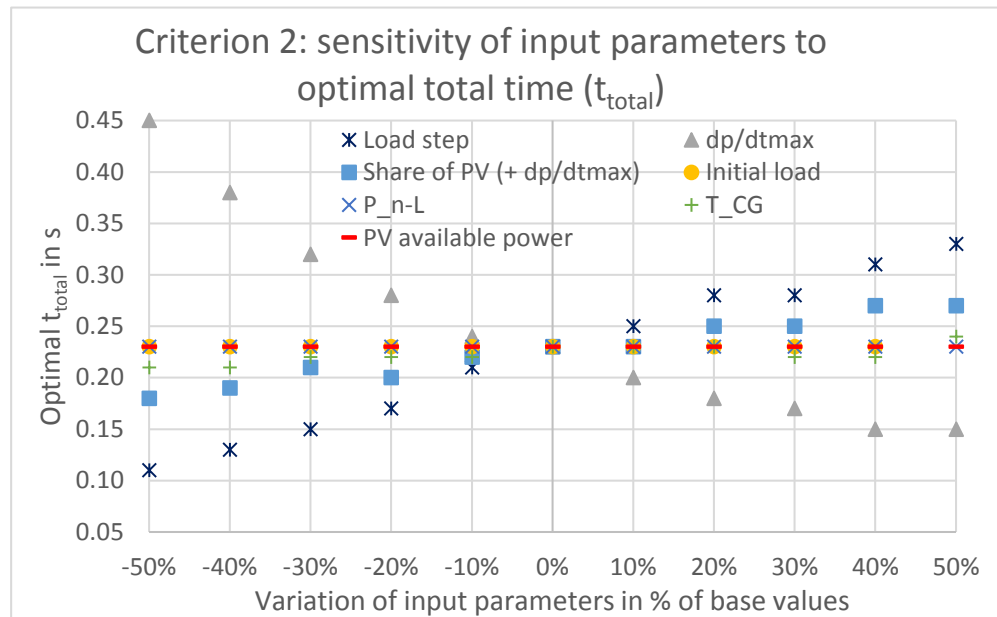
(b) Optimal total time

Figure A7: Sensitivity of input parameters to optimal outcomes (criterion 2)
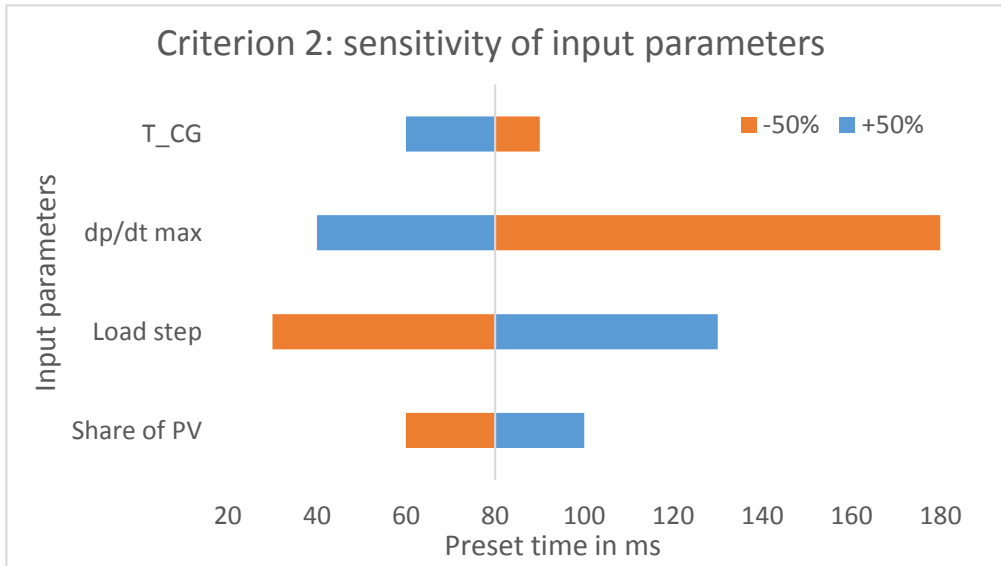
(a) Optimal preset time
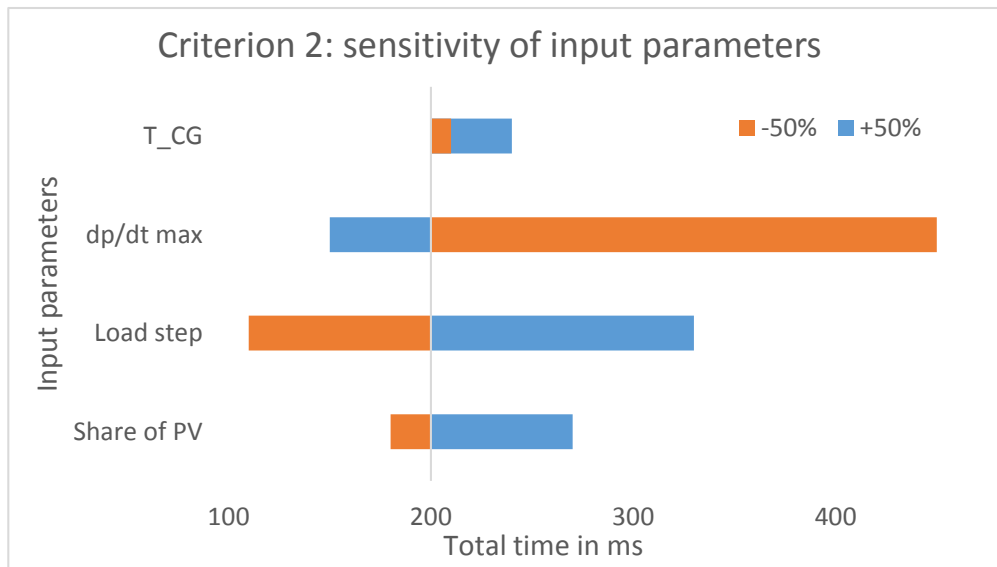
(b) Optimal total time

Figure A8: A comparison of sensitivity of input parameters to optimal outcomes (criterion 2)
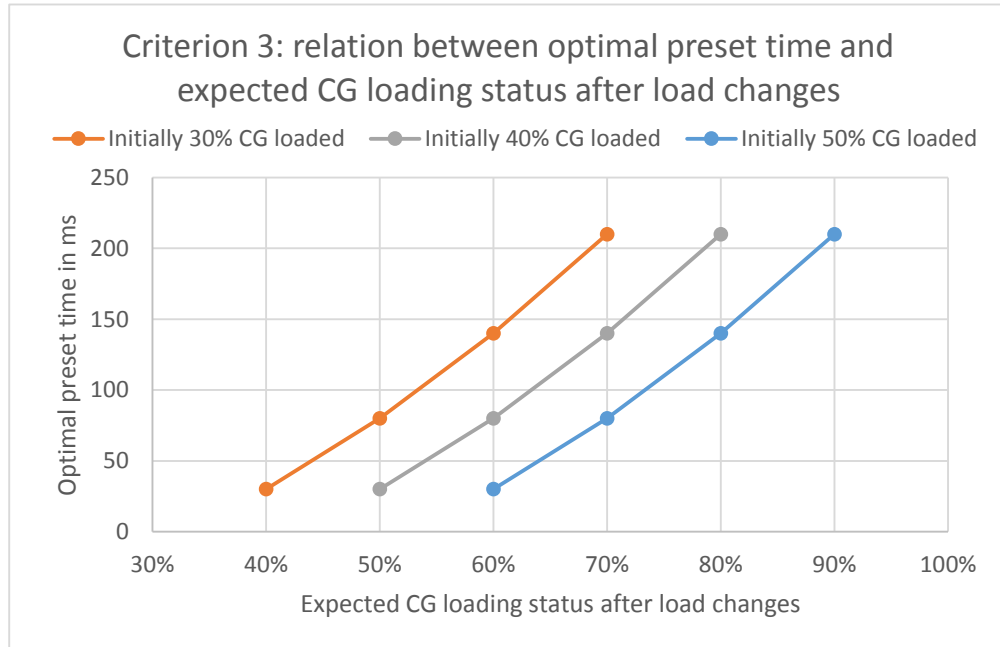
Figure A9: Relation between optimal preset time and expected CG
loading status after load changes (50% share of PV) [21]

_____

[21] Because of the system dynamics of the simulated MG, the nadir of the frequency deviation
gets critical to the system stability if a load step exceeds 0.5 p.u., even though the CG is less
than 50% loaded initially.
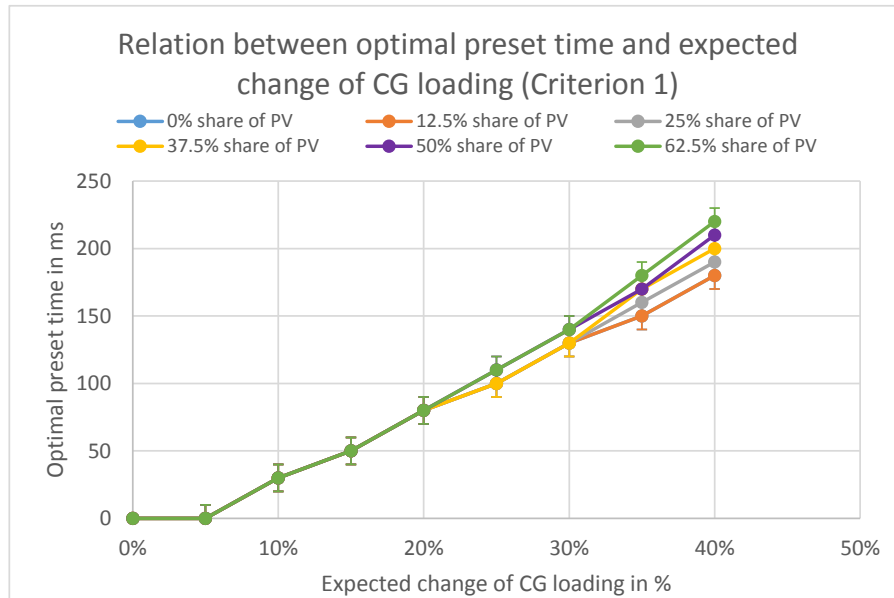
(a) Criterion 1
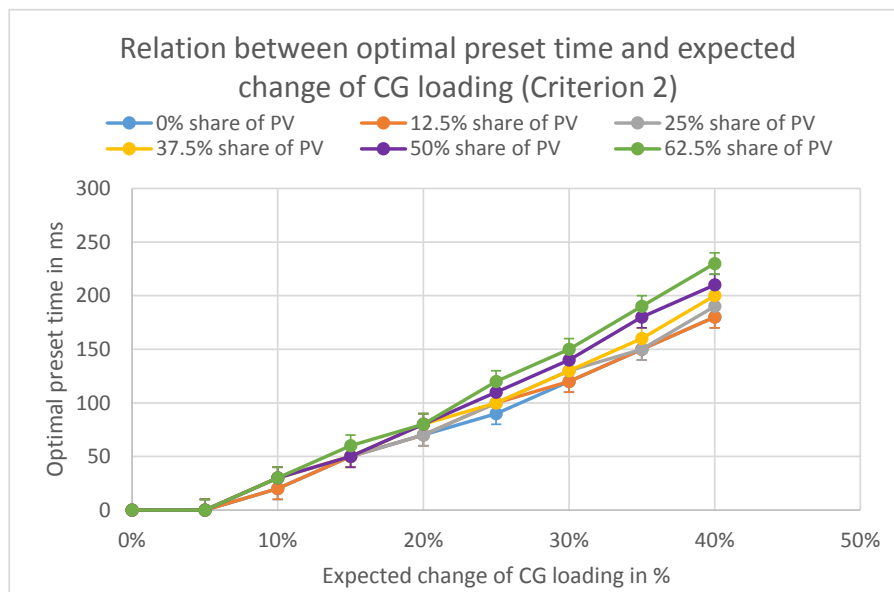
(b) Criterion 2

Figure A10: The relation between optimal preset time and the expected change of CG loading in case of a load change
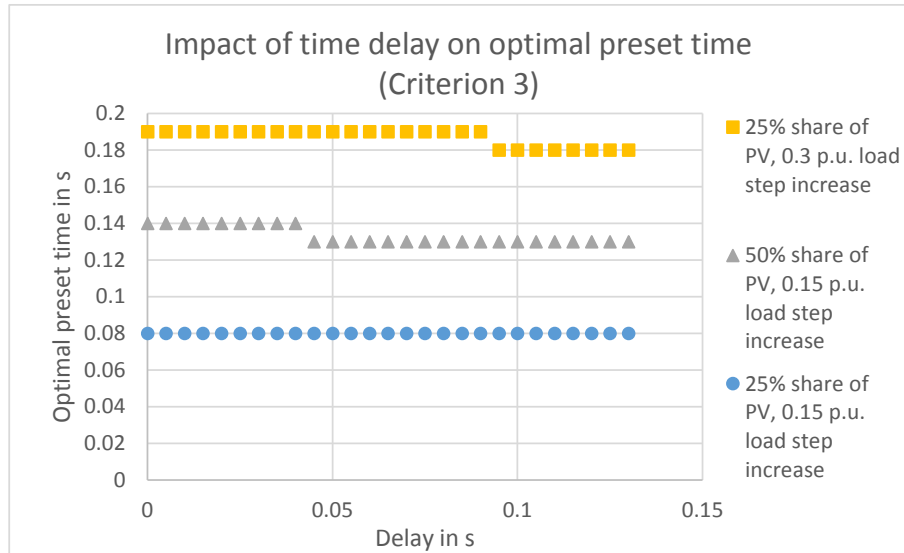
(a) Preset time
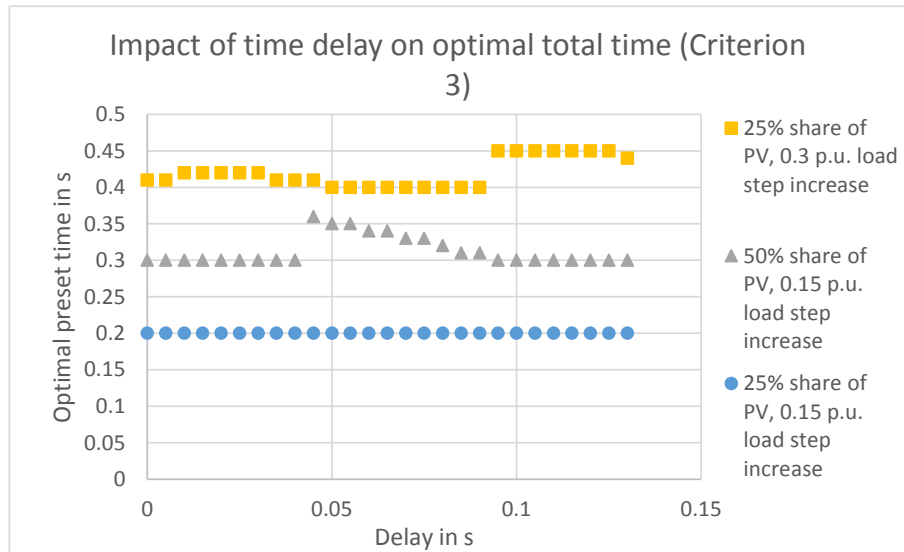
(b) Total time

Figure A11: Impact of measurement delay on optimal settings of time parameters (criterion 3)

List of Abbreviations

BB	Bang-Bang
CG	Conventional Generator
DER	Distributed Energy Resources
DG	Distributed Generation
EHV	Extra High Voltage
FCR	Frequency Containment Reserve
FRR	Frequency Restoration Reserve
GHG	Greenhouse Gases
HV	High Voltage
IEC	International Electrotechnical Commission
LC	Local Controller
LFSM-O	Limited Frequency Sensitive Mode at Over-frequency
LSP	Load Step Pre-announcement
LV	Low Voltage
MAS	Multi Agents System
MG	Microgrid
MGCC	Microgrid Central Controller
MV	Medium Voltage
NASA	National Aeronautics and Space Administration
NC RfG	Network Code on Requirements for Grid Connection of Generators
OFP	Over-Frequency Protection
p.u.	Per Unit
PCC	Point of Common Coupling
PI	Proportional-Integral
PV	Photovoltaic

ROCOF	Rate of Change of Frequency
RR	Replacement Reserve
SI	The International System of Units
TSO	Transmission System Operator
UFLS	Under-Frequency Load Shedding
UFP	Under-Frequency Protection

List of Nomenclature

$\Delta\omega$	Angular speed deviation
Δf	Frequency deviation
$\Delta f_{p.u.}$	Frequency deviation between initial set point and the value at quasi-steady-state in the islanded microgrid in per unit base
Δf_{PV}	Frequency difference between the actual frequency and $50.2\,\text{Hz}$
Δp_{CG}	Power change of the conventional generator in the islanded microgrid in per unit base
$\Delta p_{CG}(t)$	The active power change of the conventional generator in per unit base within the preset time
ΔP_D	Active power change of diesel generator
Δp_L	Expected load change in the islanded microgrid in per unit base
Δp_{PV}	Power change of the photovotaic generator in the islanded microgrid in per unit base
$\Delta f_{PV0_{p.u.}}$	Frequency difference between $50.2\,\text{Hz}$ and the initial frequency in per unit base
$\Delta f_{PV\,p.u.}$	Frequency difference between the frequency at quasi-steady-state and $50.2\,\text{Hz}$ in per unit base
$\dfrac{1}{k_{p.u.}}$	Droop setting on the base value of the maximum load demand P_{n-L} in per unit base
$\dfrac{1}{k}$	Frequency droop control setting
$\dfrac{d\omega}{dt}$	The angular acceleration of the rotational body

$\dfrac{df}{dt}$	The rate of change of frequency
$\dfrac{dP}{dt}$	The rate of the active power change of the conventional generator
$\left.\dfrac{dP}{dt}\right\|_{max}$	Limits of rate of change of power imposed by control valve rate limits of the conventional generator
$\left.\dfrac{dp}{dt}\right\|_{max}$	Limits of rate of change of power imposed by control valve rate limits of the conventional generator in per unit base
$\dot{P}_{down}$	Maximum rate of power reduction imposed by control valve rate limits
$\dot{P}_{up}$	Maximum rate of power generation imposed by control valve rate limits
ω	The angular speed of the rotor of the conventional generator
ω_i	Mechanical angular speed of ith generator
ω_n	The rated speed of a generator
$\sum P_G$	The sum of power output from all generating units
$\sum P_G(t)$	The sum of actual active power output from all generating units
$\sum P_L$	The sum of load demand in the electrical network
τ_n	The rated torque of a generator
τ_a	The net accelerating or decelerating torque
τ_{el}	Electrical torque
τ_{mech}	Mechanical torque
C	Arbitrary constant
$c_{area-ref}$	Reference point of frequency deviation area index when no LSP and BB controller are used in microgrid
c_{area}	Frequency deviation area index
$c_{sum-ref}$	Reference point of sum index when no LSP and BB controller are used in microgrid
c_{sum}	Sum index of frequency deviation band and frequency deviation area
E_{rot}	Rotational kinetic Energy

f	System frequency
$f(t)$	The actual frequency of the microgrid
f_0	Frequency set point
f_n	The nominal frequency
$f_{0_{p.u.}}$	The set point of frequency in per unit base
$f_{\_act}$	Actual system frequency in simulation model
$f_{\_ref}$	Nominal frequency in simulation model
f_{act}	Current system frequency
$f_{band-ref}$	Reference point of frequency deviation band when no LSP and BB controller are used in microgrid
f_{band}	Frequency deviation between the maximum and minimum frequency that appears in the MG dynamic frequency response after a load change
f_{base}	Base value of frequency
f_{Max}	System frequency when there is no load in the grid
f_{max}	The maximum frequency that appears in the MG dynamic frequency response after a load change
f_{Min}	System frequency at full load
f_{min}	The minimum frequency that appears in the MG dynamic frequency response after a load change
$f_{p.u.}$	System frequency in per unit base
$f_{p.u.}(t)$	The actual system frequency of the microgrid in per unit base
$f_{p.u.}(t = t_{adp})$	Approximated frequency nadir at end of inertia response in per unit base
$f_{qss_{p.u.}}$	The final frequency at the quasi-steady state after primary control
f_{qss}	The final frequency at the quasi-steady state after primary control
f_{ref}	The frequency set point
f_{set}	Set points of frequency of photovoltaic generator

J	Combined moment of inertia of generator and turbine
J_{Gi}	Individual moment of inertia of ith generator
J_i	Adapted individual moment of inertia ith generator
K_1	Very high pressure turbine power fraction
K_3	High pressure turbine power fraction
K_5	Intermediate pressure turbine power fraction
K_7	Low pressure turbine power fraction
K_i	Controller integral gain
k_{Pf}	The active power reduction rate depending on the frequency change
K_p	Controller proportional gain
l_{CG}	The loading status of the conventional generator
n_{act}	The actual speed of rotation of the rotor of the synchronous generator
n_{ref}	The reference speed of rotation of the rotor of the synchronous generator
P	Active power
p	Active power in per unit base
P_n	The nominal or rated active power of a generator
P_{0i}	Dispatched power of ith generator defined at nominal frequency
p_0	Dispatched power of the CG defined at nominal frequency
p_actual	Actual power output in simulation model
p_ref	Power set point in simulation model
p_{act}	Measured actual values of active power of synchronous generator
P_{CGmax}	The maximum power output of the conventional generator
p_{CGmax}	The maximum power output of the conventional generator in per unit base
P_{CGmin}	The minimum power output of the conventional generator

p_{CGmin}	The minimum power output of the conventional generator in per unit base
P_{CGset}	The power set point of the conventional generator
p_{CGset}	Power set point of conventional generator in per unit base
P_{CG}	The active power output of the conventional generator
p_{CG}	The active power output of the conventional generator in per unit base
$P_{CG}(t)$	The actual active power output from conventional generator
$p_{CG}(t)$	The actual active power output from conventional generator in per unit base
P_{el}	The dissipated electrical power from generator
P_{GV}	Active power output of steam turbines after speed deviations
P_{iMax}	Maximum primary control power of ith generator
P_{iMin}	Minimum primary control power of ith generator
P_{L-in}	Possible initial load of the islanded microgrid
p_{L-in}	Possible initial load of islanded microgrid in per unit base
P_{Lmax}	The upper possible steady state operating limit of the islanded microgrid
p_{Lmax}	The upper possible steady state operating limit of the islanded microgrid in per unit base
P_{Lmin}	The lower possible steady state operating limit of the islanded microgrid
p_{Lmin}	The lower possible steady state operating limit of the islanded microgrid in per unit base
P_{Lsmax}	The steady state positive load change limit
p_{Lsmax}	The steady state positive load change limit in per unit base
P_{Lsmin}	The steady state negative load change limit
p_{Lsmin}	The steady state negative load change limit in per unit base
$P_L(t)$	The actual lumped load consumption in the microgrid
$p_L(t)$	The actual lumped load consumption in the microgrid in per unit base

P_{MAX}	Maximum rate of change of power imposed by control valve rate limits
P_{mech}	The supplied mechanical power from turbine
P_{MIN}	Minimum rate of change of power imposed by control valve rate limits
P_{n-CG}	The rated power of the conventional generator in the islanded microgrid
p_{n-CG}	The rated power of the conventional generator in the islanded microgrid in per unit base
P_{n-L}	The maximum load demand can be supplied in the islanded microgrid
p_{n-L}	The maximum load demand in the islanded microgrid in per unit base
P_{n-PV}	The rated power of the photovoltaic generator in the islanded microgrid
p_{n-PV}	The rated power of the photovoltaic generator in the islanded microgrid in per unit base
P_{ni}	Rated power of ith generator
P_{ni}	The rated power of ith generator
p_{PV-in}	The initial active power infeed from photovoltaic generator in per unit base
P_{PVact}	Currently available active power of photovoltaic generator
p_{PVact}	Currently available active power of photovoltaic generation in per unit base
P_{PV}	Actual active power infeed of photovoltaic generator
p_{PV}	The active power infeed from photovoltaic generator in per unit base
$P_{PV}(t)$	The actual active power output from photovoltaic generator
$p_{PV}(t)$	The actual active power infeed from photovoltaic generator in per unit base
p_{ref}	Active power set point
s_{CG}	The share of the conventional generator in the islanded microgrid
s_{PV}	The share of PV generation in the islanded microgrid
t	Time, in seconds

T_A	System starting time constant
t_0	The time point when the load change happens in the microgrid
T_1	Controller lag compensation of speed governor
T_2	Controller lead compensation of speed governor
T_3	Valve position time constant (servomotor mechanism)
T_4	Time constant for steam chest
T_5	Re-heater 1 time constant
T_6	Re-heater 2 time constant
T_7	Crossover time constant
t_{adp}	The adapting time that the CG is needed to change its active power generation until an expected value
T_{Ai}	Mechanical starting time constant of ith generator
T_{CG}	The starting time constant of the conventional generator in the islanded microgrid
T_D	Time constant for diesel engine
T_{MG}	The system starting time constant of the islanded microgrid
T_{PV}	The starting time constant of the photovoltaic generator in the islanded microgrid
t_{qss}	The time point when the primary control of the microgrid ends
t_{set}	The time that load step pre-announcement holds an individual load switch-on or -off signal
T_{SM}	Time constant for valve actuator
t_{total}	The time that the bang-bang controller is activated
X_{act}	Actual system quantity
X_{base}	Base value of quantity

List of Figures

171

List of Tables

Bibliography

[1] I. E. A. Publications, "World energy outlook 2016," *International Energy Agency OECD Publications*, 2016. ISBN:9789264264946.

[2] NASA/GISS, "Global temperature." Website, 2017. https://climate.nasa.gov/vital-signs/global-temperature/, Accessed on April 30th, 2017.

[3] T. J. Crowley, "Causes of climate change over the past 1000 years," *Science*, vol. 289, no. 5477, pp. 270–277, 2000.

[4] J. Hansen, M. Sato, R. Ruedy, K. Lo, D. W. Lea, and M. Medina-Elizade, "Global temperature change," *Proceedings of the National Academy of Sciences*, vol. 103, no. 39, pp. 14288–14293, 2006.

[5] Eurostat, "Energy production and imports." Website, 2016. http://ec.europa.eu/eurostat/statistics-explained/index.php/Energy_production_and_imports, Accessed on April 17th, 2017.

[6] "New era for electricity in europe. distributed generation: Key issues, challenges and proposed solutions european commission: Eur 20901, 2003," tech. rep., ISBN 92-894-6262–0.

[7] C. Böhringer, T. F. Rutherford, and R. S. Tol, "The eu 20/20/2020 targets: An overview of the emf22 assessment," *Energy economics*, vol. 31, pp. S268–S273, 2009.

[8] I. E. A. Publications, "Energy, climate change and environment: 2016 insights," *International Energy Agency OECD Publications*, 2016. http://www.iea.org/publications/freepublications/publication/ECCE2016.pdf, Accessed on May 15th, 2017.

[9] G. Pepermans, J. Driesen, D. Haeseldonckx, R. Belmans, and W. D'haeseleer, "Distributed generation: definition, benefits and issues," *Energy policy*, vol. 33, no. 6, pp. 787–798, 2005.

[10] T. Ackermann, G. Andersson, and L. Söder, "Distributed generation: a definition," *Electric power systems research*, vol. 57, no. 3, pp. 195–204, 2001.

[11] N. Hatziargyriou, *Microgrids: architectures and control.* John Wiley & Sons, 2013.

[12] J. von Appen, M. Braun, T. Stetz, K. Diwold, and D. Geibel, "Time in the sun: the challenge of high pv penetration in the german electric grid," *IEEE power and energy magazine*, vol. 11, no. 2, pp. 55–64, 2013.

[13] P. Beiter, M. Elchinger, and T. Tian, "2016 renewable energy data book," tech. rep., NREL (National Renewable Energy Laboratory (NREL), Golden, CO (United States)), 2017.

[14] S. Philipps and W. Warmuth, "Photovoltaics report ©fraunhofer ise." Website, 2016. https://www.ise.fraunhofer.de/de/downloads/pdf-files/aktuelles/photovoltaics-report-in-englischer-sprache.pdf, Accessed on July 17th, 2017.

[15] G. W. E. C. Global Wind Energy Council, "Global wind statistics 2016," 2017. http://www.gwec.net/wp-content/uploads/vip/GWEC_PRstats2016_EN_WEB.pdf, Accessed on July 16th, 2017.

[16] D. E. Olivares, A. Mehrizi-Sani, A. H. Etemadi, C. A. Cañizares, R. Iravani, M. Kazerani, A. H. Hajimiragha, O. Gomis-Bellmunt, M. Saeedifard, R. Palma-Behnke, *et al.*, "Trends in microgrid control," *IEEE Transactions on smart grid*, vol. 5, no. 4, pp. 1905–1919, 2014.

[17] Y. Guo and W. Gawlik, "A novel control approach for microgrids islanded operation-load step pre-announcement and bang-bang control," pp. 1–14, Vortrag: 14. Symposium Energieinnovation EnInnov2016, Graz; 10.02.2016 - 12.02.2016, 2016. in: "EnInnov 2016 - Energie für unser Europa", Verlag der Technischen Universität Graz, ISBN:978-3-85125-447-1.

[18] R. Lasseter, A. Akhil, C. Marnay, J. Stephens, J. Dagle, R. Guttromson, A. Meliopoulous, R. Yinger, and J. Eto, "The certs microgrid concept," *White paper for Transmission Reliability Program, Office of Power Technologies, US Department of Energy*, vol. 2, no. 3, p. 30, 2002.

[19] A. Ulbig, T. S. Borsche, and G. Andersson, "Impact of low rotational inertia on power system stability and operation," *IFAC Proceedings Volumes*, vol. 47, no. 3, pp. 7290–7297, 2014.

[20] Y. Guo and W. Gawlik, "A survey of control strategies applied in worldwide microgrid projects," *Tagungsband ComForEn*, vol. 2014, pp. 47–54, 2014.

[21] Y. Guo, T. Görlich, and W. Gawlik, "Load step pre-announcement and bang-bang-controller implemented in islanded microgrids to improve frequency stability," *CIRED Workshop 2018 "Microgrids and local energy communities", Ljubljana, Slowenien*, no. 0086, pp. 1–4, 2018.

[22] Y. Guo and W. Gawlik, "Defining control strategies for photovoltaic reconnection in islanded microgrids," *e & i Elektrotechnik und Informationstechnik*, vol. 133, no. 8, pp. 402–406, 2016. DOI:10.1007/s00502-016-0441-7.

[23] J. G. Olivier, G. Janssens-Maenhout, M. Muntean, and J. A. Peters, "Trends in global co2 emissions 2015 report," 2015.

[24] U. E. I. Administration, "How dependent are we on foreign oil?." Website, 2011. http://www.eia.gov/energy_in_brief/article/foreign_oil_dependence.cfm, Accessed on April 13th, 2017.

[25] C. Hou, X. Hu, and D. Hui, "Hierarchical control techniques applied in microgrid," in *Power System Technology (POWERCON), 2010 International Conference on*, pp. 1–5, IEEE, 2010.

[26] Y. Zhou and C. N.-M. Ho, "A review on microgrid architectures and control methods," in *Power Electronics and Motion Control Conference (IPEMC-ECCE Asia), 2016 IEEE 8th International*, pp. 3149–3156, IEEE, 2016.

[27] P. Piagi and R. H. Lasseter, "Autonomous control of microgrids," in *2006 IEEE Power Engineering Society General Meeting*, pp. 8–pp, IEEE, 2006.

[28] K. De Brabandere, K. Vanthournout, J. Driesen, G. Deconinck, and R. Belmans, "Control of microgrids," in *Power Engineering Society General Meeting, 2007. IEEE*, pp. 1–7, IEEE, 2007.

[29] A. Dimeas and N. Hatziargyriou, "A multi-agent system for microgrids," in *Hellenic Conference on Artificial Intelligence*, pp. 447–455, Springer, 2004.

[30] M. Berna-Koes, I. Nourbakhsh, and K. Sycara, "Communication efficiency in multi-agent systems," in *Robotics and Automation, 2004. Proceedings. ICRA'04. 2004 IEEE International Conference on*, vol. 3, pp. 2129–2134, IEEE, 2004.

[31] M. Eremia and M. Shahidehpour, *Handbook of electrical power system dynamics: modeling, stability, and control*, vol. 92. John Wiley & Sons, 2013.

[32] F. Zeilinger, "Leistungs-frequenz-regelung, virtuelle kraftwerke, skriptum zur vorlesung 370.007," *Lecture notes*, pp. 9–11, 2014.

[33] G. Andersson, "Dynamics and control of electric power systems," *Lecture notes*, pp. 227–0528, 2012.

[34] H. Bevrani, *Robust power system frequency control*, vol. 85. Springer, 2009.

[35] E.-E. C. E. O. Handbook, "P1–policy 1: Policy 1: Load-frequency control and performance. entso-e; 2009."

[36] P. Kundur, N. J. Balu, and M. G. Lauby, *Power system stability and control*, vol. 7. McGraw-hill New York, 1994.

[37] W. Gawlik, "Energieversorgung skriptum zur vorlesung 370.002, version vom 30.09.2016," *Lecture notes*, 2016.

[38] A. Rubaai and J. Jerry, "Hybrid fuzzy bang-bang mode controller for electric motor drives applications," in *Industry Applications Society Annual Meeting (IAS), 2011 IEEE*, pp. 1–8, IEEE, 2011.

[39] E.-E. C. E. O. Handbook, "P5–policy 5: Emergency operations. entso-e; 2015."

[40] V. FNN, "Erzeugungsanlagen am niederspannungsnetz, technische mindestanforderungen für anschluss und parallelbetrieb von erzeugungsanlagen am niederspannungsnetz," tech. rep., VDE-AR, 2011.

[41] N. Hatziargyriou, *MicroGrids*. wiley-IEEE press, 2014.

[42] P. Malatestas, M. Papadopoulos, and G. Stavrakakis, "Modeling and identification of diesel-wind turbines systems for wind penetration assessment," *IEEE transactions on power systems*, vol. 8, no. 3, pp. 1091–1097, 1993.

[43] P. Pourbeik *et al.*, "Dynamic models for turbine-governors in power system studies," *IEEE Task Force on Turbine-Governor Modeling*, 2013.

[44] I. Report, "Dynamic models for steam and hydro turbines in power system studies," *IEEE Transactions on Power Apparatus and Systems*, no. 6, pp. 1904–1915, 1973.

[45] P. to Phase BV, "Synchronous machine turbine-governing systems vision dynamical analysis," 2016. http://www.phasetophase.nl/pdf/SynchronousMachineTurbineGoverningSystems.pdf.

[46] M. Dulau and D. Bica, "Simulation of speed steam turbine control system," *Procedia Technology*, vol. 12, pp. 716–722, 2014.

[47] S. A. Papathanassiou and M. P. Papadopoulos, "Dynamic characteristics of autonomous wind–diesel systems," *Renewable Energy*, vol. 23, no. 2, pp. 293–311, 2001.

[48] W. Gawlik, M. Chochole, D. Fasthuber, M. Litzlbauer, M. Heimberger, J. March-graber, Y. Guo, A. Schuster, R. Schlager, A. Kollmann, J. Reichl, K. De Bruyn, H. Steinmüller, M. Schwarz, F. Frank, E. Traxler, A. Abart, M. Streif, M. Reiter, R. Nenning, and F. Herb, "Smarte robuste regenerativ gespeiste blackout-feste netzabschnitte," *Endbericht*, 2015.

[49] W. Bartels, F. Ehlers, K. Heidenreich, R. Huttner, H. Kuhn, T. Meyer, T. Kumm, J. Salzmann, H. Schafer, and K. Weck, "Generating plants connected to the medium-voltage network," *Technical Guideline of BDEW*, 2008.

[50] B.-I. Crăciun, T. Kerekes, D. Séra, and R. Teodorescu, "Overview of recent grid codes for pv power integration," in *Optimization of Electrical and Electronic Equipment (OPTIM), 2012 13th International Conference on*, pp. 959–965, IEEE, 2012.

[51] V. VDE, "0126-1-1, automatic disconnection device between a generator and the public low-voltage grid," 2006.

[52] J. C. Boemer, K. Burges, P. Zolotarev, J. Lehner, P. Wajant, M. Fürst, R. Brohm, and T. Kumm, "Overview of german grid issues and retrofit of photovoltaic power plants in germany for the prevention of frequency stability problems in abnormal system conditions of the entso-e region continental europe," in *1st International Workshop on Integration of Solar Power into Power Systems*, vol. 24, 2011.

[53] B. PATTEN *et al.*, "Systems analysis and simulation in ecology. volume 1.," *Systems analysis and simulation in ecology. Volume 1.*, 1971.

[54] R. Antunes, V. A. González, and K. Walsh, "Identification of repetitive processes at steady-and unsteady-state: Transfer function,"

[55] W. Gao, Z. Wu, J. Wang, and S. Gu, "A review of inertia and frequency control technologies for variable speed wind turbines," in *2013 25th Chinese Control and Decision Conference (CCDC)*, pp. 2527–2533, IEEE, 2013.

[56] A. Saltelli, K. Chan, E. M. Scott, *et al.*, *Sensitivity analysis*, vol. 1. Wiley New York, 2000.

[57] "IEEE standard for synchrophasor measurements for power systems," *IEEE Std*, C37.118.1-2011.

[58] "Establishing a network code on requirements for grid connection of generators," *COMMISSION REGULATION (EU) 2016/631*, 2016.